Proteins, polymers and living cells
on titanium oxide-based nanostructured coatings:
exploitation of label-free optical sensing methods

Ph.D. Thesis

By:
Judit Nádor

Supervisors:
Róbert Horváth, PhD
Péter Petrik, DSc

Institute of Technical Physics and Materials Science,
Centre for Energy Research, Hungarian Academy of Sciences

Doctoral School of Molecular- and Nanotechnologies
University of Pannonia
Head of School: Prof. Ferenc Vonderviszt, DSc

2016

Proteins, polymers and living cells on titanium oxide-based nanostructured coatings: exploitation of label-free optical sensing methods

Értekezés doktori (PhD) fokozat elnyerése érdekében

Írta:
Nádor Judit

Készült a Pannon Egyetem – Molekuláris- és Nanotechnológiák Doktori Iskolájában

Témavezetők: Dr. Horváth Róbert, Dr. Petrik Péter

Az értekezést témavezetőként elfogadásra javaslom:

Dr. Horváth Róbert: igen / nem   …………………………..
                                                              (aláírás)

Dr. Petrik Péter: igen / nem   …………………………..
                                                              (aláírás)

A jelölt a doktori szigorlaton ……… %-ot ért el.

Az értekezést bírálóként elfogadásra javaslom:

Bíráló neve: ……………………… igen / nem   …………………………..
                                                      (aláírás)

Bíráló neve: ……………………… igen / nem   ……………………………
                                                      (aláírás)

A jelölt az értekezés nyilvános vitáján ……… %-ot ért el.

…………………………
Bíráló Bizottság elnöke

A doktori (PhD) oklevél minősítése ………………………………

…………………………
EDT elnöke

Veszprém,………………………..

Table of contents

Abstract (English)

The main topic of my doctoral work is nanostructured coatings made of titanium-oxide nanoparticles. Due to their advantageous biophysical properties, they are promising candidates for being applied as sensing surfaces on biosensors or as coatings on medical implants. In the first part of the dissertation I introduce titanate nanotube (TNT) thin films. The characterization of them was performed using atomic force microscopy, spectroscopic ellipsometry and optical waveguide lightmode spectroscopy (OWLS).

I demonstrated that OWLS sensor chips coated with these transparent nanostructured layers are still compatible with the OWLS device, the coating doesn't quench the incoupling and the propagation of the light in the waveguide, the height of the resonant peaks doesn't change considerably. I studied the adsorption of bovine serum albumin, and the adhesion of preosteoblasts and human embryonic kidney cells on the TNT coating. I revealed that the coating enhanced the adsorption of the protein, and the spreading and the strength of adhesion of living cells.

In the second part of my work I present a novel ellipsometric configuration in the Kretschmann geometry, with which the deposition of the sample can be studied *in situ* on two different surfaces simultaneously. While in this configuration the circumstances (temperature, humidity, sample concentration) are the same for the two measurements, the obtained results for the two surfaces can be compared in a more reliable way, than in the case of sequentially performed experiments.

Unlike conventional ellipsometric flow cells, multiple angles of incidence can be applied with this setup, due to the semi-cylindrical lens. The plasmon resonance, generated by a gold thin film on the substrate, improves the sensitivity of the measurements compared to previous configurations.

With this recently developed ellipsometric setup I carried out measurements in order to study the adsorption of polyelectrolytes, proteins, and living cells on surfaces coated with titania nanoparticles. I demonstrated that the coating significantly enhanced the adsorption of the proteins and the polyelectrolytes. The experiment with preosteoblasts showed, that the configuration is appropriate for studying living cells but for more exact evaluation further developments are necessary in model construction.

Magyar nyelvű kivonat

Doktori munkám központi témája titán-oxid alapú nanorészecskékből készített bevonatok, amelyek előnyös biofizikai tulajdonságaik miatt potenciálisan alkalmazhatók bioszenzorok érzékelőfelületeként, illetve orvosi implantátumok bevonataként. A disszertáció első felében titanát nanocsövekből készített rétegeket mutatok be, melyek karakterizálását atomi erő mikroszkóppal, spektroszkópiai ellipszometriai térképezéssel és optikai hullámvezető fénymódus spektroszkópiával (OWLS) végeztem.

Bizonyítottam, hogy az átlátszó nanostrukturált réteggel borított érzékelő chip alkalmas OWLS mérésekre, a bevonat nem rontja le a chip becsatolási és hullámvezetési tulajdonságait, a rezonanciacsúcsok magassága nem változik számottevően. A bevonatokon borjú szérum albumin fehérje, preosteoblast (éretlen csontképző) sejtek és humán embrionális vesesejtek kitapadását vizsgáltam. Megmutattam, hogy a bevonat elősegíti a fehérjék adszorpcióját és növeli a sejtek adhéziójának mértékét és erősségét.

Doktori munkám második részében egy olyan Kretschmann geometriájú spektroszkópiai ellipszometriai mérési összeállítást mutatok be, amellyel a vizsgált minta kitapadását egyszerre kétféle felületen, *in situ* tudjuk tanulmányozni. Mivel ebben az elrendezésben a két méréshez tartozó környezeti paraméterek (hőmérséklet, páratartalom, mintakoncentráció stb.) megegyeznek, a két felületre kapott eredmények összehasonlítása sokkal megbízhatóbbá válik, mint külön elvégzett kísérletek esetén. A korábbi ellipszometriai folyadékcellákkal szemben az üveg félhenger alkalmazásának köszönhetően több beesési szög alkalmazható, a hordozót borító arany vékonyréteg által létrehozott plazmon rezonancia pedig a módszer érzékenységét javítja a hagyományos ellipszometriai elrendezésekhez képest.

Az új mérési elrendezéssel titán-dioxid nanoszemcsékkel borított nanostrukturált felületen és arany kontrolfelületen végeztem adszorpciós kísérleteket polielektrolitok, fehérjék, valamint élő sejtek tanulmányozása céljából. A polielektrolitok és fehérjék esetében megmutattam, hogy a nanoszemcsés bevonatra nagyobb mennyiségű minta tapadt ki. Az élő sejtek vizsgálatával szemléltettem, hogy a mérési összeállítás alkalmas élő sejtek vizsgálatára, azonban a mérések pontosabb kiértékeléséhez további fejlesztések szükségesek a modellalkotás területén.

Abstract (Deutsch)

Das Hauptthema meiner Doktorarbeit ist die Herstellung verschiedener Schichten von Titan-Oxid Nanopartikeln. Durch deren vorteilhaften biophysikalischen Eigenschaften können diese Schichten als potenzielle Oberflächen von Biosensoren oder von medizinischen Implantaten verwendet werden. Im ersten Teil der Arbeit stelle ich die Dünnfilme von Titan-Nanoröhrchen (titanate nanotube - TNT) vor. Sie wurden mit Atomkraftmikroskopie, Spektralellipsometrie und OWLS (optical waveguide lightmode spectroscopy) charakterisiert.

Ich habe es demonstriert, dass die mit diesen nanostrukturierten transparenten Schichten bedeckte Oberfläche der Sensorchips mit dem OWLS-Gerät kompatibel ist. Der nanostrukturierte Dünnfilm löscht die Einkopplung und die Verbreitung in der Wellenleiter nicht, und die Höhen der Resonanzspitzen verändern sich nicht deutlich. Ich habe sowohl die Adsorption von BSA (bovine serum albumin), als auch die Haftung von Preosteoblast und Nierenzellen auf TNT untersucht. Ich habe gefunden, dass der nanostrukturierte Dünnfilm die Adsorption von Protein und die Verbreitung und die Stärke der Haftung von lebenden Zellen erhöht hat.

Im zweiten Teil meiner Arbeit habe ich eine neue Konfiguration von Ellipsometrie in dem Kretschmann-Aufbau dargestellt, in dem die Adsorption gleichzeitig auf zwei unterschiedlichen Oberflächen untersucht werden kann. Da die Bedingungen (Temperatur, Feuchtigkeit, Konzentration) für beide Messungen gleich sind, können die Unterschiede zwischen den zwei Oberflächen einfacher bestimmt werden, als im Falle von nacheinander durchgeführten Messungen.

Mit konventionellen Flüssigkeitszellen verglichen, aufgrund des Aufbaus mit einem Halbzylinder können mit dieser Konfiguration Messungen von mehreren Einfallswinkeln durchgeführt werden. Die von einem Goldfilm erzeugte Plasmonenresonanz erhöht die Sensitivität der Messung gegenüber den vorherigen Konfigurationen.

Abbreviations

AFM	atomic force microscope
BSA	bovine serum albumin
EMA	effective medium approximation
FGN	fibrinogen
GCI	grating coupled interferometry
HEK	human embryonic kidney
MQ	ultrapure milli-Q water
MSE	mean squared error
OWLS	optical waveguide lightmode spectroscope
PAH	poly(allylamine hydrochloride)
PBS	phosphate buffered saline
PSS	poly(styrene sulphonate)
SEM	scanning electron microscope
QCM	quartz crystal microbalance
RIU	refractive index unit
SE	spectroscopic ellipsometer
SPR	surface plasmon resonance
TEM	transmission electron microscope
TNP	titania nanoparticles
TNT	titanate nanotubes

1. Introduction

In the last decades label-free, surface-sensitive methods became a key in various areas of biotechnological, biophysical and biological research. An important development of these techniques was the increased sensitivity, which made possible to detect very small concentrations of the target molecules. Due to the increased throughputs of these methods, they can now be applied with improved efficiency, even in basic biological research where good quality data with statistics is crucial. Furthermore, they became more user-friendly, thus no specific qualification is needed to employ them. The optical methods became especially successful, due to the non-invasiveness of specific spectrums of optical frequencies with biological samples and the low interference with disturbing electromagnetic radiation. In addition, they can operate without the application of any dye or labeling molecules, which could modify the target molecules or their environment and increase the costs and the complexity of the measurements.

I have started my Ph.D. research work in 2012 in the Nanobiosensorics and Ellipsometric Laboratories of the Institute of Technical Physics and Materials Science. At that time several state-of-the-art techniques were available or were under development in these laboratories, such as optical lightmode spectroscopy, rotating-compensator ellipsometer, grating coupled interferometer or Corning Epic BT System. These techniques were traditionally mainly applied to investigate thin films of proteins, lipids or polymers, but there is a general tendency in biosensor research to combine these technologies with living cells or even tissues. In order to keep up with current trends, we established the first cell culture biosensorics laboratory in Hungary, where the cultured cells can be studied with the above mentioned methods on an everyday basis, opening up new research directions in materials sciences, thus increasing the portfolio of our institute.

It is especially important nowadays to employ nanostructured functional materials in biosensing or in materials sciences in general. My work focused on additive-free, titanium oxide-based nanostructured layers and their integration in various biosensing methods in a simple way. I intended to make the first steps in the research of proteins and livings cells on these novel coatings and to demonstrate that the effects of the surface roughness on the analytes can be studied in a quantitative way using these techniques.

Nowadays nanotechnology plays a more and more important role, not only in the scientific but in our everyday life. With expanding toward the nanometer and subnanometer ranges, our knowledge and possibilities grow consumedly. Our electronic devices become more efficient and complex, new medications are being developed to cure the patients on cell- or molecular levels, engineers are capable to create materials with completely new or astonishing properties.

The word "nano" can be originated from the ancient Greek word 'νᾶνος' (nanos), which means dwarf [1]. Today it indicates the one billionth (10^{-9}) of a unit in the metric system (Fig. 1.1).
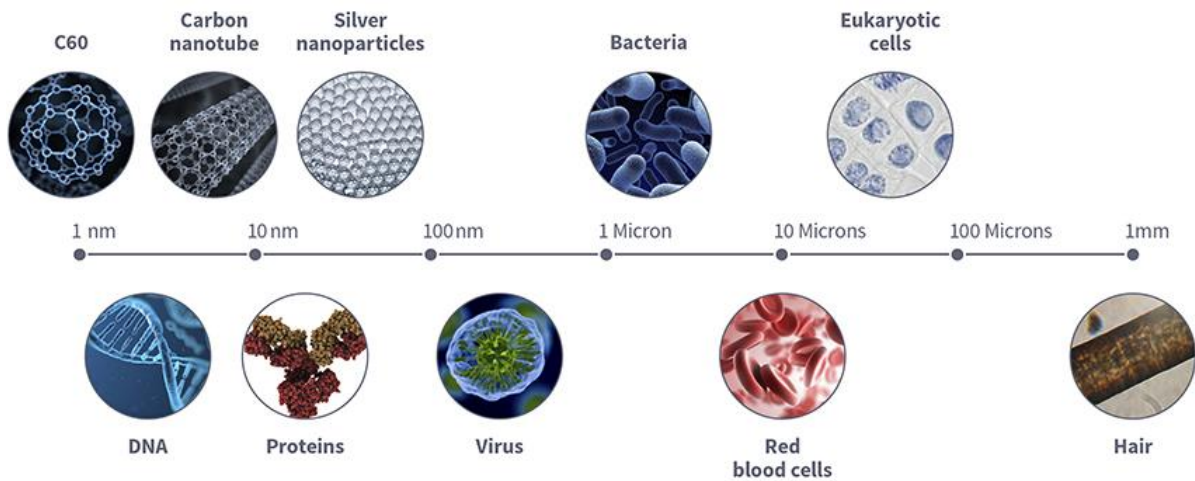

Figure 1.1. Examples for objects in the micro- and nanoscale [2].

In the next chapters I give a brief overview of the most prevalent nanoparticles and their application possibilities, and the most known coating procedures.

1.1. Morphology and applications of nanoparticles

The *criterion* of a nano-object is to have a characteristic dimension in at least one direction lower than a few 100 nm [3]. Nanostructured materials can be categorized according to their dimensionality; there are zero-, one-, two- and three-dimensional nanostructures [4].

Zero-dimensional nanomaterials (Fig. 1.2) [4] have all their dimensions in the nanometer range. In this group we can find uniform particles arrays (quantum dots), heterogeneous particles arrays, core–shell quantum dots, onions, hollow spheres or nanolenses. Their synthetization can be very diverse, and they are performed by several research groups for a long time [5]–[8]. Zero-dimensional nanomaterials are primarily applied in solar cells [9], lasers [10], light emitting diodes (LEDs) [11], single-electron transistors [12], in diagnostics and *in vivo* imaging [13], optical sensing [14] and drug delivery [15].
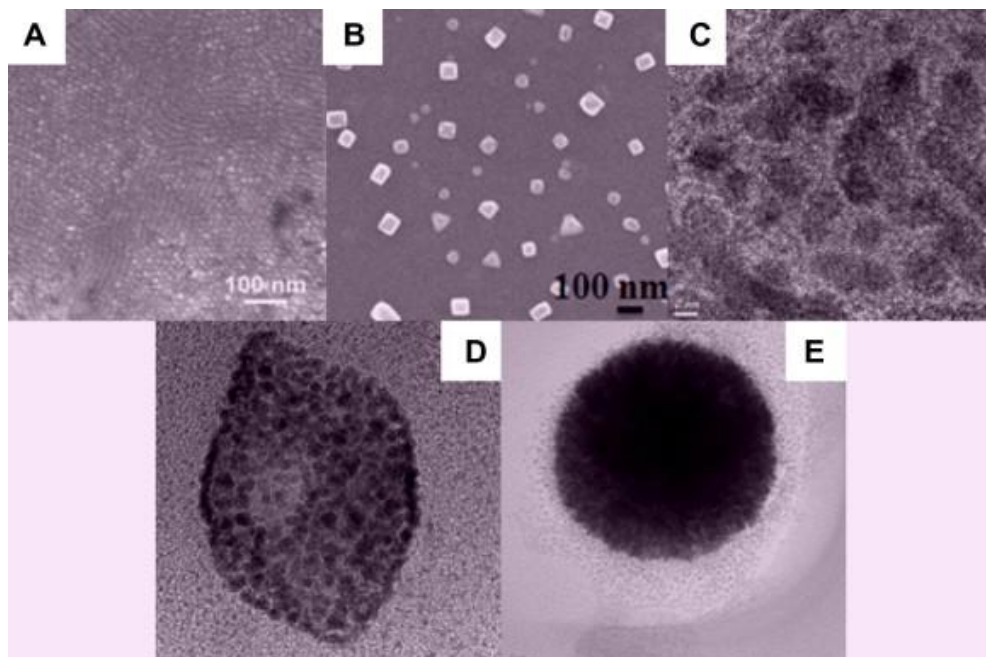

Figure 1.2. Typical scanning electron microscope (SEM) and transmission electron microscope (TEM) images of zero-dimensional nanoparticles: (a) quantum dots, (b) nanoparticles arrays, (c) core–shell nanoparticles, (d) hollow cubes, and (e) nanospheres [4].

In the one-dimensional group of nanostructures (Fig. 1.3) [4], the particles have a significantly larger expansion in one direction, than in the other two. Nanowires, nanorods, nanotubes, nanobelts, nanoribbons, and hierarchical nanostructures belong to this assembly [16]–[20]. They are often applied as interconnects or as main units in electronic, optoelectronic, and electrochemical energy devices with nanoscale dimensions [4], in electrochemical biosensors [21], and medical applications [22].
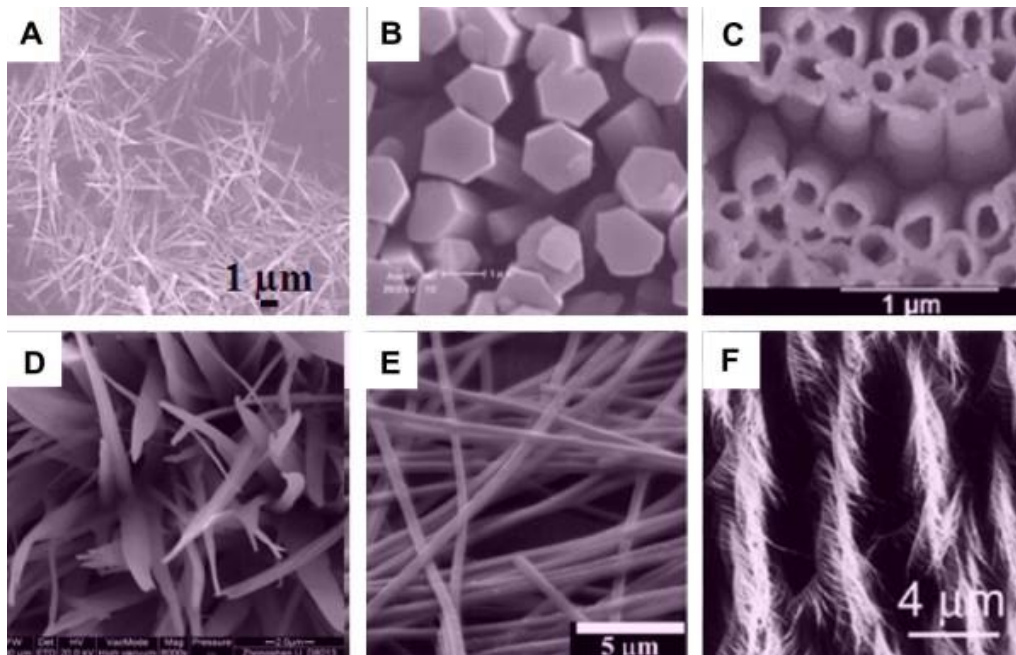
Figure 1.3. *Typical SEM images of different types of one-dimensional nanostructured materials:* ***(a)*** *nanowires,* ***(b)*** *nanorods,* ***(c)*** *nanotubes,* ***(d)*** *nanobelts,* ***(e)*** *nanoribbons, and* ***(f)*** *hierarchical nanostructures* [4].

The two-dimensional nanomaterials (Fig. 1.4) [4] are plain structures and have one dimension which is considerably smaller than the others. This group includes nanoplates, nanosheets, nanojunctions (continuous islands), branched structures, nanoprisms, nanowalls, and nanodisks [23]–[27]. Today one of the most popular two-dimensional nanostructure is doubtlessly the graphene, but beyond it we can find other promising materials that can form monolayers, such as silicene, germanene, stanene, and phosphorene [28], [29]. These types of nanomaterials are widely studied and are hopeful candidates for being employed in electrical applications, like field-

effect-transistors or single-electron-transistors [30], [31], solar cells [32], or in highly efficient thermoelectric applications [29]. They are also popular in medical fields and were successfully applied in cellular imaging, drug delivery, gene delivery, tissue engineering [33], [34], and also in electrochemical and optical biosensors [35].
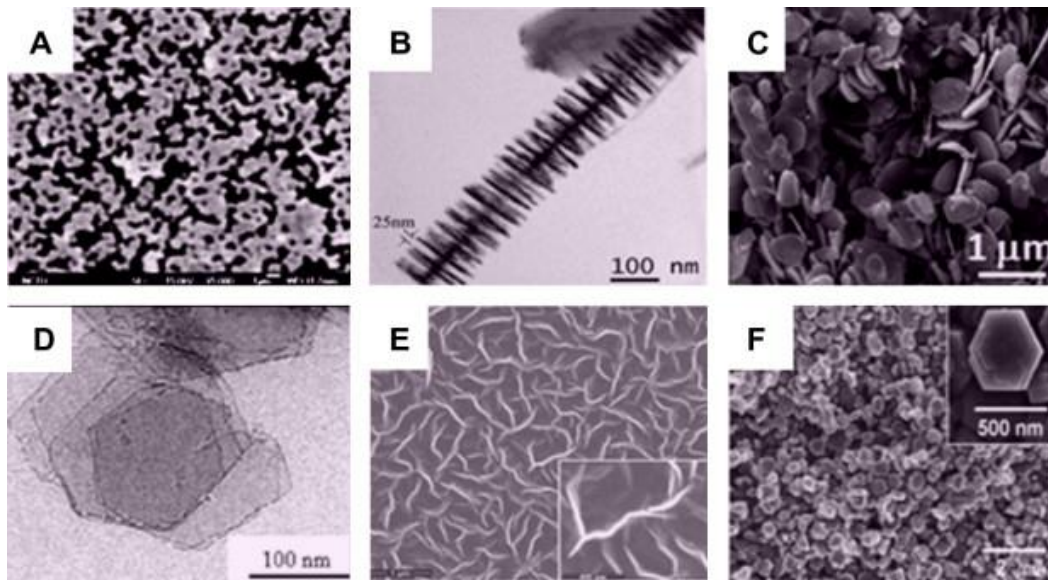
Figure 1.4. Typical SEM and TEM images of different types of two-dimensional nanostructures: (a) junctions (continuous islands), (b) branched structures, (c) nanoplates, (d) nanosheets, (e) nanowall, and (f) nanodisk [4].

The three-dimensional nanostructures (Fig. 1.5) can possess preferable properties over their bulk counterparts, due to their huge specific surface area [4]. The most typical three-dimensional nanostructures are nanoballs (dendritic structures), nanocones, nanocoils, nanoflowers and nanopillars [36]–[41]. The application possibilities of these three-dimensional nanostructures are very wide, so only a non-exhaustive list of examples is given here. Their unique properties can be exploited in electronic systems, like flexible solar cells [41], microfluidic devices with integrated electronics, chemical and biological sensors, or photonic and optoelectronic systems that combine unconventional materials with conventional silicon-based electronics [42] and rechargeable batteries [43], [44]. They can be applied in medicine as biomaterial scaffolds [45], in drug [46] and gene delivery [47], and in biological targeting [48].
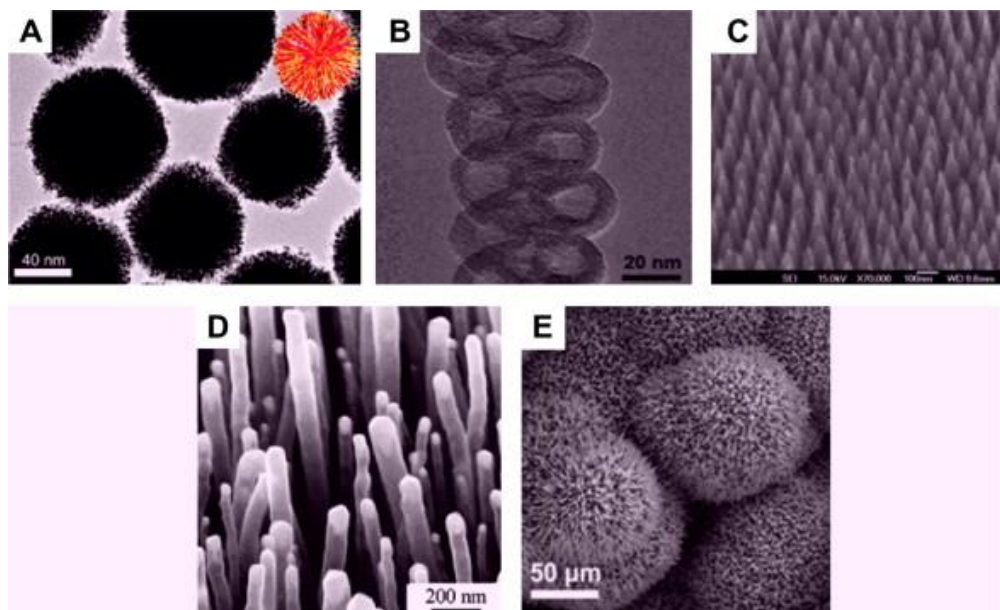
*Figure 1.5. Typical SEM and TEM images of different three-dimensional nanoparticles: **(a)** nanoballs (dendritic structures), **(b)** nanocoils, **(c)** nanocones, **(d)** nanopillars, and **(e)** nanoflowers* [4].

Many types of nanoparticles from the above introduced groups could be exploited as surface coatings for various biosensing applications. When the aim is to determine concentration, affinity or adsorption of a target biomacromolecule (e.g., proteins), using label-free methods such as optical waveguide lightmode spectroscopy, spectroscopic ellipsometry or quartz crystal microbalance, the target objects are first required to be captured by a sensor. Therefore making the sensor surface as large as possible is beneficial, because more analytes can be captured. A popular method to accomplish that requirement and to improve adhesion is to nanostructure the surface which is accompanied by the increase of the specific surface area [T1].

Another possible role of surface nanostructuring is that the changes of the surface roughness have an effect on the behavior of living cells (Fig. 1.6) [49]–[51]. Among other biophysicochemical properties of the substrate, like composition or topography, the surface roughness can be an effective tool in controlling cell adhesion, spreading or proliferation.
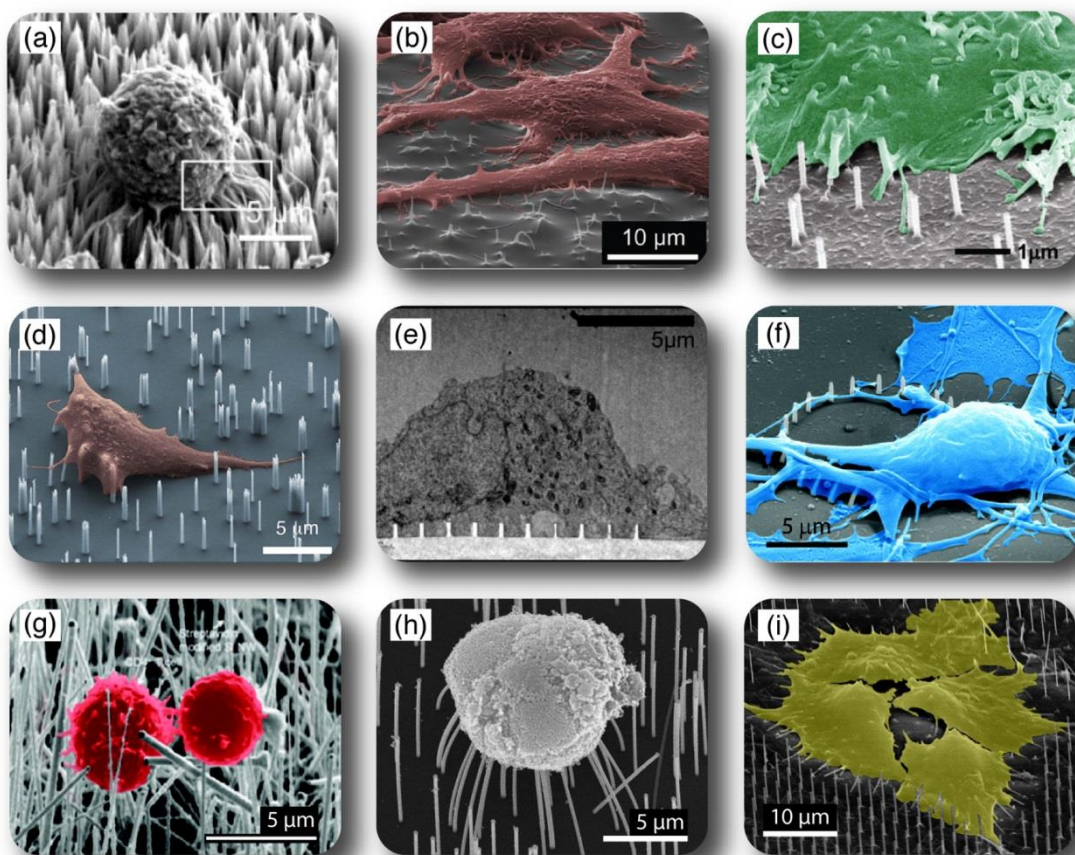
Figure 1.6. *Cells on arrays of NSs.* [52] *A549 cell on silicon NSs **(a)** [53], HeLa cells on copper oxide NSs **(b)** [54], CHO or HeLa cell on hollow aluminum oxide NSs **(c)** [55], natural killer cell on silicon NSs **(d)** [56], cortical neuron cell on quartz NSs **(e)** [57], cortical neuron cell on a ring of platinum NSs **(f)** [58], T lymphocyte cells on silicon NSs **(g)** [59], retinal cell on gallium phosphide NSs **(h)** [60], and HEK293 cells on indium arsenide NSs **(i)** [52].*

1.2. Coating preparation procedures

There are plenty of fabrication methods for preparing coatings. They can be classified in four general categories (Table 1.1), which are atomistic deposition, particulate deposition, bulk coating and surface modification [61]. In atomistic deposition processes, atoms are condensing onto a substrate surface and migrating to nucleation and growth sites to form the film. In this case the atoms can't always reach their lowest possible energy configurations, therefore many structural imperfections (voids, dangling bonds, lattice mismatches) can be found in the resulting films. In particulate deposition

technologies solid or molten particles are used for depositing the coating, and the solidification and sintering steps are very important part of the method, which have a great effect on the resulting microstructure. Bulk coating processes require great amount of the coating material to be applied on the surface at once. In surface modification methods the surface composition or other properties are modified by chemical, mechanical, thermal or ion treatments [62].

Atomistic deposition	Particulate deposition	Bulk coating	Surface modification
Vacuum environment • Evaporation • Molecular beam epitaxy • Ion beam deposition *Plasma environment* • Sputter deposition • Ion plating • Plasma polymerization • Glow discharge deposition *Electrolytic environment* • Electroplating • Electroless deposition *Chemical vapor environment* • Chemical vapor deposition • Spray pyrolysis *Liquid phase epitaxy*	*Thermal spraying* • Plasma spraying • Flame spraying • Detonation gun *Fusion coating* • Enameling • Electrophoresis	*Wetting processes* • Printing • Dip coating • Spin coating *Printing* *Cladding* • Explosive • Roll-binding *Weld coating*	*Chemical conversion* • Anodic oxidation • Nitridation *Leaching* *Thermal surface treatment* *Ion implantation* *Laser glazing*

Table 1.1. *The classification of coating procedures* [61].

2. State of the art

In this section I introduce the most important evanescent wave- and ellipsometry-based techniques. The last subsection is about surface structuring, which is often combined the highlighted novel technologies in order to improve the sensitivity of the method or the accessibility of immobilized receptors.

2.1. Evanescent field-based sensing

When an electromagnetic wave strikes an interface at an angle greater than the critical angle, it undergoes total reflection at the boundary, but a small part of the wave can penetrate into the adjacent medium. It generates the so-called evanescent field, which has an exponentially decreasing intensity orthogonally to the interface (Fig. 2.1). The evanescent field-based (bio)sensors utilize the fact, that the interaction or adsorption of (bio)molecules within the penetration depth (d_p) of the evanescent field can cause the change of the effective refractive index for the guided mode and it leads to the change of the incoupling angle (θ).

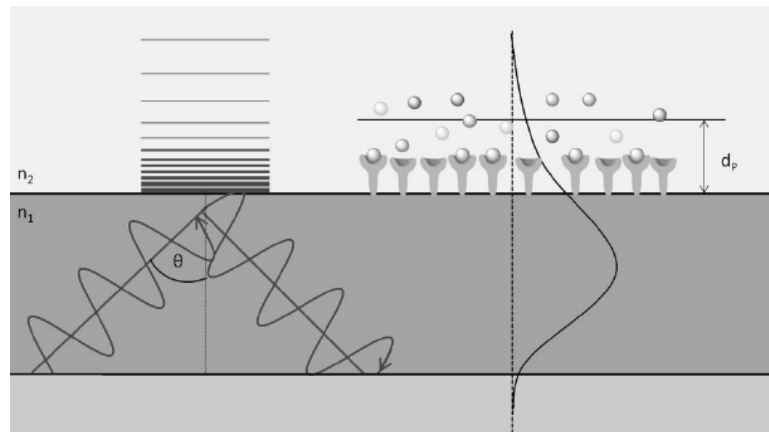*Figure 2.1. The schematic image of evanescent field-based sensing. Total internal reflection and the evanescent wave penetrating into the adjacent medium (n_2) with an exponentially decreasing intensity are represented. The interaction with (bio)molecules within the penetration depth (d_p) of the evanescent field may lead to absorption or to a change of the effective refractive index for the evanescently guided mode* [63]*.*

2.1.1. Optical waveguide lightmode spectroscopy

Optical waveguide lightmode spectroscopy (OWLS) is a very popular label-free sensing method, where a dielectric waveguide layer forms the surface of the sensor chip (Fig. 2.2). It is based on the sensitive monitoring of refractive index changes near the surface, when the observed analytes (bacteria, proteins, cells etc.) are adsorbing onto the surface.

In the OWLS sensor chip there is a shallow surface grating in the planar waveguide, in order to excite the guided modes. The plane-polarized measuring light from the source (e.g., He-Ne laser) is diffracted from the grating and via total internal reflections it can propagate in the waveguide. At certain angles the numerous successive internal reflections will interfere and excite a guided mode. The light exits from the layer and is detected by photodiodes, placed next to the sensor. The light can be incoupled only at certain angles of incidence, and these angles are conditioned by various circumstances, for example the wavelength of the illuminating beam, the grating constant of the sensor, or the refractive index inside the evanescent field above the grating.
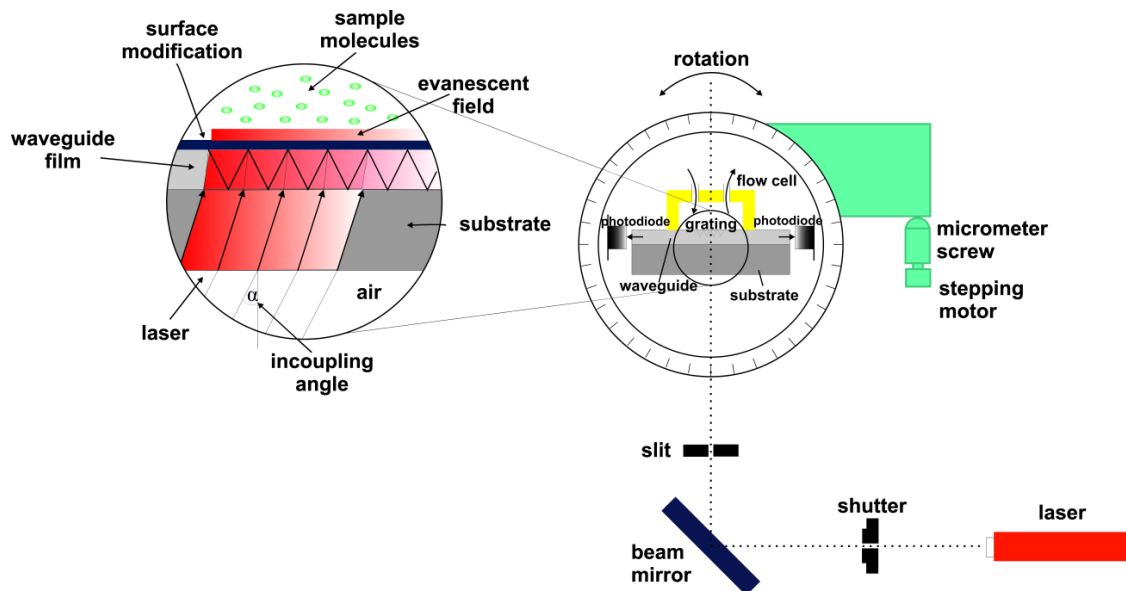

Figure 2.2. The schematic image of the measurement configuration of the optical waveguide lightmode spectroscopy [64]. *Due to refractive index changes near the surface the incoupling angles are shifted, from which the adsorbed mass density can be calculated.*

19

The changes of the refractive index in the evanescent field alter the conditions of the incoupling, which causes the change of the incoupling angles. During the measurement a high precision goniometer is rotating the sensor chip relative to the illuminating beam, and the incoupling angles can be determined from the positions of the sharp resonant peaks in the function of the measured light intensity and the angle of incidence. From the incoupling angles the effective refractive index and accordingly the adsorbed mass density of the studied objects (e.g. proteins, cells, bacteria) can be calculated [64], [65] (see section 4.7, Eq. (3), Eq. (4), Eq. (5)).

The sensitivity of the OWLS can be as low as 10 pg/mm^2 in adsorbed mass density or 3.4×10^{-5} RIU in refractive index [66] and its typical temporal resolution is around 2-20 s [67]. The commercially available standard OWLS sensor chips has coatings made of SiO$_2$, TiO$_2$, Ta$_2$O$_5$, ITO, ZrO$_2$ or Al$_2$O$_3$ thin films, PTFE (polytetrafluoroethylene) or silicone thick films for passivation or APTES ((3-aminopropyl)-triethoxysilane) for silanization [68], but nanostructured sensor coatings are not available.

OWLS is widely used for studying surface processes *in situ*, especially in biological and medical fields, like the adsorption of proteins [69], living cells [70], [71] or bacteria [72] or it can be applied as immunosensor as well [73]. It is important to stress that optical waveguide-based sensors are now available in microtiter plate format (96, 384 wells) and successfully employed to monitor cell adhesion [74], [75], and cell signaling [76].

2.1.2. Surface plasmon resonance sensors

One of the most popular label-free optical biosensor is the surface plasmon resonance (SPR) sensor (Fig. 2.3). This method is based on the phenomenon, that when a conductor/dielectric material interface is illuminated by a light beam with specific wavelength in a specific angle, resonant oscillation of conduction band electrons occurs on the surface. Usually the exciting light is incoupled by a prism and undergoes total internal reflections from the interfaces of the conductor film, thus an evanescent field

will penetrate into the flow channel where the studied events (e.g. adsorption, capturing) are happening (see Fig. 2.3). The intensity of the detected light has minimum values at the angles and wavelengths where plasmon excitation happens, and from the changes of these parameters the mass of the adsorbed molecules can be calculated.

The sensitivity of the method is typically 10^{-5}–10^{-8} RIU [66], [77]. SPR can be employed as a separate technique for detecting molecular adsorption, like protein, DNA or polymer adsorption, [78], [79], or it can be combined with other techniques (e.g. Raman scattering [80], anodic stripping voltammetry [81], ellipsometry [82]) in order to enhance their sensitivity or provide complementary information.
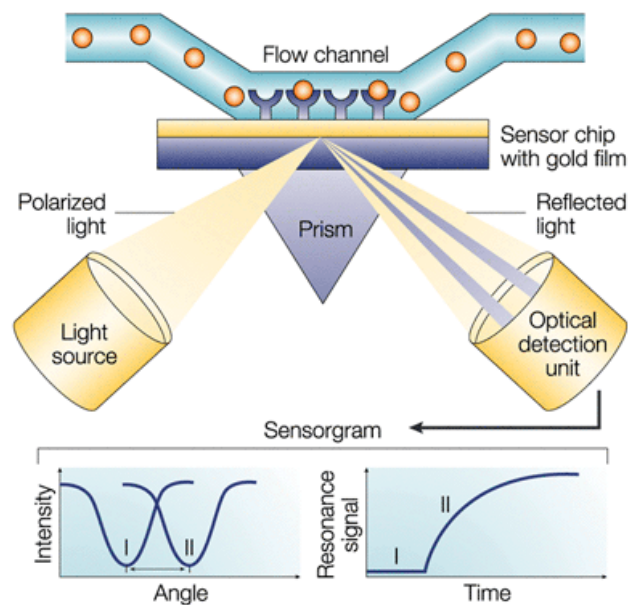
Figure 2.3. *A typical setup for a surface plasmon resonance biosensor* [83]. *The capturing of the target molecules on the sensor surface leads to changes of the angle of incident at which the plasmon enhancement happens.*

2.1.3. Grating coupled interferometry

One of the most sensitive label-free biosensors on the market is the grating coupled interferometer [84], [85]. The sensing method (Fig. 2.4) is based on a planar optical waveguide sensor chip with two incoupling and one outcoupling grating. With an

expanded beam the two incoupling gratings are illuminated simultaneously, but one half of the beam is phase-modulated by a laterally divided two-cell liquid crystal modulator, in order to obtain the interference signal. The incoupled measuring and reference light beams interfere, and the third grating leads out the interference signal through an optical fiber to the detector. The studied phenomenon (e.g. protein adsorption) happens on the sensing surface between the two incoupling gratings, and alters the refractive index of the material in the evanescent field, thus the phase of the measuring beam will change compared to the reference beam. The surface sensitivity of this method was demonstrated to be below 0.1 pg/mm^2 [85].

The GCI is ideal for measurements requiring high sensitivity and real time detection. A possible application can be in the field of fragment-based screening, where the interactions between receptors and very small (~100-200 Da) drug molecule fragments are investigated. The sensitivity of the GCI can be utilized for the detection of low concentration samples as well.
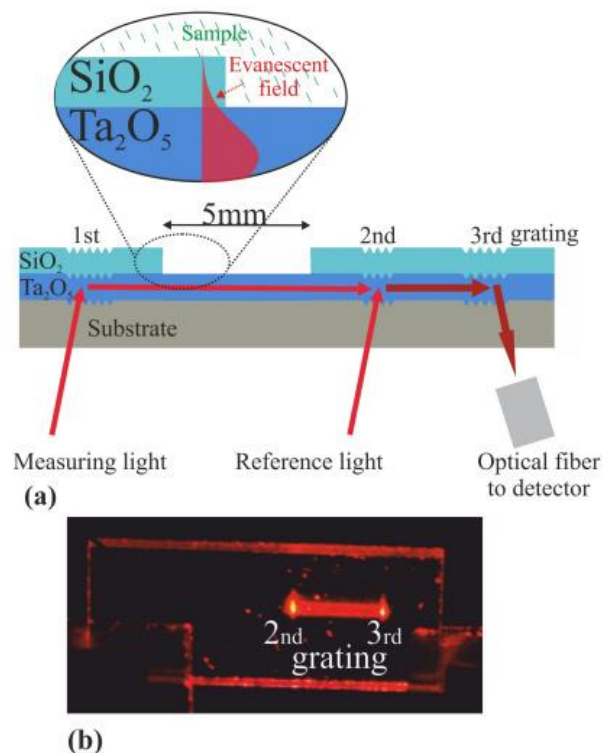

Figure 2.4. The working principle of the grating coupled interferometry (a) and the waveguide chip with the incoupled light between the second and the third gratings (b) [85].

2.1.4. Fiber-optic evanescent wave sensors

Evanescent waves can also be exploited in fiber-optic arrangements [86], [87], where a single optical fiber is applied as the sensor and also as the transmission line of optical signals. In an optical fiber a part of the light wave propagates in the core, but the 5-40% of the total propagating power penetrates out of the fiber as an evanescent wave [88].

Optical fibers can be combined with surface plasmon resonance [89], [90], where the fiber is coated with thin metallic layer(s), and plasmon waves can be excited on its surface by the evanescent wave of the guided fiber mode. Resolution of 7×10^{-7} RIU was achieved by a multiple-peak SPR fiber-optic sensor [91], and sensitivity of 3161 nm/RIU was accomplished by applying metal-ZnO bilayers [92]. Another method was developed for increasing the sensitivity by replacing the standard polymer optical fiber with a three-layer structure in the sensing region to increase the intensity and the penetration depth of the evanescent wave. The new structure resulted a 3.91-fold improvement in the detection of the target antibody relative to a conventional sensor, and a lower limit of detection of 0.2 ng/L [93]. Fiber-optic evanescent wave sensors were successfully applied for detecting oligonucleotides [94], [95], antibody [93] or gas [89].

2.2. Ellipsometric methods

Ellipsometry is also a non-destructive label-free method, based on the phenomenon that if a light beam is reflected from an interface between two materials with different refractive indices, the polarization state of the light changes [96], [97]. There are numerous types of ellipsometers, but the most popular ones are the rotating-polarizer, the rotating-analyzer and the rotating-compensator ellipsometers.

The basic ellipsometric configuration (Fig. 2.5) is made up of two co-planar optical arms with adjustable included angle between them, and the controlling and processing electronic elements. One of the optical arms contains the light source and the polarizer, the other contains the analyzer and the detector. The compensator (optional) can be placed behind a polarizer or in front of an analyzer and it is employed to convert linear polarization to circular polarization and vice versa. After getting through the polarizer

the light beam becomes linearly polarized in the plane, which is determined by the actual state of the polarizer. Then the light reaches the sample and is reflected in a different (usually elliptically) polarized state. After getting through the analyzer the light beam becomes linearly polarized again and enters the detector [96].
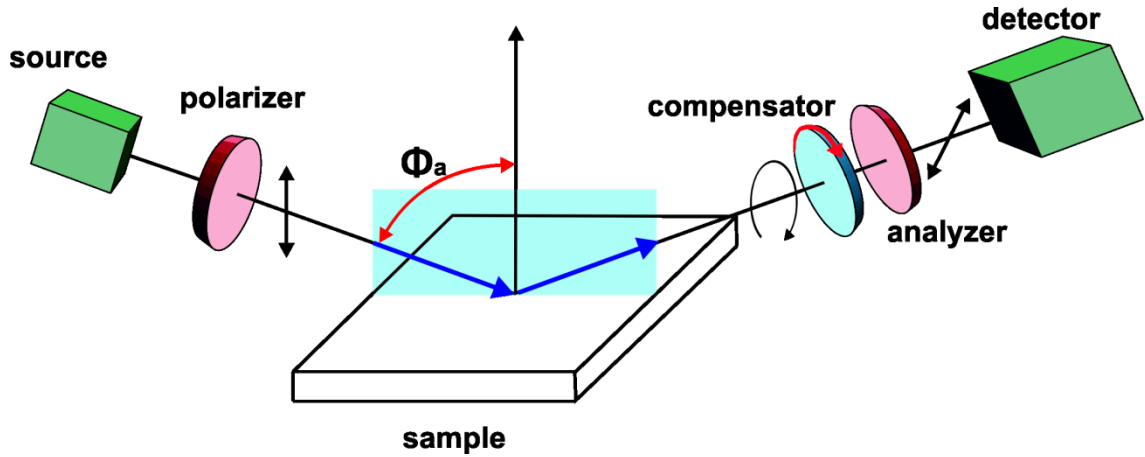
Figure 2.5. *Typical geometry of a rotating-compensator spectroscopic ellipsometry measurement with the indication of the angle of incident (Φ_a) and the polarization state of the measuring light beam [98].*

In the case of a rotating-compensator ellipsometer, due to the continuously rotating compensator the detected intensity signal will have a sinusoidal shape. It can be Fourier analyzed to determine the ellipsometric angles Δ and Ψ (Fig. 2.6) defined from the ratio of the amplitude reflection coefficients for p- and s-polarizations (Eq. (1)). Ψ and Δ represent the changes in the ratio of the amplitudes and phase-shift between the two perpendicular (p- and s-polarized) components of the light during the reflection from the sample, respectively.

$$\rho = \tan \Psi e^{i\Delta} = \frac{r_p}{r_s} \qquad \text{Eq. (1),}$$

where ρ is the complex reflection coefficient, Ψ and Δ are the amplitude ratio and the phase difference between p- and s-polarizations, respectively and r_p and r_s are the amplitude reflection coefficients for p- and s-polarizations, respectively.
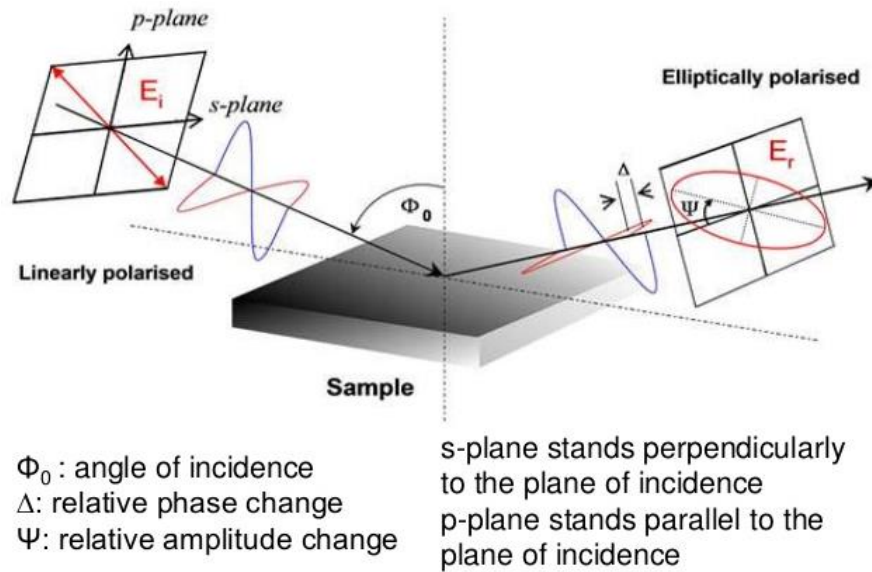
Figure 2.6. *The schematic image of the principle of ellipsometry, demonstrating the ellipsometric angles Ψ (relative phase change) and Δ (relative amplitude change)* [96].

Ellipsometry is an indirect method, which means that we can't measure directly the data which we are interested in, like refractive index, surface roughness or layer thickness. Instead, we must have some *a priori* knowledge about the structure of our sample, and have to set up an optical model based on that information (Fig. 2.7). Then the parameters of the optical model are varied (fitted) in order to make the experimental and calculated spectra overlap, which leads to the capability of reconstructing complex material systems, such as depth profiles [99], semiconductors [100], or three-dimensional protein structures [101].
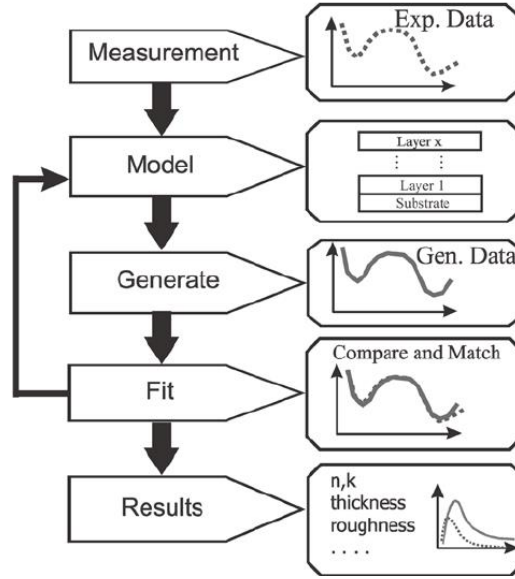
Figure 2.7. The process of the ellipsometric data evaluation [102]. Using regression analysis, the hypothetic model is adjusted to find the requested parameters (e.g. optical constant, layer thickness) that generate data curves that best match the measured spectra.

The quality of the fit of the required parameters in the data evaluation can be determined by calculating the mean squared error (MSE) by the following equation:

$$\text{MSE} = \sqrt{\frac{1}{N-P-1}\sum_{i=1}^{N}\left[\frac{(\Delta_i^M - \Delta_i^C)^2}{\sigma_{\Psi_i}^M} + \frac{(\Psi_i^M - \Psi_i^C)^2}{\sigma_{\Delta_i}^M}\right]} \qquad \text{Eq. (2),}$$

where N is the total number of data points taken, P is the number of unknown (fitted) parameters, Ψ and Δ corresponding to the amplitude and phase change during reflection of polarized light from the sample surface, respectively. Superscripts M and C signify "measured" and "calculated" data, respectively. If the MSE is around 1, the fit has a good quality. For more samples with more layers and complex structure, MSE values below 10 are acceptable.

The history of ellipsometry began in 1945, when the word 'ellipsometer' was first used by Rothen, who applied the device to determine the thickness of barium stearate thin films deposited on metal slides [103]. Soon he used the ellipsometer for biological purposes; he studied films of antigens and antibodies on polished metal surfaces with a

26

sensitivity of ~0.3 Å [104], [105]. The following steps were the thickness measurement of unhydrated protein layers [106], and the development of the recording ellipsometer [107] and its combination with a cuvette, which makes possible to follow and record reactions (both adsorption and desorption) at solid-liquid interfaces continuously while the substrate is immersed in solution. It was employed for studying enzyme reactions, where proteins were applied as the solid substrate [108], [109]. With a similar recording ellipsometer blood clotting on tantalum-sputtered glass substrates was also studied [110].

In the middle of the 1970s the first spectroscopic ellipsometer was developed, which applied a spectral range from the near infrared to the near ultraviolet range [111]. Some years later an automated ellipsometer was introduced with unique properties of speed (1 measurement/2-3 s) and sensitivity (5 Å), making possible to follow biochemical reactions (e.g. protein adsorption, protein–protein interaction) at interphases with a high degree of accuracy [112]. The first ellipsometric studies related to the human body were the thickness measurements of the skin exposed to sunshine, and the investigation of the effectiveness of cosmetic products [113]. From the 1980s the biological studies carried out by spectroscopic ellipsometry became more and more popular. Adsorption kinetics and optical properties of various protein layers on different surfaces [114]–[117] were studied applying such devices. It was followed by the development of imaging ellipsometry, which can be applied for the quantification and the three-dimensional visualization of the lateral thickness distribution of transparent thin films on solid substrates with high layer thickness sensitivity (0.5 nm), high lateral resolution (5 μm) and high sampling speed (less than 1 s) [118].

In the same time the improvement of the surface plasmon resonance enhanced ellipsometry (also known as total internal reflection ellipsometry) also took place [119], [120]. A very good sensitivity can be achieved, if the conditions are appropriate for total internal reflection and surface plasmon effects are generated by employed thin metal films [121]–[123]. The advantages of this method can be exploited in many fields, such as in the characterization of fragmented antibody layers and estimating the orientation of antibody active sites from the experimental data [124], the detection of hazardous gas [125], [126] or low molecular weight environmental toxins, like simazine, atrazine and T2 mycotoxin [127], furthermore it can be combined with imaging ellipsometry [128].

Although, the first ellipsometric studies of cellular microexudates (also called cell coat materials) of different tissue cultured cells were published already in 1960 [129], [130], the first ellipsometric experiments with living cells were only performed a half century later. A surface plasmon resonance imaging ellipsometer was applied for studying adhesion properties and dynamics, cell-substrate and cell-cell interaction of different cell types [131]. Recently, the optical properties of mouse myoblast cells with different population densities were studied using spectroscopic ellipsometry [132].

In certain cases, it is beneficial to combine ellipsometry with other methods in order to get additional information about the studied object or phenomena. Two examples of these combinations and some examples for their applications are introduced below. The combination of ellipsometry and quartz crystal microbalance (QCM) is one of the oldest and most popular methods. The combination with grating coupled interferometry (GCI) is a very recent development, and its improvement is still in progress in our institute.

Quartz crystal microbalance enables label-free mass detection, based on measuring the frequency of a piezoelectric quartz crystal oscillator (Fig. 2.8). Due to small mass changes on the surface of the wafer the resonant frequency of the quartz is being altered, from which the surface mass density can be calculated. It is widely used as biosensor [133], it can be applied for studying living cells [134], aptamer-protein interactions [135], or for nucleic acid hybridization assays [136], [137].
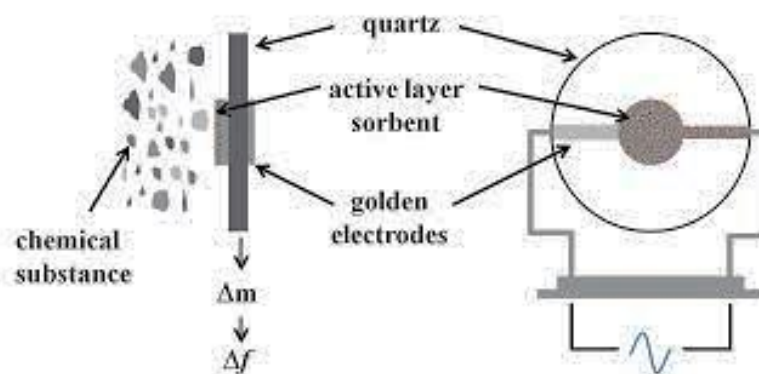

Figure 2.8. *The working principle of the quartz crystal microbalance* [138]. *The change in the mass (Δm) due to the adsorption of the monitored substance causes the change in the resonant frequency (Δf).*

The first study in which ellipsometry and a quartz crystal microbalance were applied simultaneously was published in 1990. The complementary information received from the combination of the methods was used for the determination of the apparent density of the growing polyaniline thin film on an electrode surface sputtered onto the quartz crystal [139].

The buildup of polyelectrolyte multilayers was studied *in situ* with the combination of spectroscopic ellipsometry and quartz crystal microbalance with dissipation monitoring (QCM-D) in a single device. From the measured parameters the hydration of the polyelectrolyte multilayers could be calculated layer by layer [140]. *In situ* generalized ellipsometry combined with a similar QCM-D was applied for studying the deposition of engineered titanium dioxide nanoparticles on three-dimensional nanostructured slanted columnar thin films with controlled roughness [141].

GCI (see section 2.1.3) can also be combined in a single device with the spectroscopic ellipsometer, in order to exploit the high sensitivity of GCI and the spectroscopic capabilities of ellipsometry. Fibrinogen adsorption and layer-by-layer deposition of polyelectrolytes were studied so as to demonstrate the advantages of the combined device [142].

2.3. Surface micro- and nanostructuring

Micro- and nanostructured materials and surfaces got in the center of interest because of the remarkable novel properties (optical, catalytic, electronic, magnetic, ferroelectric or mechanical), which appear when the characteristic size of the material is reduced significantly [143]. In the 1960s the application of the first lasers [144] enabled the micropatterning of semiconductor surfaces with a characteristic size of around 2 μm [145]. Later the development of various lithographic, deposition and surface modifying technologies induced the improvements in micro- and nanostructuring, such as achieving smaller and more controllable characteristic sizes [146], [147], higher aspect ratios [148], [149] or special surface properties [150], [151].

The behavior of different biomolecules on micro- or nanostructured surfaces started to be widely studied in the last decades, as novel biosensing techniques, medical implants

and biocompatibility, antibacterial and antifouling coatings are of great interest.The investigation of protein adsorption on a coating is essential in the field of implants, because the implant integration always begins with protein adsorption, cell adhesion happens subsequently. Hence the adsorption of proteins is a significant factor in determining the biocompatibility of a material [152].

Enhancing the protein adsorption can be beneficial in surface sensitive methods to increase the sensitivity of the biosensing device or on biomaterials to be implanted, in order to enhance advantageous cell adhesion and tissue responses. Some studies examined that beyond the increased surface area the microtopography [153] and nanotopography [154]–[157] of surfaces with the same chemical composition are also able to enhance the adsorption of proteins. Protein desorption promoting surfaces were also constructed by creating nano-scale superhydrophobic surfaces, which can be applied in microfluidic devices, where protein adsorption on the walls can cause problems [158]. In another study natural lotus leaves were applied as templates in replica molding in order to enhance the protein resistance and cell adhesion suppression of their antifouling coatings [159].

Since the failure of implants and prosthetic devices are often caused by bacterial infection, bacterial behavior is widely investigated on structured or patterned surfaces by various research groups. The morphological, genetic, and proteomic properties of adherent *Escherichia coli* bacteria were demonstrated to be altered by the different nanoroughness values of glass and gold surfaces [160]. The adhesion of *Staphylococcus aureus* and *Escherichia coli* was also studied on nanostructured silicon wafers with systematically varied, ordered surface topographies [161]. The same bacteria species were investigated on titania thin films with controlled and reproducible nanostructures. The results revealed that bacterial adhesion and biofilm formation was affected by the nanoroughness in a non-monotonous way: the highest cell adhesion rate was observed on the surface with a roughness of 20 nm, and in the cases of smaller and greater roughness values the number of bacteria decreased [162].

In the case of studying the behavior of living cells an important role can be attributed to the surface topography. Intrinsically cell-repulsive hydrogels were turned into adhesion- and spreading-supportive surface for fibroblast cells by linear micropatterning in the presence of proteins [163]. Nanostructured platforms were fabricated from silicon by a

novel laser approach, and their functionalities were investigated using cervical cancer cells. The experiments revealed that the cancer cells couldn't attach to the nanostructured patterns and started to migrate to untreated, flat areas [164]. Increased fibroblast response was observed on nanostructured polymer demixing of polystyrene and polybromostyrene compared to the flat surface. The cells showed gene up-regulation in the areas of cell signaling, proliferation, cytoskeleton, and production of extracellular matrix proteins [165].

Since titanium is very stable but light in weight, non-toxic material and it is not rejected by the body, it is widely used as dental or medical implants since the 1950s [166]–[168]. Therefore it is very important to emphasize the results of the studies about living cells on titanium- or titanium-oxide-based surfaces. There were (and still are) numerous *in vivo* animal experiments for testing titanium and titanium alloy implants, in order to reveal their physiological effects on the tissues [169]–[172].

From the 1970s the porous and the micro- or nanostructured titanium surfaces became popular biological and medical topics, and the greater part of the studies concluded consistently that structuring and increased roughness enhance the osseointegration and the bone regeneration [173]–[175]. *In vitro* studies also contributed to the better knowledge of how structured, rough surfaces affect the behavior of living cells, with special emphasis of osteoblasts and osteoblast-like cells. Numerous reviews were prepared about these topics [176]–[180], which concluded that surface topography has a great impact on the adhesion, proliferation, migration and other properties of living cells, however more detailed studies are needed to determine the correspondences between topography and cell behavior in a more exact way. Some examples of the most important studies are introduced below.

Different sizes (submicron to nanometer) of surface features and aligned patterns on titanium thin films were investigated and compared to flat titanium surfaces. The structuring was proved to be advantageous for cell adhesion for both endothelial and bone cells [181]. Micron and submicron structures were produced on titanium surfaces applying anodic oxidation and SaOS-2 human osteoblast-like cells were seeded on the surfaces. Enhanced cell adhesion and spreading were observed on the structured surfaces, and the results were explained by the phenomena, that porous structures can act as positive attachment sites for the filopodia of anchorage-dependent cells [182].

Fibroblast cells were studied on polished Ti-6Al-4V titanium alloy surfaces with 6 different average roughness values between 2.75–30.34 nm, and it was demonstrated that the roughness had a significant influence on the adhesion, proliferation and morphology of the cells [183]. Titanium substrates with rough and grooved surfaces were compared by culturing primary osteoblast-like cells on their surfaces. The grooved surface was demonstrated to enhance the cell attachment and proliferation compared to the rough surface [184]. Nanotubular titania surfaces were fabricated by a simple anodization process. *In vitro* measurements with marrow stromal cells and *in vivo* experiments with Lewis rats showed that the nanotubular surfaces enhanced the cell adhesion, proliferation and viability and did not cause adverse immune response [185].

3. Motivation and aims

In the first part of my work my aim is to prepare coatings from novel, additive-free titanate nanotubes on sensor chips, that are compatible with optical waveguide lightmode spectroscopic (OWLS) measurements and to apply them for various biosensing experiments. For the film fabrication I'm going to use the very simple and fast spin coating method. The nanostructured films have to be homogeneous and dense, but not too thick, because it could decrease the quality of the measurements. The required thickness would be between 5-15 nm, at which it is expected to well cover the surface, but doesn't increase the optical thickness significantly.

I plan to characterize the micrometer-scale homogeneity of the coating with atomic force microscopy, and the millimeter-scale homogeneity and the film thickness with spectroscopic ellipsometry. The changes in the light guiding capabilities of the coated OWLS chip will be studied with the OWLS itself, by comparing the incoupling resonant peaks of the coated and uncoated sensor chips.

After the proper coating procedure is found, I would like to carry out protein adsorption and living cell adhesion measurements with the OWLS to study the effect of the coating. For the protein adsorption measurements I'm going to use bovine serum albumin and for the cell adhesion experiments I'm going to use human embryonic kidney cells and preosteoblasts. I also plan to incubate the living cells on coated and uncoated substrates for a longer time, and to monitor them with inverted microscopy and examine the effect of the coating on the behavior of the cells. I also would like to monitor these living cells on the nanostructured TNT coatings by a new digital holographic microscope, HoloMonitor M4. Therefore I plan to develop a new cuvette configuration that enables the long-term monitoring of living cells on spin-coated surfaces by the HoloMonitor.

In the second part of my work I'm going to take part in the development and the application of a new flow cell which can be instantly employed with the commercially available spectroscopic ellipsometers. This novel ellipsometric configuration can incorporate many advantageous properties of other conventional configurations, such as multiple angle of incidence, low sample consumption, *in situ* measurement, plasmon

enhancement and time-sharing two-channel monitoring. For the two-channel measurement, I intend to find a method to prepare substrates partially coated with titania nanoparticles. The untouched part of the gold surface can serve as the control in the measurements.

With the new configuration, at first I would study the layer deposition of polyelectrolytes on the nanostructured coating and on the uncoated surface. Afterwards I plan to carry out similar two-channel measurements with fibrinogen protein and preosteoblast cells and to reveal the effects of the coating on protein adsorption and cell adhesion.

4. Materials and methods

In this section I describe the methods and the materials that I applied in my experimental work, and give the types and operational details of the instruments I used. First I introduce two techniques for characterizing the size distribution and refractive index of the sample solutions, then I specify the processes of substrate cleaning and coating. Later I give the details of solution preparation procedures for the different experiments, and I describe the applied microscopic methods. Finally I introduce the devices and calculation methods applied in the adsorption measurements.

4.1. Applied methods for the characterization of the solutions

4.1.1. Particle size distribution

Characterization of TNPs in ethanolic solution was carried out using dynamic light scattering (DLS) (Fig. 4.1) using a Malvern ZetaSizer NanoZS device. In the DLS measurements disposable plastic cuvettes with 500 μL solution were used. Three measurement cycles were carried out, and each cycle consisted of 10 measurements. The wavelength of the laser in our instrument was 632.8 nm, and the data were collected at 20 °C.

DLS measurements are suitable for determining particle size distribution, molecular weight or zeta potential (electrokinetic potential in colloidal dispersions) for nanoparticles and colloid systems. When small particles are irradiated by a light with wavelength that is comparable to the particle size, the light scatters in all directions. The particles are undergoing Brownian motions and the distance between them is changing constantly, so the scattering intensity fluctuates over time. By analyzing these intensity fluctuations, the size of the particles can be concluded.
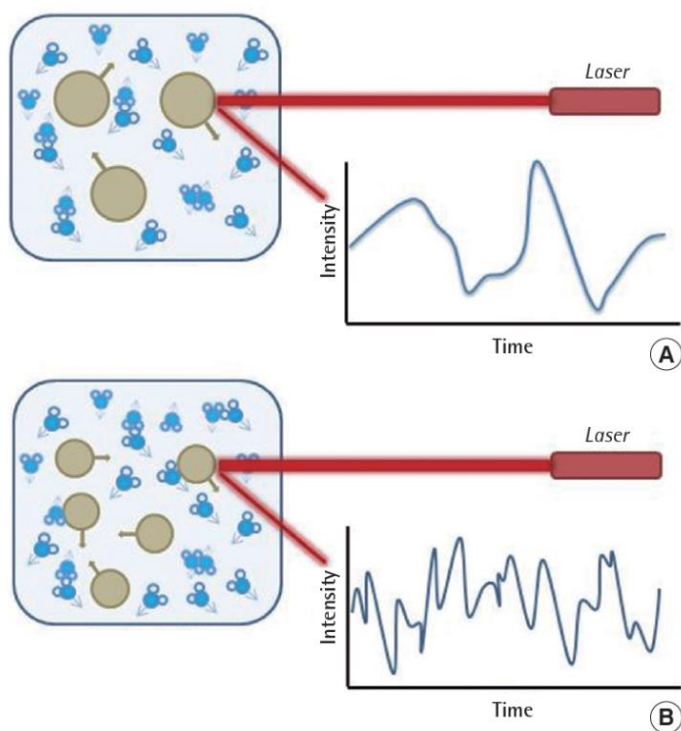
Figure 4.1. The schematic image of the theory of dynamic light scattering measurements with **(a)** larger and **(b)** smaller particles. Larger particles generates higher scattering intensity than smaller particles [186].

4.1.2. Refractive index determination

The refractive indices of the buffer and protein solutions were determined by a full automatic Rudolph J157 refractometer in order to use them in the evaluation process of the OWLS and ellipsometric measurements. The refractive index measurements were carried out at 20 °C and the wavelength of the measuring laser light was 632.8 nm.

The theory of operation of this device is based on that the direction of propagation of the light changes when the light beam passes through a boundary between two different materials with different refractive indices (Fig. 4.2). A light beam from a point source enters a prism with high refractive index, and bends when reaching the sample. Above a certain "critical" angle the bending becomes so great, that total reflection is occurred, so the light is actually reflected from the sample and through the prism it can reach the diode array detector. The transition from light to dark is detected and the refractive index can be calculated from that.
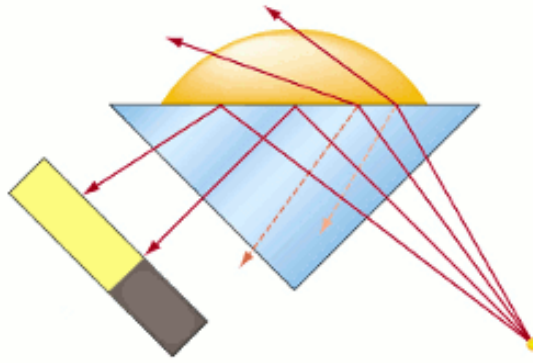
Figure 4.2. *The working principle of the refractometer* [187]. *Above the critical angle the light is reflected from the interface and enters the detector.*

4.2. Substrate preparation processes

I applied spin coating method (Fig. 4.6) for fabricating nanostructured coatings from sols containing titanate ($H_2Ti_2O_5 \times H_2O$) nanotubes [188] or titania (TiO_2) nanoparticles. It is a reliable and reproducible method for rapid deposition of thin coatings on flat substrates [189], [190]. The substrate to be coated is held on a rotatable disc by vacuum, and before or during the spinning, the coating solution is dispensed onto the substrate surface. Due to the rotation the solution is spread out and generates the coating of the chosen material.
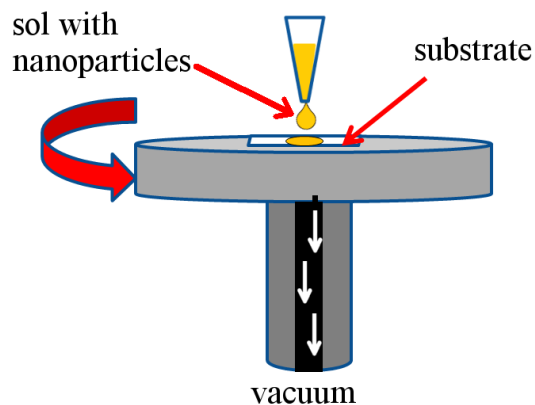

Figure 4.6. *Schematic image of the spin coating procedure. The substrate is fixed on a rotatable disc and due to the spinning a uniform coating is composed from the dispensed solution.*

4.2.1. Titanate nanotubes

The titanate nanotubes (TNTs) were synthetized using a previously reported protocol by László Kőrösi and his coworkers [188], our group received the ready-to-use TNT sols from them. These open ended nanoparticles have a diameter of 4-7 nm, and their length is around a few hundred nanometers (Fig. 4.7).
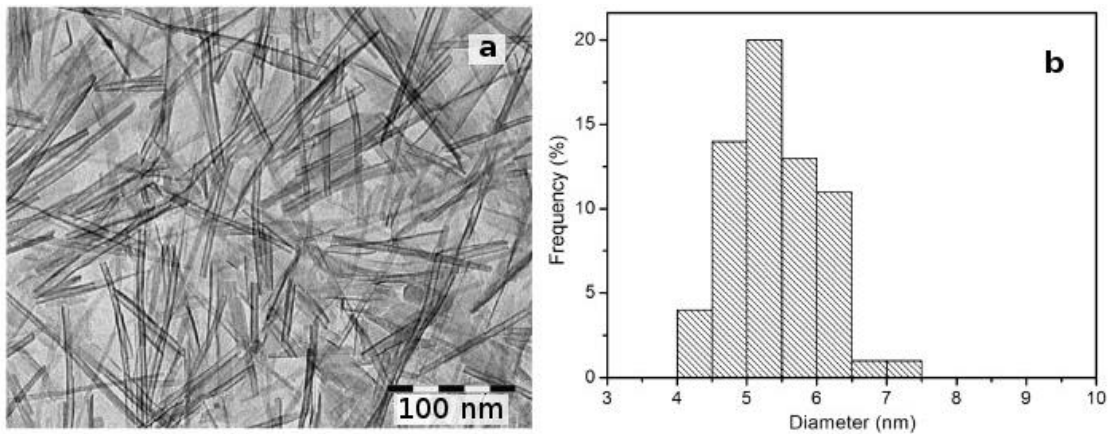

Figure 4.7. *Transmission electron microscopic image of the titanate nanotubes (a) and the distribution of the diameter of the nanotubes (b)* [188].

I prepared the TNT coatings on three different substrates: on OW2400 (Microvacuum Ltd.) $Si_{0.6}Ti_{0.4}O_2$ optical chips for the OWLS measurements, on 1×1 cm pieces of silicon (1,0,0) substrates (covered by 3 nm thick native oxide) for the ellipsometric characterization and on microscope slides (MENZEL-GLÄSER, 1 mm thick, Thermo Scientific) for the AFM characterization.

The optical chips consist of a 0.5 mm glass substrate (n=1.53) and a ~200 nm waveguide layer with high refractive index (n=1.77). The incoupling of the laser beam into the waveguide layer is provided by a grating with 20 nm depth and 0.4166 µm periodicity. Before preparing the nanotube coatings on the optical chips, they were steeped in chromic acid (Merck) for 3 min, in ultrapure milli-Q water (MQ) for 2 s, in 0.5 M KOH solution (Merck, analytical grade) for 10 s and in MQ again. At last, the chips were sonicated in MQ water with an S 15 H Elma sonicator for about 30 min. The water was exchanged to fresh MQ water in every 3 minutes.

The Si plates were cleaned with hot 'Piranha solution' (a 3:1 mixture of 95% H_2SO_4 (AnalaR NORMAPUR® ACS) and 30% H_2O_2 (Scharlab EMSURE® ACS)) for 15 min and subsequently profusely rinsed with MQ water.

The glass plates were steeped in Cobas Integra cleaner solution (300 mM HCl, 1% detergent, Roche Diagnostics) and were sonicated for 15 minutes, then in water for another 15 minutes. Subsequently they were exposed to an O_2 plasma (Plasma Prep II, Structure Probe Inc.) for 5 min.

The fast and simple spin coating procedure was carried out at room temperature on the three substrates, using a Convac St 450 spin coater. The spinning time was 20 s, the spinning speed was 3000 rpm and the volume of the dropped sol was 50 μL. After the substrates were drying for some minutes at room temperature, the highly transparent nanostructured coatings were ready to use.

4.2.2. Titania nanoparticles

The synthesis of titania nanoparticles (TNPs) and the sol preparation was also performed by László Kőrösi and his group, but so far no SEM or TEM images were taken of these nanoparticles. The preparation process was mostly similar to that described previously [188], [191], [192], except that in this procedure neither doping agents nor solvothermal treatment were applied. 50 mL of 2-propanol and 100 mL of distilled water was added to 13.3 mL of $TiCl_4$, then 250 mL of 1.5 M NaOH solution was added dropwise to the solution during dynamic stirring. The emerging white precipitate was copiously washed with water and ethanol. Afterwards, dispersing ultrasonically the precipitate in ethanol, a stable dispersion of TNPs was formed. To obtain monodisperse nanoparticle mixture, the ethanolic dispersion was centrifuged at 12 000 rpm (13 225 × g) for 30 min, and then the separated supernatant with a solid content of 0.45 w/v% was used for the spin coating process.

I determined the size distribution of the TNPs in the ethanolic solution using Zetasizer Nano Zs (Malvern Instruments). The average size of the nanoparticles was found to be 11.34±1.97 nm.

The TNP coatings were applied in the *in situ* ellipsometric adsorption measurements, so I prepared them on specific substrates required by the ellipsometric configuration. The substrates were consisting of three layers: a cover glass, a 2 nm thick Cr_2O_3 layer, and a 20 or 30 nm Au layer. Cover glass slides coated with Cr_2O_3 and gold thin film by e-beam evaporation were purchased from Optilab Ltd., Hungary. Prior to the spin coating of the TNPs, the substrates were rinsed with MQ water, then steeped in methanol (VWR Chemicals) and acetone (VWR Chemicals) for 10 s each. The substrates were dried with nitrogen gas between and after the cleaning steps.

The parameters of the spin coating procedure were the same as described for the TNT coatings, but additional steps were needed to create partially coated substrates for the multichannel *in situ* ellipsometric measurements. First I wrapped one half of the sample surface with a specific stick-on foil (Wafer Tape SWT 10+R) before spin coating the TNPs on it. The spinning time, the spinning speed and the volume of the dropped sol were the same as in the previous procedures. The spin coating was followed by the removal of the foil with the TNPs on it, thus half of the substrate surface remained clean and uncoated.

It was verified by the ellipsometric measurements performed on the uncoated part of the surface before and after the application of the foil. Several samples were measured before and after the foil application and the spectra within the wavelength range of 400-1700 nm were compared (Fig. 4.8). The average difference between the 'before foil' and 'after foil' states was 0.08° for Ψ and 0.34° for Δ, which is equivalent to ca. 0.2 nm change in roughness, which can be considered negligible and can also be the result of the poor reproduction of the measuring position on the substrate.
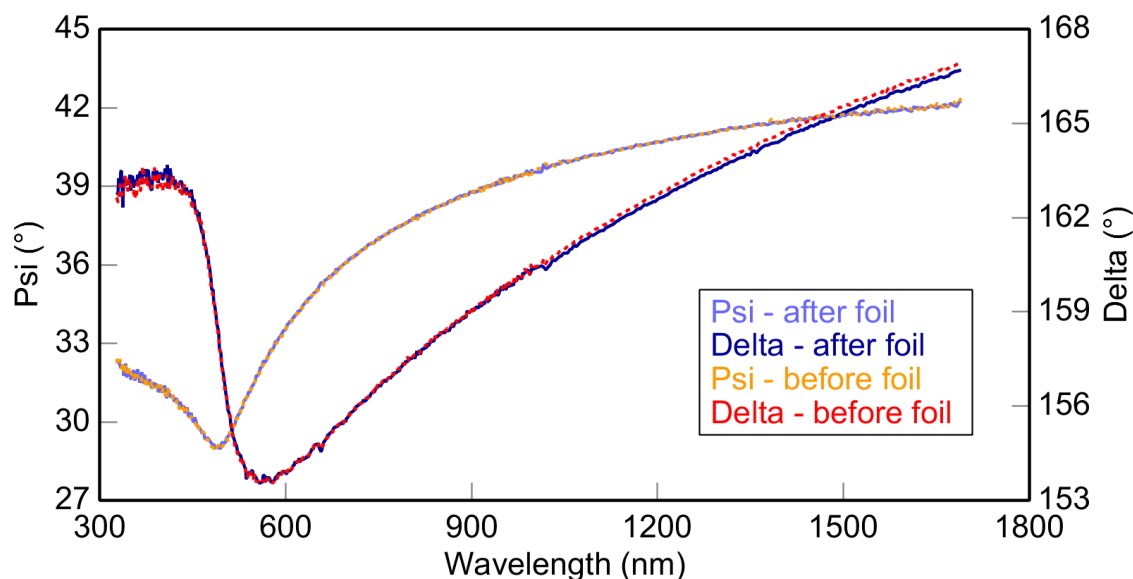
Figure 4.8. *Typical ellipsometric spectra of the substrate (coated by a 10 nm thick gold layer) before and after the application of the stick-on foil on the surface, recorded at an incidence angle of 70°.*

4.3. Sample solutions in the OWLS measurements

For the protein and cell sample solutions, 10 mM phosphate buffer with pH 7.4 was prepared from phosphate-buffered saline (PBS) tablets (Sigma–Aldrich). One of the tablets was dissolved in 200 mL MQ water and the solution was sonicated until dissolved (10-15 min).

Bovine serum albumin (BSA) solution with a concentration of 1 mM was prepared from powder (Sigma–Aldrich) dissolved in 10 mM PBS at room temperature. Human embryonic kidney (HEK293) and preosteoblast (MC 3T3-E1) cells were cultured in incubator (37 °C, 5% CO_2, 20% O_2) in Dulbecco's modified Eagle's medium (DMEM) and alpha-MEM respectively, both supplemented with 10% fetal bovine serum (FBS), 4 mM L-glutamine, 40 g m/L gentamycin and 0.25 g m/L amphotericin. Both types of the cells were trypsinized with 1.0% trypsin–EDTA warmed to 37 °C. Trypsin was removed before the cells detached completely. The activity of the trypsin was blocked by adding culture medium containing 10% FBS. Harvested cells were centrifuged at 380 × g for 7 min and the cell pellet was resuspended in assay buffer with intensive but gentle pipetting.

41

4.4. Sample solutions in the in situ ellipsometric measurements

4.4.1. Polyelectrolyte adsorption measurements

For the polyelectrolyte adsorption measurements 0.5 mM Poly(allylamine hydro-chloride) (PAH) solution was prepared from powder (Alfa Aesar), and 0.5 mM Poly(styrene sulfonate) (PSS) was prepared from powder (Sigma-Aldrich) dissolved in MQ water. The pH of both solutions was adjusted to pH 4 and pH 8 with HCl (VWR Chemicals) and NaOH (VWR Chemicals) solutions, respectively. The pH of the solutions was measured using Hydrion MicroFine pH test paper set (Sigma-Aldrich.)

4.4.2. Protein adsorption and cell adhesion measurements

For preparing the protein solution, fibrinogen powder (Sigma–Aldrich) was dissolved in 10 mM PBS (see section 4.3) at room temperature. The fibrinogen concentration of the solution was 1 mM.

For preparing the cell sample, preosteoblast (MC3T3-E1) cells were cultured in an incubator (37 °C, 5% CO_2) in Minimum Essential Medium (MEM) Alpha Medium, supplemented with 10% fetal bovine serum (FBS), 2 mM L-glutamine, 100 U/mL penicillin, 100 µg/mL streptomycin solution and 0.25 µg/mL amphotericin. The cells were trypsinized with 0.05% (w/v) trypsin, 0.02% (w/v) ethylenediaminetetraacetic acid (EDTA) warmed to 37 °C. Trypsin was removed before the cells detached completely. Afterwards the cells were taken up in Hank's Balanced Salt Solution (HBSS) containing 20 mM 4-(2-Hydroxyethyl)piperazine-1-ethanesulfonic acid (HEPES) buffer (pH 7.0). The preosteoblasts were seeded onto the uncoated and the TNP-coated surfaces, and were left (still surrounded by the buffer) for 1 h at room temperature to adhere before I started the ellipsometric measurement.

4.5. Applied microscopic methods

4.5.1. Atomic force microscopy

The topography of the transparent nanoparticle coatings was studied by AFM (Aist-NT, DigiScope1000) in tapping mode with MikroMasch SPM probes with a tip radius of 8 nm and resonance frequency of 325 kHz. The AFM images were processed using the data leveling, background subtraction and false color mapping operations of Gwyddion 2.37 software [193].

Atomic force microscope (AFM) (Fig. 4.3) is developed from scanning tunneling microscopes in order to enable the investigation of the surface of non-conducting materials [194]. This microscope operates by measuring very small forces (10^{-18} N) between a probe and the sample. Usually the probe is a sharp tip attached to a cantilever. During scanning over the surface the vertical and lateral deflections of the cantilever are caused by the close-range, attractive and repulsive forces between the tip and the surface. The deflections are measured by reflecting an incident laser beam from the cantilever to a position-sensitive photodetector. If the direction of the reflected beam is changed due to surface rugosity, it can be recorded by the four-segment photodetector. The vertical resolution of a modern AFM can reach 0.1 nm, the best lateral resolution is around 0.4 nm, [195] so even atomic resolution could be achieved [196].

By now AFM has become a routine technique and it is often applied for the fast mapping of surface topographies and for nanopatterning [197].
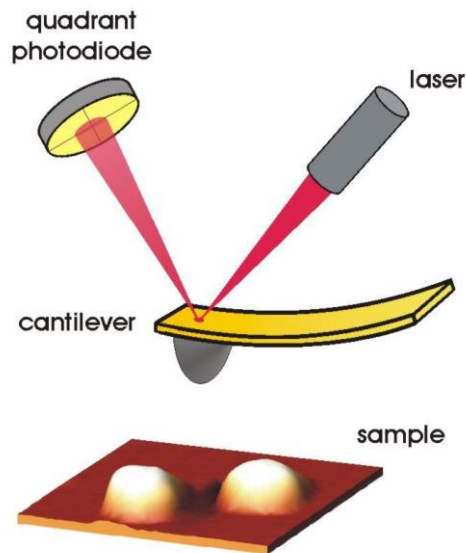
Figure 4.3. *Schematic image of the atomic force microscope* [198]. *During the surface scanning with the sharp tip, the cantilever deflections cause the changes of the direction of the reflected laser beam.*

4.5.2. Digital holographic microscopy

For the three-dimensional visualization of preosteoblast cells adhered on the nanostructured TNT coating, an incubator adapted holographic microscope, the HoloMonitor M4 was applied (Phase Holographic Imaging PHI AB, Lund, Sweden). During the imaging process, the cells and the HoloMonitor were placed in a Panasonic MCO-5AC-PE incubator, at 37 °C in a humidified atmosphere at 5% CO_2 in air.

This technique is a modern, label-free and non-invasive imaging method, primarily used for three-dimensional time-lapse visualization and both quantitative and qualitative investigation of living cells [199]–[201]. It is based on that a laser beam is split into a sample and a reference beam, and only the sample beam goes through the sample (Fig. 4.4) experiencing a given phase-shift compared to the other beam. Afterwards, the two beams are rejoined to create an interference pattern, the hologram. In digital holography this resulted pattern is recorded digitally, and the real image is calculated by the computer. The main advantage of this recently developed device [202] is, that as it is compatible with incubators, the real-time and long-term monitoring of living cells is possible at controlled temperature and gas composition.
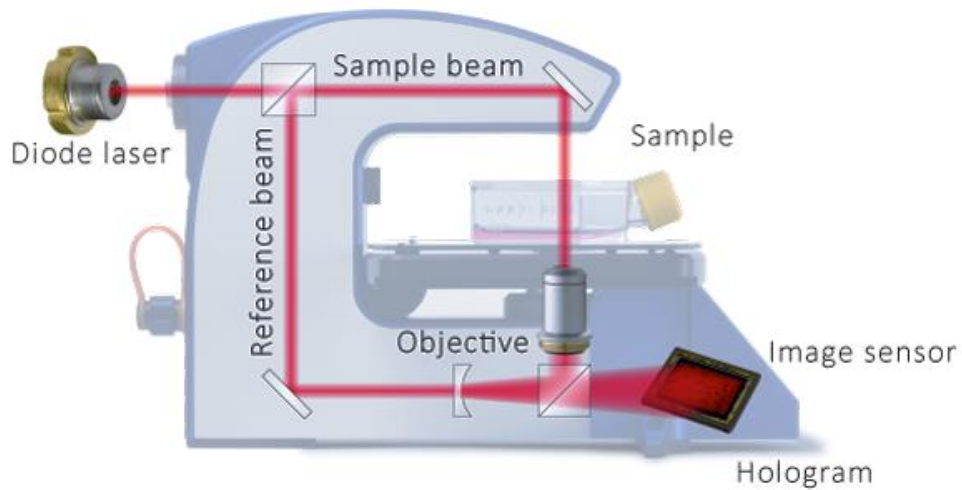
Figure 4.4. *Schematic image illustrating the working principle of the phase holographic microscope* [203]. *The measuring light is divided into two beams, a sample beam and a reference beam by a beam splitter. After the sample is illuminated by the sample beam, the two beams are combined to create the holographic image.*

4.5.3. Phase contrast microscopy

The phase contrast microscopic images of the living cells were taken using an inverted Zeiss Axio Observer A1 microscope.

There are structures, called 'amplitude objects' which can change the amplitude of scattered light directly by absorption and can be observed applying simple bright field microscopy. However small objects without dyes and pigments (e.g. cells) hardly change the amplitude of the light, therefore they can't be seen well using a bright field microscope. The refractive indices of certain parts of the cells, such as the cell membrane or the organelles, are slightly differ from the surrounding medium, thus the phase of the light changes when passing through these structures.

Phase contrast microscopy (Fig. 4.5) is based on translating this phase shift to an amplitude difference. The light first goes through the condenser annulus and then passes through the specimen. The direct light which is not deviated by the object goes through the phase-altering pattern of the phase plate which modifies the wavelength. Those rays that pass through the object structures with different refractive index are deviated, and

45

cross the part the phase-plate that is not covered by the phase altering pattern, therefore the wavelength remains the same as for the incident light. Eventually the difference of the wavelengths will improve the contrast of the image and makes the object clearly visible.

For the invention of the phase contrast microscope, the Nobel Prize in Physics was awarded to Frits Zernike in 1953 [204], [205].
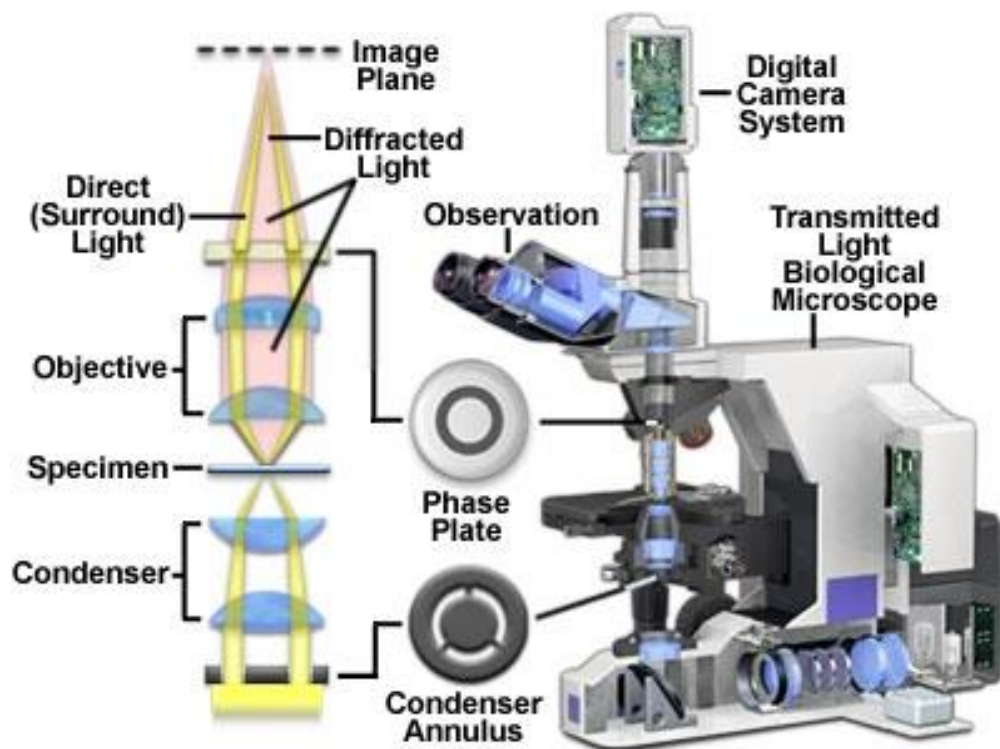

Figure 4.5. *A schematic illustration of the phase contrast microscope and the phase contrast optical train* [206]. *Its working principle is based on translating a phase shift into an amplitude difference.*

4.6. Applied instruments for the coating characterization and the in situ adsorption experiments

4.6.1. Optical waveguide lightmode spectroscopy

The characterization of the light-guiding capabilities of the nanostructured coatings and *in situ* protein adsorption measurements were performed using an OWLS210 integrated optical scanning instrument (Microvacuum Ltd, Hungary), and Biosense 2.8 and 3.0 softwares. For the cell adhesion measurements [207]–[209] I employed a laboratory-built OWLS device and a BIOS-1 instrument (Microvacuum Ltd, Hungary) with the same operating method [210]. The illuminating beams of the devices have the wavelength of 632.8 nm. Each experiment was typically repeated three times.

4.6.2. Spectroscopic ellipsometry

The millimeter-scale homogeneity and thickness of the TNT and TNP layers were characterized with a rotating-compensator spectroscopic ellipsometer (Woollam M2000DI) in mapping mode. The angles of incidence of the mapping beam were 70° and 75°. The results were evaluated with CompleteEASE 4.72 software. For the *in situ* two-channel adsorption measurements the same instrument was used integrated with recently developed mountings, described in details in subsection 5.3.1.

4.7. Calculation methods in the adsorption measurements

4.7.1. Measuring principle of OWLS

If a mono-mode waveguide is applied in the OWLS measurement, the precondition is that the phase shift during one total internal reflection equals zero, and it only occurs at two distinct angles of incidence, represented by the effective refractive indices for the two polarization modes, transverse electric (NTE) and transverse magnetic (NTM) [64].

In the OWLS measurement the incoupling of the measuring light occurs, the effective refractive index of the guided mode (N) can be calculated using the following equation:

$$N = n_0 \sin\alpha + l\left(\frac{\lambda}{\Lambda}\right) \qquad \text{Eq. (3),}$$

where N is the effective refractive index of the excited guided mode, n_0 is the refractive index of air, α is the incoupling angle, l is the diffraction order, λ is the wavelength of laser and Λ is the grating constant.

If a protein film is adsorbing onto the surface of the waveguide from the sample, the refractive index (n_A) and the thickness of the adsorbed layer (d_A) can be determined by applying N from Eq. (3) in the next correlation:

$$0 = \frac{2\pi}{\lambda}\sqrt{(n_F^2 - N^2)}\left(d_F + d_A \cdot \frac{n_A^2 - n_C^2}{n_F^2 - n_C^2}\left(\frac{\left(\frac{N}{n_C}\right)^2 + \left(\frac{N}{n_A}\right)^2 - 1}{\left(\frac{N}{n_C}\right)^2 + \left(\frac{N}{n_F}\right)^2 - 1}\right)^\rho\right) -$$

$$\arctan\left(\left(\frac{n_F}{n_C}\right)^{2\rho}\frac{\sqrt{(N^2 - n_C^2)}}{\sqrt{(n_F^2 - N^2)}}\right) - \arctan\left(\left(\frac{n_F}{n_S}\right)^{2\rho}\frac{\sqrt{(N^2 - n_S^2)}}{\sqrt{(n_F^2 - N^2)}}\right) \qquad \text{Eq. (4),}$$

where λ is the wavelength of laser light, n_F and d_F are the refractive index and the thickness of the waveguide, n_A and d_A are the refractive index and the thickness of the deposited adlayer, n_S is the refractive index of the substrate, $\rho=0$ for TE and $\rho=1$ for TM polarization modes.

4.7.2. The de Feijter formula

In OWLS measurements we obtain n_A and d_A parameters (refractive index and the thickness of the deposited adlayer) as described above in section 4.7.1. In ellipsometry we get these parameters by fitting them in the optical model.

But due to surface inhomogeneities or changes in the density of the adsorbed layer these data can be incorrect and misleading. In order to eliminate this mistake, n_A and d_A should be converted directly to surface mass density (Γ) using *de Feijter*'s formula [211]:

$$\Gamma = d_A \frac{n_A - n_C}{\frac{dn}{dc}} \qquad \text{Eq. (5),}$$

where Γ is the surface adsorbed mass density, d_A is the thickness of the adsorbed layer, n_A is the refractive index of the adsorbed layer, n_C is the refractive index of the cover medium, dn/dc is the refractive index increment of the buffer medium containing the adsorbing molecules (usually 0.18 cm³/g is used for protein adsorption studies [212]).

5. Results and discussion

5.1. Characterization of the coatings

In this part I summarize the results of the characterizations of the prepared nanostructured coatings. First the surface morphology and homogeneity was characterized by atomic force microscopy, afterwards the thicknesses of the layers were studied by spectroscopic ellipsometry. Finally, the light-guiding capability of a TNT-coated OWLS chip was examined by OWLS. The results of this section were published in Colloids and Surfaces B: Biointerfaces [T1].

5.1.1. Surface morphology and optical characterization of the coatings

From both of the nanoparticles, a dense and homogeneous coating was required to be prepared to be compatible with the OWLS and ellipsometric measurements. Moreover the thickness of the coatings needed to be between 5 and 15 nm, at which it can be expected to well cover the substrates without increasing the optical thickness of the original waveguiding layer significantly (geometric thickness typically 170–180 nm, with a refractive index of about 1.77) [213] or the gold coated (20-30 nm) substrate.

The TNT and TNP coatings were characterized with atomic force microscopy (AFM) [194], [214], [215] on various substrates in tapping mode (Fig. 5.1 and 5.2). The images were recorded at different parts of the substrate surface, so they clearly showed that both the TNTs and the TNPs covered the whole surface uniformly. The arithmetic average roughness (R_a) and root mean squared roughness (RMS) [216], [217] of the surface were calculated from the AFM data by the Gwyddion 2.37 software [193] based on the following equations:

$$R_a = \frac{1}{N}\sum_{n=1}^{N} |r_n| \qquad \text{Eq. (6)},$$

$$RMS = \sqrt{\frac{1}{N}\sum_{n=1}^{N} r_n^2} \qquad \text{Eq. (7)},$$

where N is the number of measured data points and r_n is the nth measured value.

For the TNT coating R_a was 4.67±0.57 nm and RMS was 5.93±0.69 nm, and for the TNP coating R_a was 2.13±0.36 nm and RMS was 2.84±0.52 nm. The uncoated surfaces were featureless with R_a<1 nm.
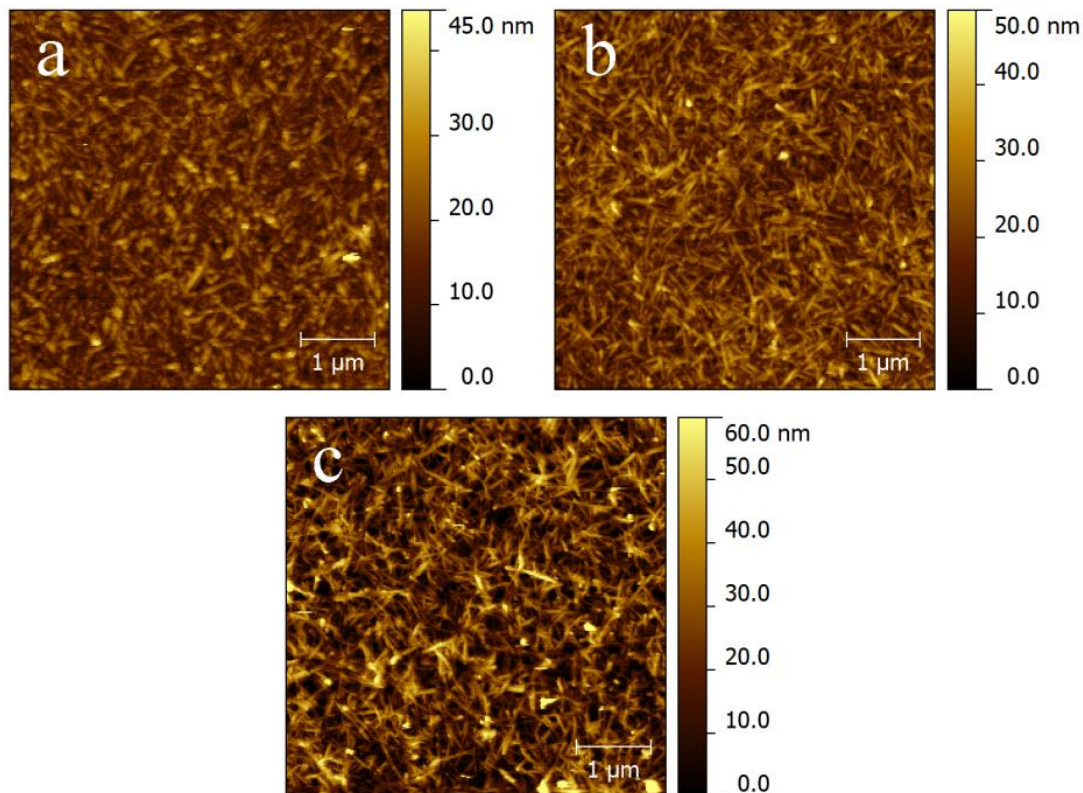

Figure 5.1. *Representative AFM images of the titanate nanotube coating prepared on a silicon wafer (a), an OWLS sensor chip (b), and a glass slide (c)* [T1]**.**
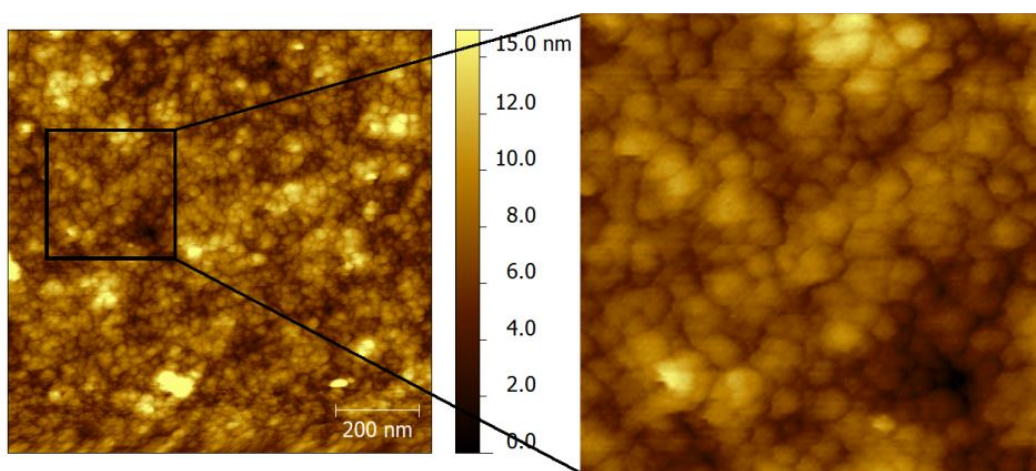

Figure 5.2. *AFM image of a titania nanoparticle coating spin-coated on a gold-coated glass substrate. The magnified area is 300 nm × 300 nm* [T2].

5.1.2. Thickness characterization with spectroscopic ellipsometry

I used a spectroscopic ellipsometer in mapping mode for characterizing the thickness of the TNT coatings prepared on small pieces of silicon wafers [218]–[220]. A two-layer optical model was applied in the evaluation of the measured data. On the single-crystalline Si substrate a native oxide layer (the thickness of which was fixed at the value obtained from measurements before the preparation of the TNT layers), and a TNT layer was placed. The optical properties of the TNT layer were described by the Cauchy dispersion relation [221] (Eq. (8)), which is an empirical polynomial approximation for the refractive index function of semiconductors and insulators below the band-gap [222]. Usually, only the first three terms of the summation is used:

$$n = A + B/\lambda^2 + C/\lambda^4 \qquad \text{Eq. (8),}$$

where n is refractive index of the layer, λ is the wavelength, A, B, C are coefficients to be determined by fitting (or known from previous measurements).

The best fit could be achieved when I used a vertical grading (a built-in feature in the CompleteEASE software) of the refractive index within the Cauchy layer of the TNT coating. In this case the graded layer contained 5 sublayers, and the refractive index changed from one sublayer to another in a linear way. The inhomogeneity of the grading, which defines the refractive index changes between the top and the bottom layer, was found to be around 60%.

The ellipsometric maps (Fig. 5.3a) showed that in the central part of the area the thickness of TNT coating is around 9-13 nm. According to our aim to prepare these coatings on OWLS sensor chips, this central part of the surface is the most important, as the 1-mm^2 sensing zone of the chip is located in the center. The quality of the fit (MSE) (Eq. (2)) is also acceptable at this central area (Fig. 5.3b).
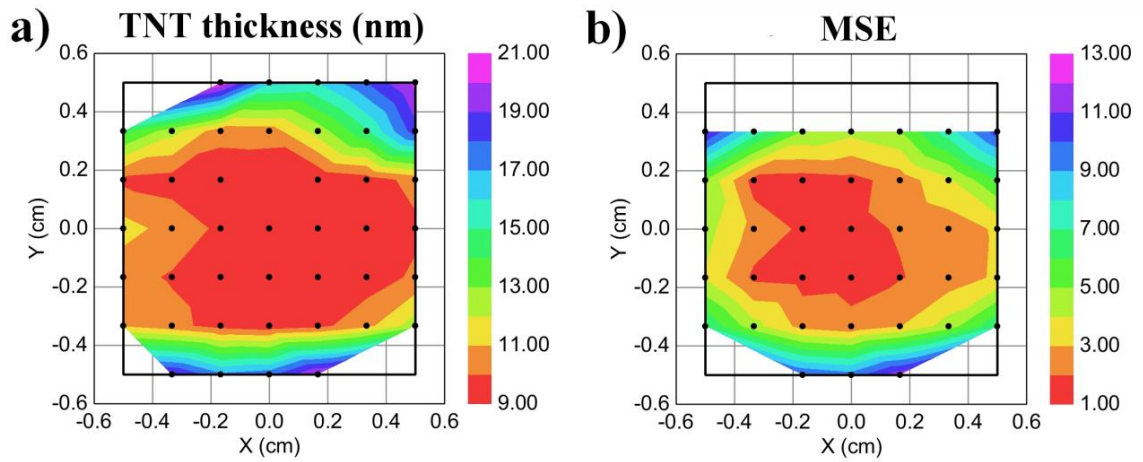
Figure 5.3. *A representative thickness map of a TNT-coated silicon plate **(a)** and the fit quality (MSE) values of this measurement **(b)** measured by spectroscopic ellipsometry. The central part of the area is coated by a 9–10 nm thick TNT film, and the quality of the fit is very good (MSE<3) in this area* [T1].

The thicknesses of the TNP coatings were also characterized by ellipsometry. The TNP-coated slide was modeled by a three-layer optical model on a BK7 glass substrate. On the glass a 2-nm Cr_2O_3 layer and a 20 nm or 30 nm thick gold layer were placed. Above them the TNP layer was located which is found to be 10-12 nm thick during the evaluation. It is in agreement with the dynamic light scattering measurements, where diameter of the nanoparticles was determined to be 11.3 nm. In the ellipsometric model the coating was represented by a homogeneous layer of effective medium approximation (EMA) (Eq. (9)) [192] of TiO_2 (50-55%) and void (45-50%), and could be perfectly fitted. In addition, the resulted proportion of the volume of void and TiO_2 is also in good agreement with the spherical geometry of the TNPs (the volume fraction of a monolayer consists of contiguous spheres is very close to our results). Because of the big difference between the refractive indices of the TNP and the gold layer, the uncertainty of the evaluation is acceptable (0.04% for the TNP thickness, and 0.21% for the EMA% of void).

5.1.3. Light-guiding capabilities of the TNT-coated OWLS chips

If we intend to apply a TNT-coated OWLS sensor chip in adsorption measurements, it is very important that the coating doesn't quench the propagation of light. By OWLS measurements, I demonstrated that the resonant incoupling peaks are slightly shifted to higher angles by the coating, but the height of the peaks didn't change significantly (Fig. 5.4).
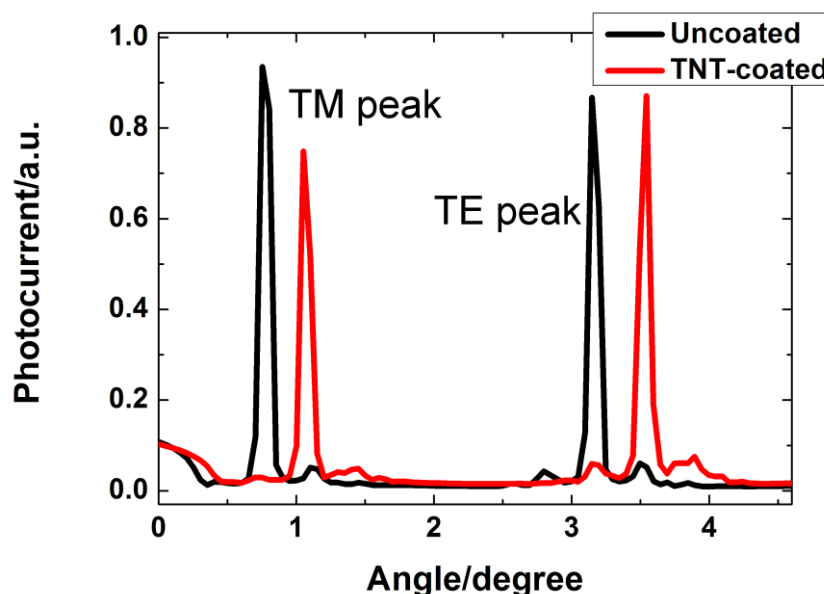

Figure 5.4. *The typical resonant incoupling peaks of an uncoated and a TNT-coated OWLS sensor chip* [T1]*.*

The thickness and the refractive index of the guiding film of the uncoated and TNT-coated sensor chips were calculated from the positions of the resonant peaks [65], [213], [223]. By the coating process the refractive index (n_F) decreased from 1.77494 to 1.77217 and the thickness (d_F) increased from 175 nm to 183 nm, which is in good agreement with the results of the ellipsometric measurements.

5.2. OWLS measurements on the TNT coatings

In this chapter I summarize the results of the OWLS measurements. First, protein adsorption experiments with bovine serum albumin (BSA) were performed on

TNT-coated and uncoated sensor chips. They were followed by experiments with living human embryonic kidney (HEK) cells and preosteoblasts. The strength of their adhesion was also investigated and presented by phase contrast microscopic images. At last a new cuvette configuration was developed in order to study living cells on spin-coated surfaces by HoloMonitor. The results of this section were published in Colloids and Surfaces B: Biointerfaces [T1] and the second part of subsection 5.2.2 in Journal of Biomedical Optics [T3].

5.2.1. Protein adsorption on the TNT coating

In the protein adsorption measurements BSA, a widely used, relatively small (66.5 kDa) protein was studied. Before the measurements the sensor chips were steeped in the buffer for one night. In the beginning of the experiment pure buffer was flowing in the cuvette for 1-2 h in order to record a stable baseline. Then the protein solution was introduced for 2 h, and at last the surface was washed with pure buffer again. For introducing the buffer and the protein solution a peristaltic REGLO Digital MS-4/12 (Ismatec) pump was applied at a flow rate of 1 μL/s. The temperature in the OWLS cuvette was kept at 25 °C during the experiments.

After the washing step the surface adsorbed mass density of the BSA was 130±20 ng/cm^2 for the uncoated chip, and 250±20 ng/cm^2 for the TNT-coated chip, which means a 92±16% increase on the nanostructured coating. The kinetic curves for both surfaces (Fig. 5.5) shows a saturation section during the adsorption with minor desorption during the washing step which indicates that a stable monolayer was formed on the surface [224].

It is important to note, that the limiting factor of protein desorption is the high energy barrier caused by the strong interfacial interaction. Even at very high flow rates, the diffusion boundary layer is orders of magnitude wider than the size of a protein molecule, so no hydromechanical force affects the protein [67], [224].
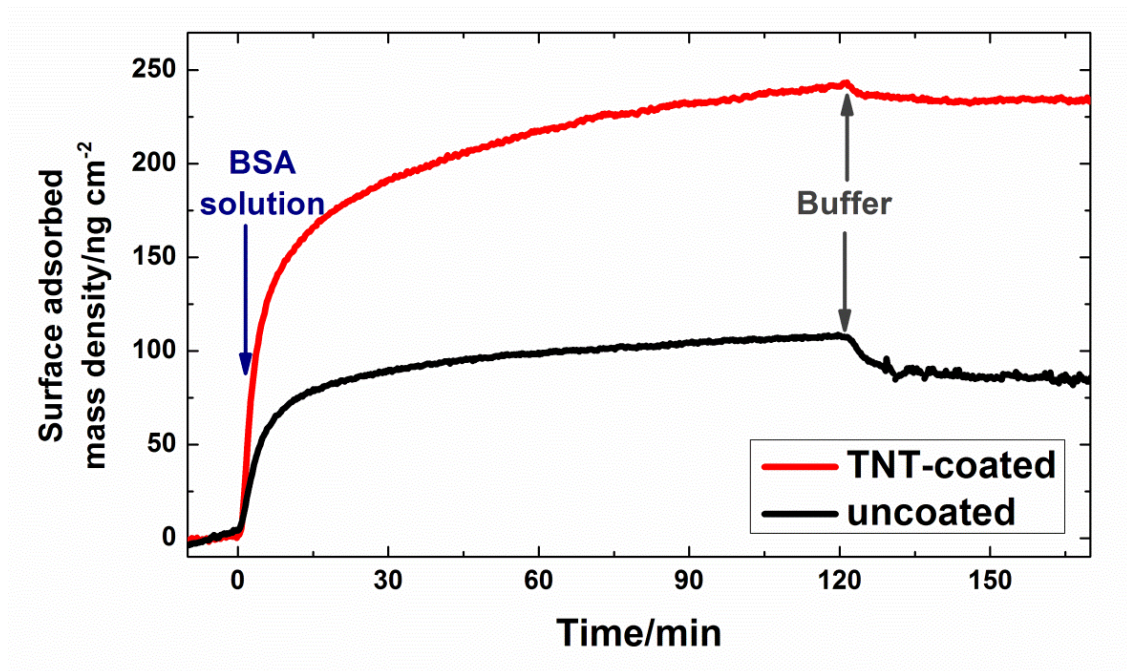
Figure 5.5. *Representative OWLS measurements of BSA adsorption on uncoated and TNT-coated OWLS sensor chips* [T1].

5.2.2. Cell spreading kinetics and adhesion strength on the TNT coating

The adhesion of living HEK cells were studied using a laboratory-built OWLS device dedicated to live cell studies, containing a closed cuvette without flow into which the buffer and cell solution were introduced using a pipette [67]. At first pure buffer was pipetted into the cuvette, above the sensor chip, and the position of the resonant peaks were measured. After a stable baseline was recorded the buffer was removed and 25 000 cells in 500 μL of medium were introduced into the cuvette, and the resonant peaks were measured for 2 h. The adhesion and spreading of the cells caused the resonant peaks to shift to higher angles. In the case of the nanostructured surface a larger signal could be observed (Fig 5.6), which means that the TNT coating enhanced the cell adhesion [225].
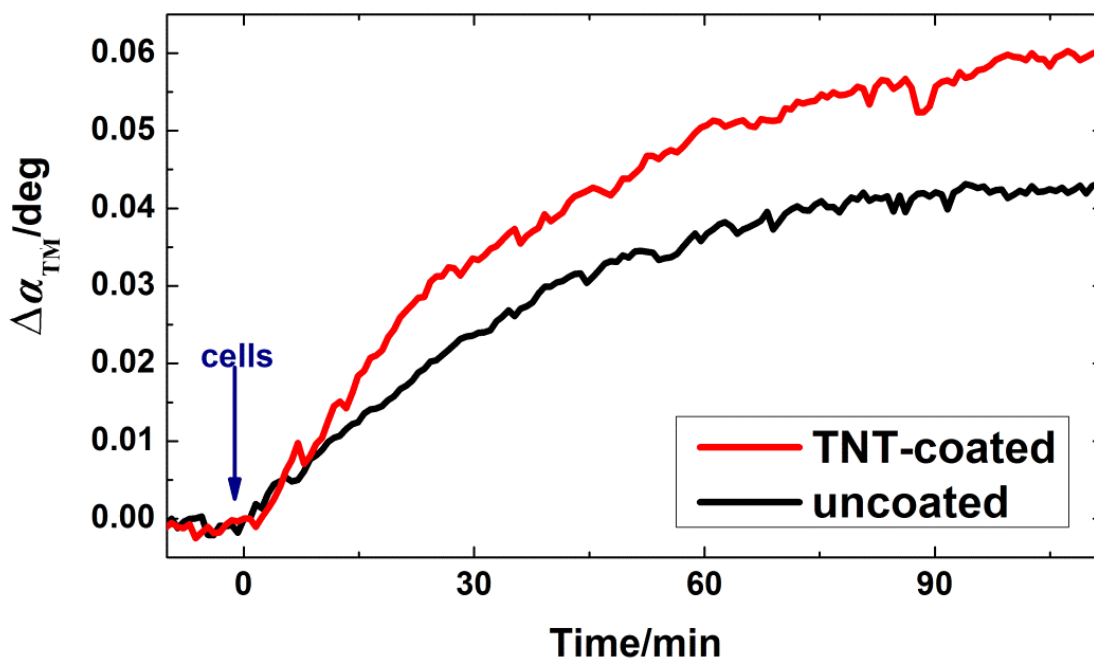
Figure 5.6. The typical curves of the adhesion and rapid spreading of HEK293 cells on bare and TNT-coated surfaces measured by OWLS. The ordinate plots the shift of the peak position (in degrees) of the zeroth transverse magnetic guide lightmode (ΔTM_{center}), which is proportional to the contact area of the attached cells [T1].

An additional experiment was performed with the same type of HEK cells (Fig. 5.7). The cells were seeded on uncoated and TNT-coated glass substrates and were cultured in incubator at 37 °C with 5% CO_2 and 20% O_2. For 6 days I took phase contrast images of the cells on the two surfaces each day using a phase contrast microscope. The images showed that the cells were spreading and proliferating in a similar way and speed. On the seventh day the substrates were washed with an intense flow (~350 µL/s) of cell culture medium and the cells were investigated with the microscope. While the cell coverage on the surface of the uncoated substrate decreased drastically, the coverage on the TNT-coated substrate remained the same, clearly indicating, that the cells could adhere more strongly on the nanostructured TNT film.
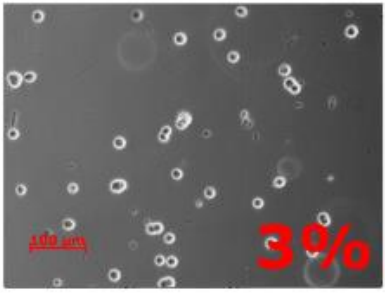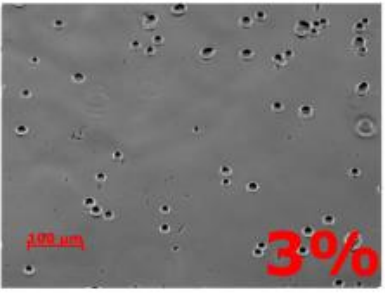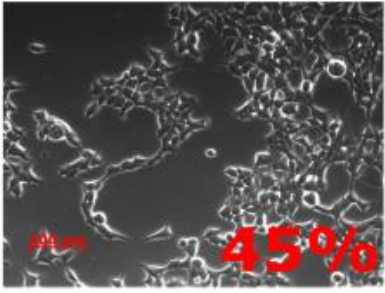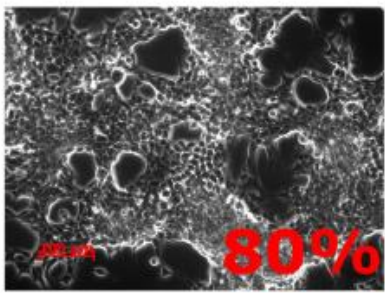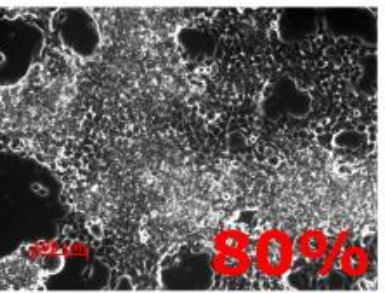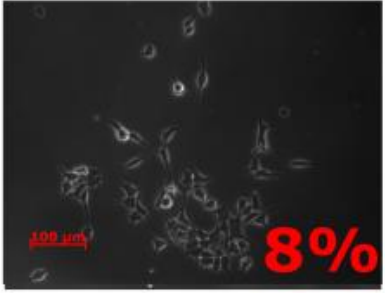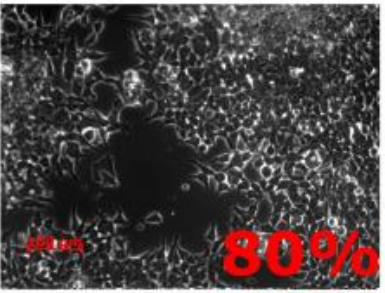
Figure 5.7. *Phase contrast images of the cultured HEK293 cells 1 day, 3 days and 6 days after seeding on uncoated and TNT-coated glass substrates, and after washing with medium. All scale bars are 100 μm. On the images the estimated cell-covered area percentages (calculated by using ImageJ software) are designated* [T1].

Another cell type, MC 3T3-E1 preosteoblast cells, that are more relevant for possible biomaterial applications, was also investigated in similar experiments. In contrast to the HEK cells, these cells could not been removed by washing from neither of the surfaces, indicating that this cell line can adhere stronger, which was confirmed by the OWLS measurements also, as the obtained signal was significantly larger for these cells.

The adhesion kinetics of the preosteoblasts was studied in the same way as the HEK cells. The results showed that the TNT coating enhanced the adhesion by about 30% compared to the uncoa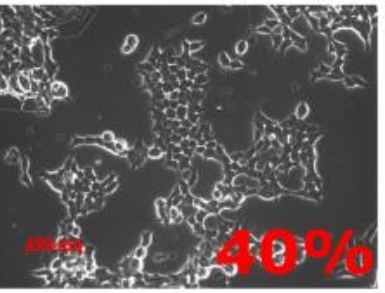ted sensor chip surface (Fig. 5.8). This is a promising result toward the intention of using this type of coating on implants to promote tissue regeneration.
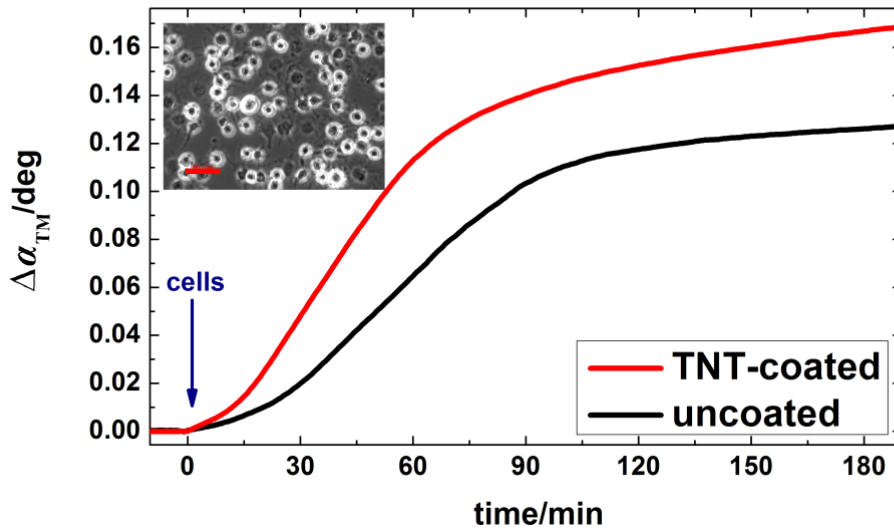
Figure 5.8. *A typical OWLS measurement of preosteoblast cell (MC 3T3-E1) attachment and rapid spreading on uncoated and TNT-coated OWLS chips. The ordinate plots the shift of the peak position (in degrees) of the zeroth transverse magnetic guide lightmode, which is proportional to the cell contact area. The inset shows the spread cells after the experiment (the scale bar is 50 μm)* [T1].

In order to study the adhesion of these cells in more detail, they were investigated by HoloMonitor M4, a digital holographic microscope. For the measurements, a new cuvette configuration had to be developed, so the cells could be studied *in situ* on spin-coated substrates by the HoloMonitor (Fig. 5.9). Cover glass substrates were coated with TNTs beforehand, using the same method that was introduced in subsection 4.2.1.

Then an O-ring was lubricated with silicone grease and was placed on the coated substrate and preosteoblast cells in cell culture medium (3×10^4 cells in 140 μl) were pipetted on the area inside the O-ring. The O-ring and the cell suspension were carefully covered with another glass slide, to prevent the ingress of bubbles, evaporation and disturbing meniscus effects which can limit the image quality.
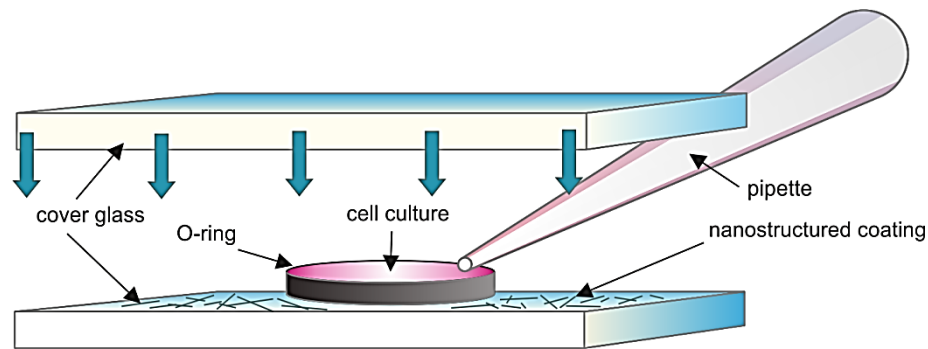
Figure 5.9. Schematic image of the developed cuvette setup where the cells are seeded on the TNT-coated substrate and surrounded by an O-ring. It enables long-term monitoring of living cells on coated surfaces by HoloMonitor M4 [T3].

The cells were incubated and observed for 24 h, images were taken in every minute for 3 h, and later in every 5 min. In Fig. 5.10 the three-dimensional visualization of the cells and the cross-sectional view of a typical cell can be seen 5 min, 3 h and 24 h after seeding. The height of the cells can be observed to be reduced from 14 μm to about 5 μm in the first 3 h, and remained similar for the rest 21 h of the experiment.
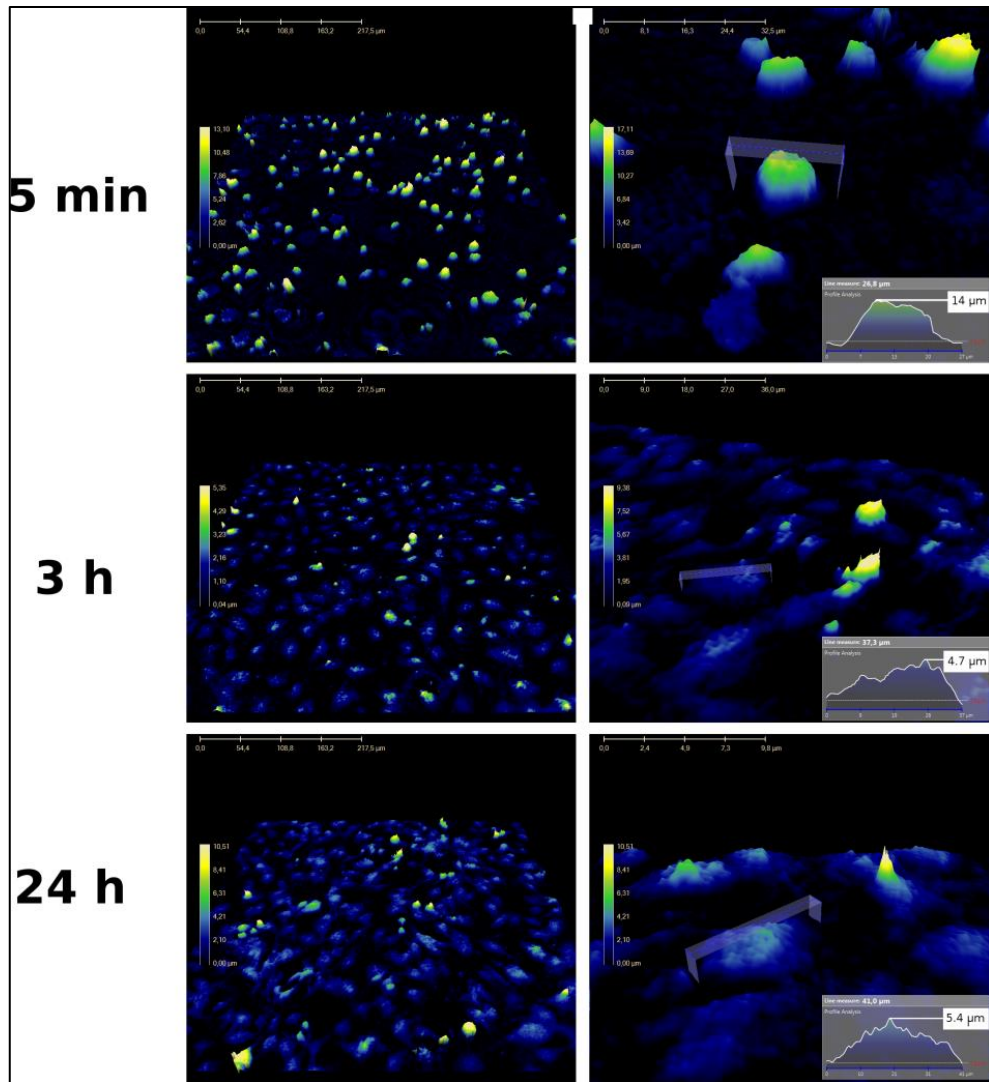
Figure 5.10. *The three-dimensional visualization of preosteoblast cells on nanostructured TNT coatings and the cross-sectional view of a representative cell at different moments of the measurement* [T3].

By this experiment I demonstrated that by applying the new cuvette configuration, one is able to visualize living cells on a spin-coated surface (like the TNT coating) with good resolution applying the HoloMonitor. With further investigations and calculations we also showed, that the vertical resolution of this technique is limited, and it has to be taken into account, when flattened, spread cells like preosteoblasts are monitored [T3].

5.3. New time-sharing two-channel ellipsometric configuration and its applications in in situ adsorption measurements

In this chapter I introduce the development of the new ellipsometric configuration and its advantages. It is followed by the presentation of three applications: the monitoring of polyelectrolyte layer deposition, protein adsorption and living cell adhesion. The results presented in this section were summarized in a publication in Optics Express [T2].

5.3.1. The new setup and its advantages

Our group developed a new ellipsometric configuration where a flow cell is combined with a semi-cylindrical glass lens (Fig. 5.11, Fig. 5.12a), in internal reflection Kretschmann geometry [121], [122]. The flow cell can be easily placed onto the mapping stage of a spectroscopic ellipsometer and applied for multiple angle of incidence measurements. In contrary to the conventional ellipsometric flow cells [101], [226], [227], where a fix angle of incidence has to be used, determined by the layout of the cell, in this new Kretschmann configuration, due to the semi-cylinder any angle can be chosen between 45° and 90°. I chose the angle of incidence of a measurement, at which the plasmon resonance was the highest on the TNP-coated surface.

Another advantage of the semi-cylindrical lens is that the substrate is illuminated through a glass lens, not through the sample solution which absorbs the infrared range of the light. Therefore the spectral range between 350 nm and 1689 nm can be used in the evaluation.
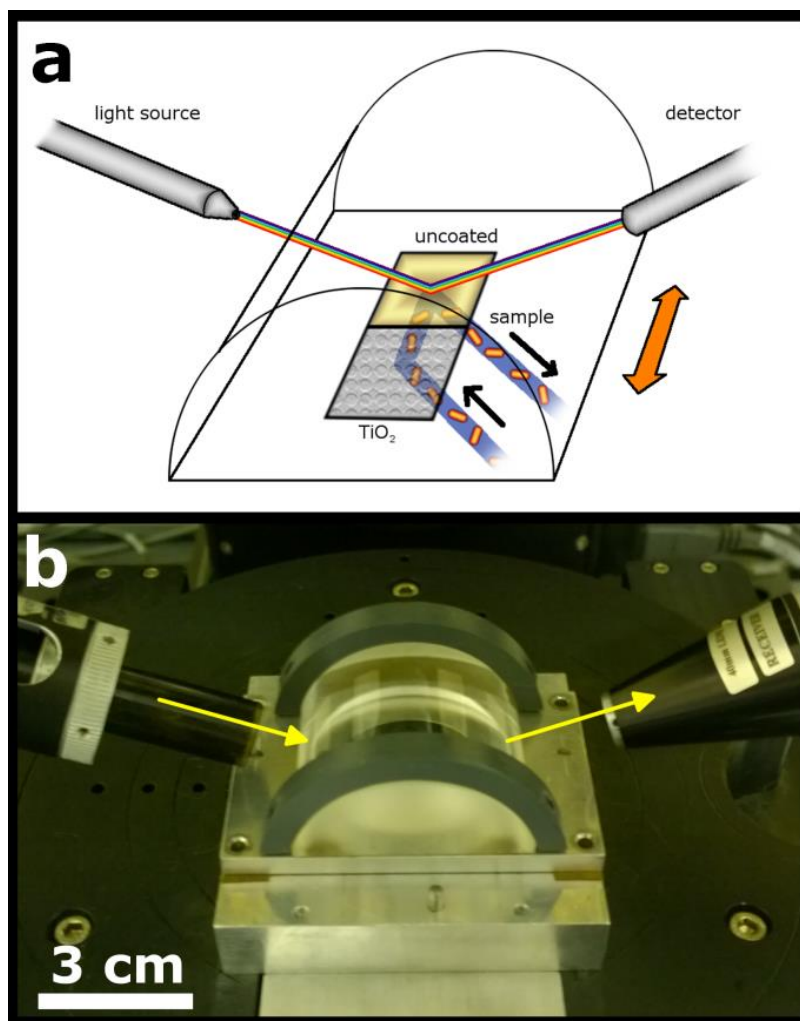
Figure 5.11. A schematic image (a) and a photo (b) of the developed in situ *multi-channel plasmon-enhanced ellipsometric configuration in the Kretschmann geometry* [T2].

The illuminating light beam is focused by a custom lens and reaches the substrate in a ~0.9 mm × 0.3 mm spot. After being reflected, the light is collimated and reaches the detector with the same intensity as in the case of the basic ellipsometer. Therefore it takes only about 1 s to measure the whole spectrum with a relatively low noise.

The studied process takes place in the flow cell (Fig. 5.12b) with a volume of ~10 µl, which ensures the fast sample blending and low sample consumption. The protein or polyelectrolyte solution and the buffers are flowing continuously during the real-time monitoring of the adsorption processes.
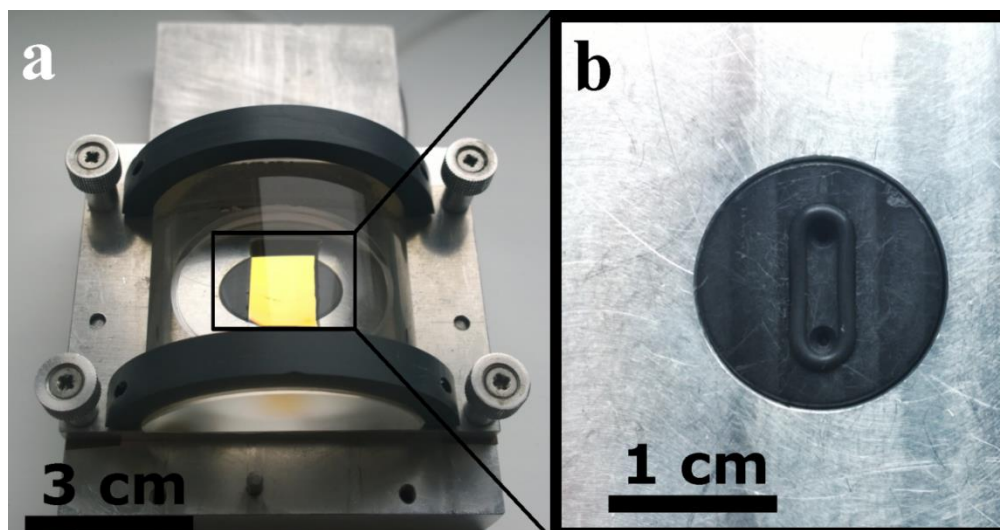
Figure 5.12. *A photo of the gold covered substrate placed between the flow cell and the semi-cylindrical glass lens **(a)** and the 10-μl flow cell from above **(b)*** [T2].

During the experiment, the substrate with the semi-cylindrical lens and the flow cell is shifted back and forth by the precisely positionable automatic mapping stage, so that the light beam is projected on the coated and the uncoated surface alternately (Fig. 5.11a). The main advantage of this method is that the studying of the adsorption on the two different surfaces takes place in the same process, thus the conditions of the experiments (temperature, pH, humidity, sample concentration etc.) are the same, and the results can be compared more reliably, because systematic errors can be ruled out and concerns about repeatability can be minimized in this way.

In order to achieve a higher sensitivity, surface plasmon resonance effect was combined with the ellipsometric method. On the employed glass substrates gold thin films with a thickness of 20 and 30 nm was evaporated, which enables plasmon resonance during the measurements. Therefore, at certain angles of incidence, sharp peaks appear in certain wavelength ranges of the spectra (see Fig. 5.16a). Due to the plasmon enhancement the sensitivity of the method improves by several orders of magnitude.

5.3.2. The construction of the ellipsometric model

The spectral range of the *in situ* multichannel measurements was 191-1689 nm, but as the light penetrated through the glass semi-cylindrical lens, the UV range was absorbed. Thus in the evaluation only the range between the wavelengths of 350 nm and 1689 nm was used. The spectral step was 1.59 nm between 191 and 999 nm and 3.46 nm between 999 and 1689 nm.

The cross-sectional view of the physical layers and the constructed optical model can be observed in (Fig. 5.13). The glass semi-cylinder and the glass substrate are located on top of the layers, modeled by a BK7 glass (from SCHOTT) ambient. Between the glass and the gold film there is an intermediate 2 nm thick chromium-oxide layer in order to ensure the adhesion of the gold layer. The optical parameters of the gold and the chromium oxide layers were determined applying B-spline parameterization, where a low-degree polynomial function is applied to parameterize an arbitrary dielectric function [228]. The optical constants determined in this way were in good agreement with the data in the database of the employed ellipsometer.

The layer of the spin-coated titania nanoparticles are modeled by the effective medium approximation (EMA) [96], [101]. The EMA is applied when the studied thin film is macroscopically homogeneous but microscopically heterogeneous. In this case the size of the distinct parts inside the layer is smaller than the wavelength of the measuring light, thus the diffraction and scattering on heterogeneities are negligible, but the volumes of these parts are large enough to have the optical properties of the bulk materials. In this approximation the medium is considered as the mixture of material with known refractive indices. In his theory, Bruggeman assumed that the dielectric function of the host material is equal to the requested dielectric function of the effective medium. His solution of the EMA was the following equation:

$$\sum_{n=1}^{N} f_n \frac{\varepsilon_n - \varepsilon}{\varepsilon_n + \gamma_d \varepsilon} = 0 \qquad \text{Eq. (9),}$$

where N is the number of the constituents, f_n is the fraction of the nth constituent, ε_n is the dielectric function peculiar to the bulk state of the nth constituent in the layer, ε is the dielectric function of the effective medium, and γ_d is a factor related to the screening and the shape of the inclusions (e.g. γ_d=2 for spheres).

In the model the TNP layer is represented by a ca. 12 nm thick EMA layer which is a compound of TiO_2 (50-55%) and water (45-50%), the latter represents the buffer. For the TiO_2 material also the reference from the database of the ellipsometer was applied, which was confirmed by the accurate fit and the good agreement between the layer thickness and the diameter of the nanoparticles resulted by the dynamic light scattering measurements. The refractive index of the buffer were modeled by fitting Sellmeier's dispersion equation (Eq. (10)) to Palik's data [229]. The equation is based on the Cauchy formula (Eq. (8)), but it was improved by Sellmeier to give a more precise approximation in the ultraviolet and infrared wavelength ranges. The most frequent form of the equation contains only the first three terms of the summation:

$$n^2(\lambda) = A + \frac{B_1\lambda^2}{\lambda^2 - C_1} + \frac{B_2\lambda^2}{\lambda^2 - C_2} \qquad \text{Eq. (10),}$$

where n is refractive index of the layer, λ is the wavelength, *A, B, C* are coefficients to be determined by fitting (or known from previous measurements) [230].

Below the TNPs, the studied adsorbed layer of proteins or polyelectrolytes is placed. The monolayer of proteins was approximated with the Cauchy dispersion (Eq. (8)). I modeled the adsorbing protein layer with a Cauchy layer having fixed thickness and fitted refractive index (parameter A was fitted, the other parameters were B=0.01 and C=0 [226], [227]). The adsorption process can be visualized as the following: a fixed volume above the surface is filled by pure buffer in the beginning of the measurement while the baseline is being recorded. Later, when the protein solution is flowing, the fixed volume is started to being filled up with protein molecules, thus its refractive index starts to increase.

The optical parameters of the deposited polyelectrolyte layers were also defined by the Cauchy equation (Eq. (8)) using the same dispersion parameter as for proteins (B=0.01), and parameter *A* was being adjusted in order to have the same refractive index at the wavelength of 632.8 nm as in Ref. [231]. In this case the thickness of the layer was fitted and all of the Cauchy parameters were fixed. At the bottom of the model there is a PBS buffer layer, which was modeled as water with the Sellmeier dispersion (Eq. (10)).
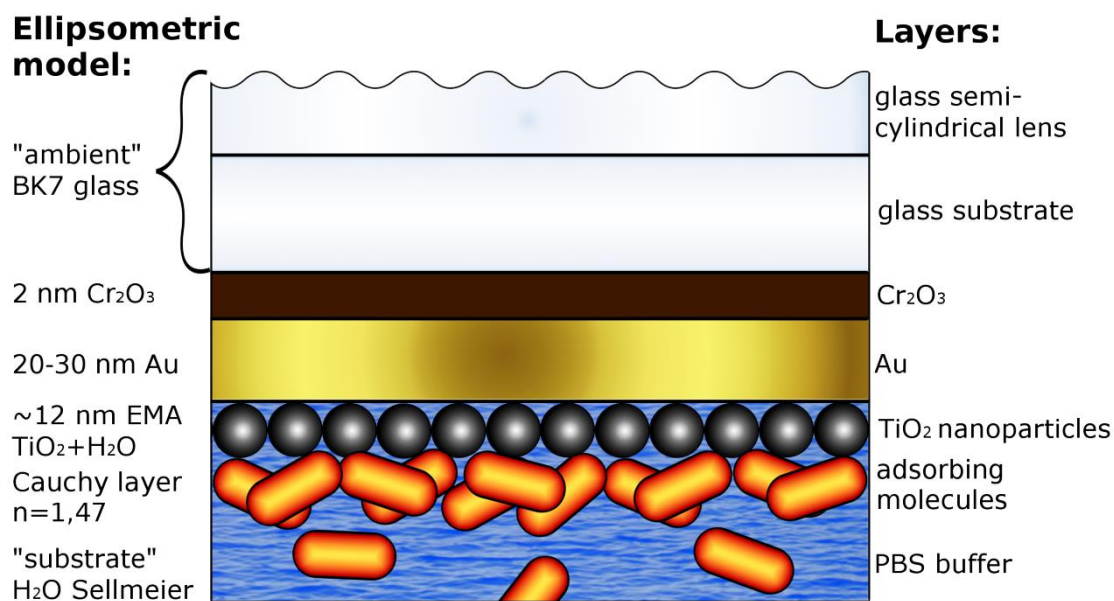
Figure 5.13. *Schematic image of the cross-sectional view of the physical layers and the corresponding layers of the optical model in the measurement* [T2].

Before each experiment a map of the complex reflection coefficient (ρ) (Fig. 5.14) was prepared for the actual substrate, where ρ was plotted as a function of the wavelength and the angles of incidence. In the measurements the angles of incidence were chosen to be at the regions where the plasmon resonance is the largest (the lowest ρ values on the map), which was typically around the angles of 64° and 65°.
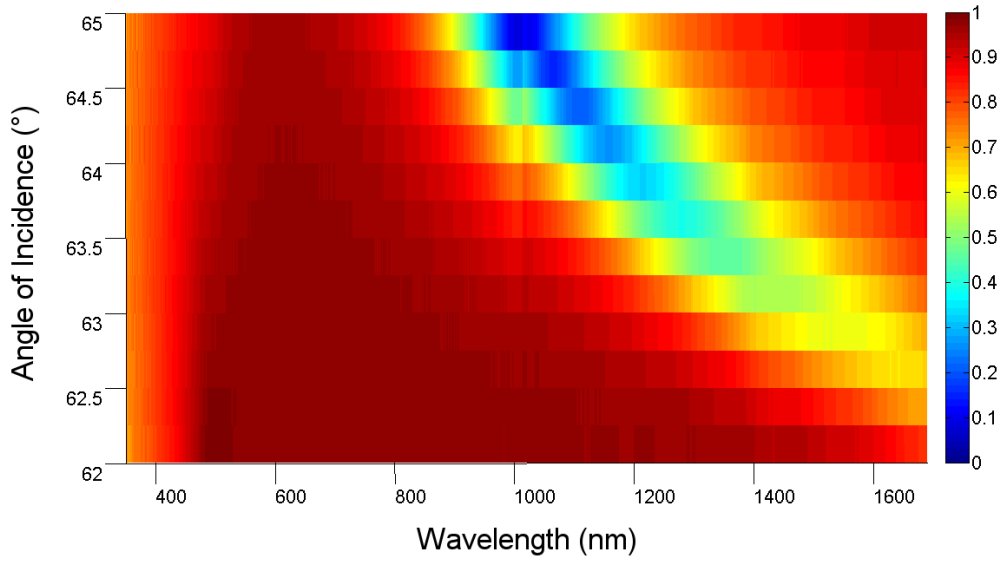
Figure 5.14. *A typical map of the absolute value of the complex reflection coefficients (ρ=tan(Ψ)e^(iΔ)) plotted as a function of the wavelength and the angle of incidence, measured on a substrate with 30 nm thick gold layer. The lower the values at a point of the map, the larger the plasmon resonance is* [T2].

The mean standard deviation of the baselines of the protein adsorption measurements was calculated for 5 min long sections, applying the following equation:

$$s = \sqrt{\frac{1}{N-1}\sum_{n=1}^{N}(x_n - \bar{x})^2}$$ Eq. (11),

where N is the number of the measured values, n=1, 2, 3 … N, x_n is the nth measured value.

The limit of detection (defined as the treble of the mean standard deviation) was determined to be 2.3° for the Δ ellipsometric angle in the most sensitive range, which means a sensitivity of 40 pg/mm^2 in surface adsorbed mass density.

5.3.3. Polyelectrolyte deposition on the TNP coating

The application of the new ellipsometric configuration was first demonstrated with the monitoring of polyelectrolyte multilayer deposition. Poly(allylamine hydrochloride) (PAH) and poly(styrene sulfonate) (PSS) were applied as positively and negatively charged polyelectrolytes, respectively.

First the measurement was carried out at pH 8 (Fig. 5.15a), where both the gold and the titania surfaces are negatively charged. Beginning with a PAH layer, 10 pairs of layers were built with 10 min long deposition and 5 min long washing (MQ) sections. In the optical model the polyelectrolyte layers were approximated with a Cauchy layer with a refractive index of 1.47 [231]. The kinetic curves of polyelectrolyte layer deposition on the TNP-coated and uncoated surfaces revealed that the coating enhanced the layer formation, and significantly thicker layers were built on it.

The experiment was also performed at pH 4, where both of the surfaces have positive charges on the surface. The comparison of the adsorption curves for the different pH-s shows that the deposited layers at the acidic pH were significantly thinner than at the basic pH (Fig. 5.15b). This difference between the bilayer thicknesses at the basic and acidic pH can be interpreted by the fact that the polyelectrolyte deposition has a strong pH-dependence [232].
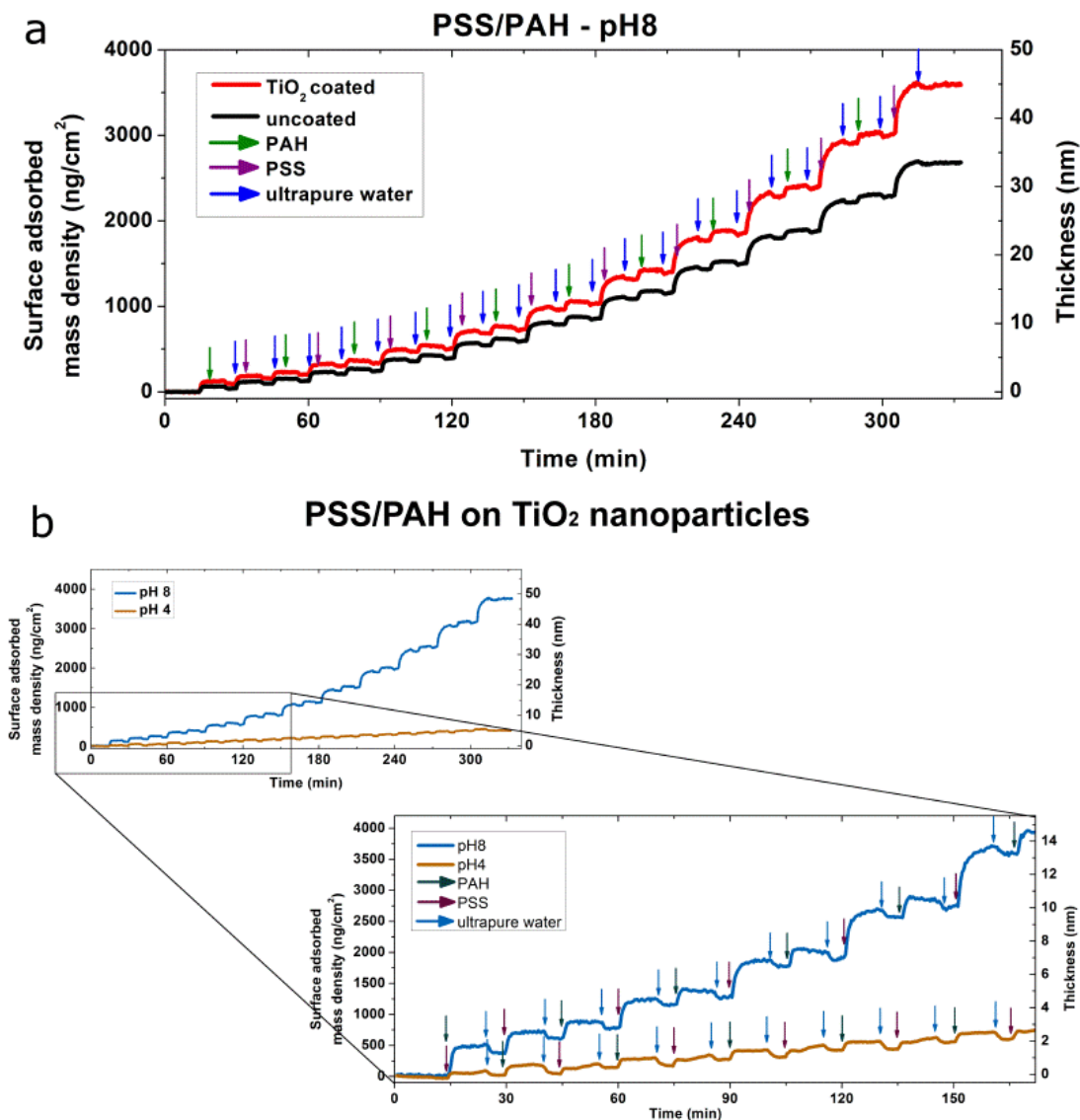
Figure 5.15. Typical kinetic curves of the polyelectrolyte measurements. Comparison of 10 pairs of PSS/PAH layers deposited at pH 8 on TNP-coated and uncoated surfaces (a), and on TNP-coated surface at pH 8 and pH 4 (b) [T2].

5.3.4. Protein adsorption on the TNP coating

For the investigation of protein adsorption on the TNP-coated surface I applied a widely used stable protein, fibrinogen (Fgn). In the beginning PBS buffer was flowing in order to achieve a stable baseline. Afterwards Fgn solution (1 mg/mL) was introduced for 30 min, and the measurement was ended with a washing step with the buffer.

The resonant peaks in the recorded spectra (Fig. 5.16a) can be observed at the wavelength of 1000-1200 nm. The quality of the fit of the modeled data to the measured spectra was satisfactory in the wavelength range of 350-1689 nm. Utilizing the fitted refractive index data and the other fixed (known) parameters, the value of the adsorbed mass density of the proteins on the surface can be determined, using de Feijter's formula (see in section 4.7.2, Eq. (5)) [211].

By plotting the adsorption curves (Fig. 5.16b) of the proteins on the two different surfaces, the difference between the nanostructured and control surface can be demonstrated. It is clearly seen that the TNP-coated surface enhanced the adsorption of the fibrinogen, which is in good agreement with my previous results that the titanate nanoparticles facilitated the adsorption of BSA. Both phenomena can be explained by the specific surface enlargement, the value of which can be easily approximated in the case of the titania nanoparticles. According to the AFM images, we can assume that they are globular shaped and densely deposited on the surface. Then their specific surface area can be approximated with the area of contiguous hemispheres which means an increase of 81% compared to a plane surface.
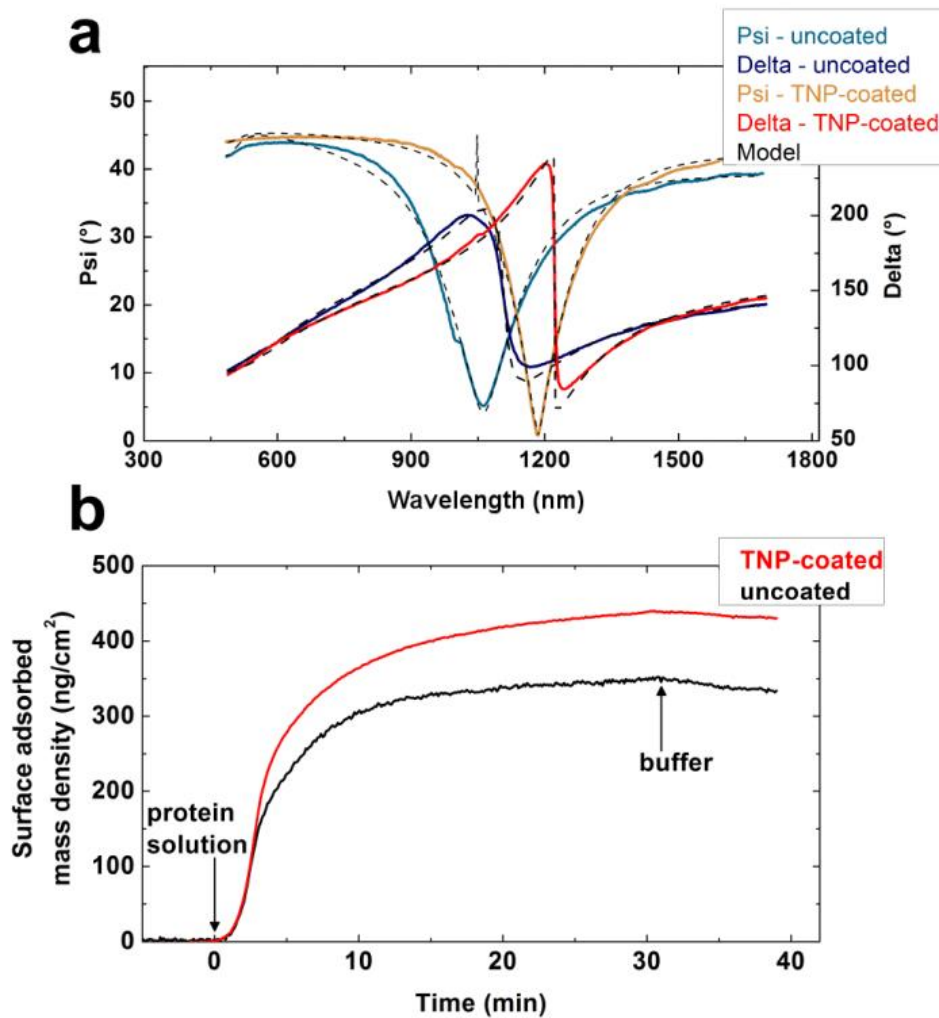
Figure 5.16. Spectra of the measured ellipsometric angles (Ψ and Δ), at the beginning of the measurement on the TNP-coated and uncoated surfaces, and the fitted spectra (a). The kinetic curves of representative in situ *ellipsometric measurements of Fgn adsorption on TNP-coated and uncoated surfaces (b)* [T2].

5.3.5. Ellipsometric experiment with living cells on the TNP coating

I performed *in situ* two-channel ellipsometric measurements with the new setup for monitoring the previously studied preosteoblast cells on titania nanoparticles. While in this configuration the substrate was upside-down during the measurement, the process of the cell adhesion couldn't be monitored, only the spreading and the washing of them. In the beginning of the measurements the cells were seeded on the substrates partially coated with titania nanoparticles, and were left for one hour to adhere on the surface. Afterwards, I assembled the cell-covered substrate with the flow cell and the

semi-cylinder and started the *in situ* measurement. The cells were measured for 30 min while being at rest, and then buffer was flowing slowly for 30 min. It was followed by the injection of trypsin-EDTA (ethylenediaminetetraacetic acid), which was let to exert its cell-detaching effect for 3 min. Then buffer was flowing rapidly for 1 min and slowly for two more hours. Further developments are needed in creating a proper optical model for living cells to evaluate the results properly. But if we look at the Δ plotted as a function of time (Fig. 5.17a), we can establish that the periods of the measurement can be dissevered easily, so the new configuration is appropriate for the investigation of living cells.

After the measurement, I took phase contrast images with a microscope in order to observe the residual cells on the substrate (Fig. 5.17b). In a control experiment, osteoblasts were incubated on a control substrate which was a similar gold coated glass slide partially covered by titania nanoparticles (Fig. 5.17c). Comparing the TNP-coated and the uncoated gold surfaces in the images, we can see that more cells remained on the coated surface after measurement and more cells could be observed on the coated control substrate after 4 days of incubation. These results indicate that the cells preferred the nanostructured surface and adhered stronger to it as well.
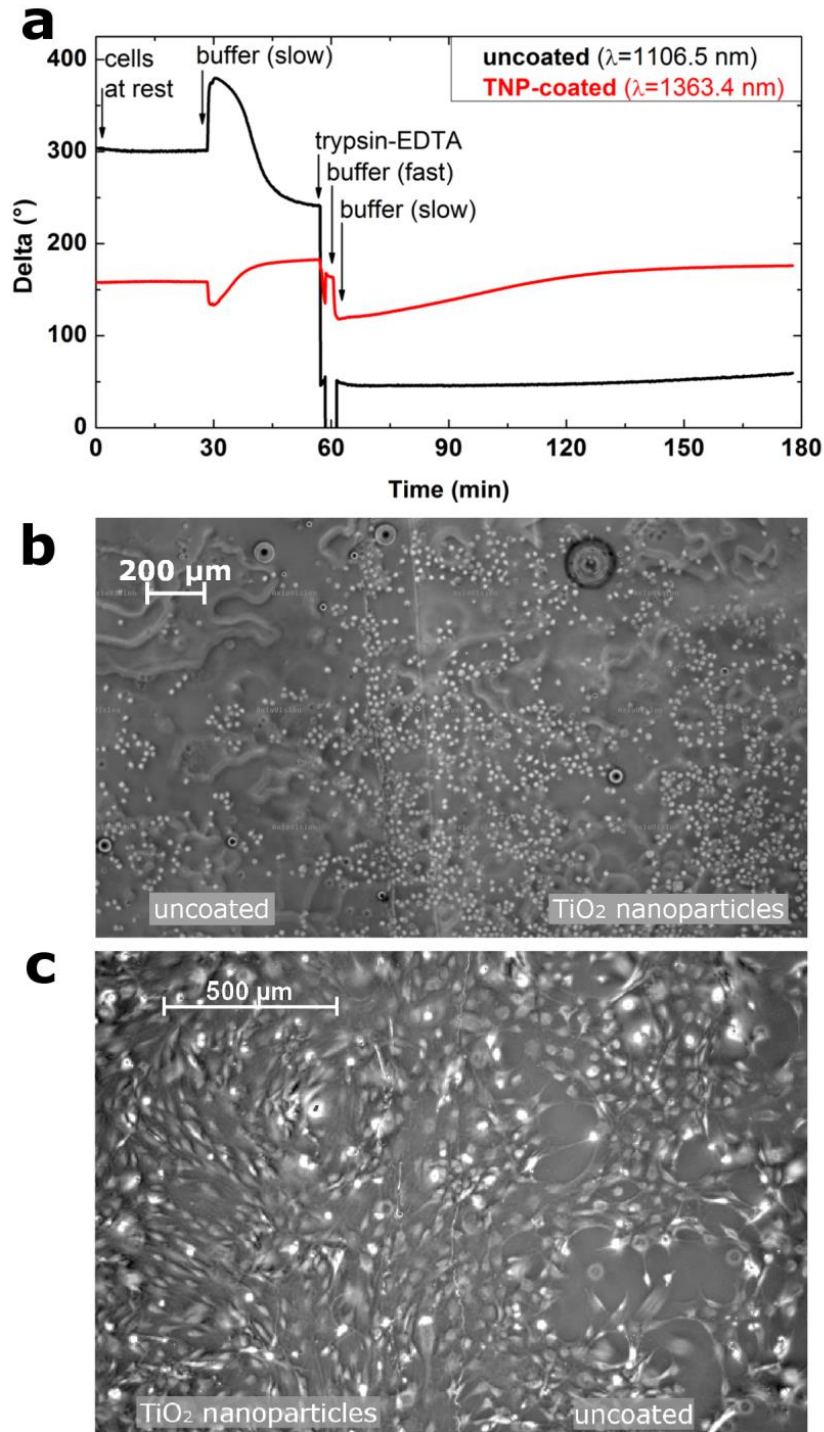
Figure 5.17. *The alterations of the Δ (ellipsometric angle) in the living cell experiment on the TNP-coated and uncoated surfaces, plotted at the wavelengths where the plasmonic effect was the highest (a). Phase contrast microscopic images of the preosteoblast cells at the boundary of the TNP-coated and uncoated surfaces on the substrate applied for the ellipsometric measurement (b), and on the control substrate after being incubated for 4 days (c)* [T2].

6. Summary and outlook

In my Ph.D. work I prepared highly transparent nanostructured coatings from additive-free titanate nanotubes (TNT) and titania nanoparticles (TNP) using a simple, fast, inexpensive, room temperature spin-coating method.

The surface morphology, homogeneity, thickness and light-guiding capabilities of the coatings were characterized by atomic force microscopy, spectroscopic ellipsometry and optical waveguide lightmode spectroscopy (OWLS). The obtained results confirmed that the coatings are appropriate for *in situ* OWLS and ellipsometric measurements with biomolecules, like proteins or living cells.

I performed protein adsorption experiments that revealed that the surface-adsorbed mass density of bovine serum albumin proteins was by 92±16% larger on the TNT coating compared to the uncoated surfaces. With another OWLS device I demonstrated that living cells (human embryonic kidney cells and preosteoblasts) could spread and adhere better on the TNT-coated chips. Parallel microscopic experiments showed that the cells adhered much stronger on the nanostructured surface and significantly fewer cells could be removed by an intense flow of cell culture medium.

These results can be further developed in various directions. For surface-sensitive optical methods, the sensitivity can be improved by increasing the specific surface area of the sensor chips, thus enlarging their analyte capture capacity. The TNT coatings could possibly be fabricated by dip-coating method and potentially be prepared on medical implants to enhance or control cell adhesion and regeneration processes. The very simple and fast fabrication method of the nanostructured films makes them especially promising candidates for such applications.

In the second part of my Ph.D. work I took part in the development of a new ellipsometric configuration and applied it for studying various adsorption processes. In this configuration I applied a 10-μL flow cell with a semi-cylindrical lens in the Kretschmann geometry with a standard spectroscopic ellipsometer and mapping stage for multi-channel, multiple angles of incidence, multi-wavelength, internal reflection, plasmon-enhanced ellipsometry. In the measurements the wavelength of the light beam was in the range of 350-1689 nm and the angles of incidence can vary from 45° to 90°.

The illuminating spot was focused to be smaller than approximately 0.5 mm at the axis of the semi-cylinder by using custom lenses and designed mountings. I developed a custom sample preparation method to create substrates partially coated with 10 nm titania nanoparticles for this ellipsometric configuration. The application of the new configuration with the partially coated substrates made possible to perform time-sharing multi-channel *in situ* measurements on nanoparticle coated and uncoated reference surface in the flow cell, in the same run. The two-channel measurement can be performed by scanning the substrate back and forth parallel to the axis of the semi-cylinder, so that one spot on the coated and another one on the uncoated control surface can be measured one-by-one alternately. The measurements on the two different surfaces are performed in the same process, under the same conditions (temperature, pH, concentration etc.), thus the comparison of these measurements are more reliable than before, ruling out most of the systematic errors, and minimizing concerns about repeatability.

A sensitivity of ~40 pg/mm^2 could be achieved by optimizing the parameters of the measurements (thickness of the plasmonic layer, the angle of incidence and the wavelength range) and the time resolution of the measurements was approximately 1 s.

I applied the developed ellipsometric setup for monitoring polyelectrolyte deposition and revealed that thicker layers were built on the TNP-coated surface. The measurements were performed at both pH 4 and pH 8 and their comparison showed that significantly thicker layers were created at pH 8. Experiments with fibrinogen proteins and preosteoblast cells were also performed on similar substrates partially coated with titania nanoparticles. In the case of fibrinogen the measurements clearly indicated that the nanostructured coating enhanced the adsorption of the proteins, (similarly to the titanate nanotubes described above) due to the increased specific surface area and nanoroughness. In the living cell experiments the sequent measurement sections could be distinguished according to the curves with the ellipsometric angles as a function of time. For a more detailed evaluation further developments are needed in creating optical models for living cells.

7. Thesis highlights

1. For the first time, I used novel types of additive-free titanate nanotubes (TNTs) and titania nanoparticles (TNPs) prepared by our collaborator for fabricating thin films that can be used as coatings on optical waveguide lightmode spectroscopy (OWLS) sensor chips. I demonstrated with atomic force microscopic images, that the layers cover the surface uniformly, and in the aspect of optical modelling they can be considered approximately homogeneous. I used spectroscopic ellipsometry in mapping mode to characterize the thickness of the layers. For both types of the nanoparticles, the thickness of the coating was revealed to be 10-12 nm on the central area of the surface of the substrates which is relevant in the *in situ* optical measurements. I proved with OWLS measurements, that due to the coatings prepared on sensor chips the resonant peaks were shifted to higher incoupling angles, but their amplitudes didn't change considerably, so the nanostructured coating didn't quench the incoupling of the laser light and the propagation of the excited waveguide mode [T1].

2. For the first time, protein adsorption and living cell adhesion were studied on TNT coatings using OWLS. I demonstrated that the nanostructured layer enhanced the adsorption of bovine serum albumin. The mass density of the irreversibly adsorbed protein derived from the OWLS measurements was higher by ca. 92% on the coated surface compared to the uncoated one. I carried out living cell adhesion experiments applying OWLS and phase contrast microscopy, and it was revealed that the TNT films have a promotive effect on the adhesion of human embryonic kidney (HEK) cells and preosteoblasts. The adhesion of HEK cells and preosteoblasts increased by ca. 43% and ca. 36%, respectively. When surfaces with ca. 80% HEK cell coverage were washed, the cell coverage on the uncoated substrate decreased to 8%, while on the TNT-coated surface it remained 80%, accordingly the coating increased the strength of cell adhesion.

I developed a new cuvette configuration for the HoloMonitor M4 digital holographic microscope that enables to take high-quality images of living cells under favorable circumstances on spin-coated layers for long periods of time (min. 24 hours) [T1], [T3].

3. For the first time, I applied multiple angle of incidence, internal reflection, plasmon-enhanced spectroscopic ellipsometry in Kretschmann configuration for time-sharing multi-channel *in situ* adsorption measurements. I developed a substrate preparation method, which enables coated and reference surfaces to be studied by ellipsometry simultaneously under same experimental conditions, which makes the comparison of the measurement results more reliable. Multiple angle of incidence and time-sharing multi-channel measurement was enabled by using a semi-cylindrical glass lens. Low sample consumption and rapid blending was ensured by the small volume (~10 μL) of the flow cell. In the measurements I used substrates with gold thin films on their surface, in order to achieve the plasmon resonance effect. Thanks to plasmonic enhancement the sensitivity of the method increased, the limit of detection – compared to the ca. 80 pg/mm^2 value for the ellipsometric measurements applying conventional flow cells – decreased to 40 pg/mm^2 [T2].

4.a For the first time, I studied the deposition of sodium poly(styrene sulfonate) and poly(allylamine hydrochloride) polyelectrolyte layers using the ellipsometric setup presented in thesis highlight 3. I showed that among the simultaneously built polyelectrolyte layers, the layers on the TNP coating had a greater effective thickness derived from optical measurements (by ~35% for 10 pairs of layers), performed at pH 8. By comparing the total thickness of the layers built on nanostructured TNP surface at pH 4 and pH 8, I revealed that the layers were about 9.7 times thicker in the case of pH 8 [T2].

4.b   I applied the new ellipsometric arrangement to study the adsorption of fibrinogen from bovine serum on TNP coating and gold control surface in the same process. The results of the measurements demonstrated that the nanostructured coating enhanced the adsorption of the proteins, the effective surface mass density derived from optical measurements was greater by 30% for the TNP-coated surface.

For the first time, living cells were studied with time-sharing two-channel *in situ* spectroscopic ellipsometry in Kretschmann geometry. I demonstrated that the various measurement sessions are distinguishable based on the measured data, furthermore the sets of data for the two surfaces significantly differ from each other. After the experiment, I took phase contrast images of the cells on the substrate, and proved that after the washing step clearly more cells remained on the TNP coating than on the gold control surface [T2].

Tézispontok

1. Külső partner által egy újfajta eljárással előállított, adalékanyag-mentes titanát nanocsöveket (TNT), illetve titán-dioxid nanorészecskéket (TNP) tartalmazó szolokból elsőként készítettem olyan vékonyrétegeket, amelyek alkalmazhatók optikai hullámvezető fénymódus spektroszkópiai (OWLS) szenzorchipek bevonataként. Atomi erő mikroszkópiával igazoltam, hogy a nanorészecskékből álló rétegek egyenletes lefedettséget biztosítanak, az optikai modellezés tekintetében jó közelítéssel homogénnek tekinthetők. Spektroszkópiai ellipszometriai térképezéssel megmutattam, hogy a bevonat vastagsága mindkét nanorészecske esetében 10-12 nm a hordozó felületének középső, az *in situ* optikai mérések szempontjából releváns részén. OWLS műszerrel igazoltam, hogy a szenzor chip felületén elkészített bevonat hatására a rezonancia csúcsok a nagyobb becsatolási szögek felé tolódnak, de az amplitúdójuk nem változik számottevően, tehát a nanostrukturált bevonat nem rontja a lézerfény becsatolódását és a gerjesztett hullámvezető módus terjedését [T1].

2. Elsőként végeztem fehérjeadszorpciós és sejtadhéziós méréseket OWLS-sel TNT bevonatokon. Megmutattam, hogy a borjú szérum albumin kitapadását elősegíti a nanostrukturált TNT réteg, a felületre irreverzibilisen kitapadt fehérje OWLS mérésekből származtatott effektív tömegsűrűsége kb. 92%-kal nagyobb volt a bevonatos, mint a bevonat nélküli chipen. OWLS-sel és fáziskontraszt mikroszkóppal végzett kísérletekkel megmutattam, hogy a humán embrionális vesesejtek és a preosteoblast (éretlen csontképző) sejtek kitapadását is jelentős mértékben elősegítette a TNT bevonat. A vesesejtek adhéziója kb. 43%-kal, a preosteoblastoké pedig kb. 36%-kal nőtt. Vesesejtekkel kb. 80%-osan borított felületek lemosásakor a bevonat nélküli hordozón a sejtborítottság kb. 8%-ra csökkent, míg a TNT rétegen nem változott, tehát a sejtkitapadás erősségét is növelte a réteg.

Egy új küvettaelrendezést fejlesztettem a HoloMonitor M4 digitális holografikus mikroszkóphoz, mely lehetővé teszi, hogy forgótárcsás rétegképzéssel létrehozott bevonatokon hosszú időn (min. 24 óra) keresztül jó minőségű képeket lehessen készíteni élő sejtekről a számukra megfelelő körülmények között [T1], [T3].

3.   Elsőként alkalmaztam Kretschmann elrendezésű, belső reflexiójú, plazmongerjesztéses, több beesési szögű spektroszkópiai ellipszometriát időosztásos kétcsatornás *in situ* adszorpciós mérésekhez. Kidolgoztam egy olyan hordozó-előkészítési eljárást, ami lehetővé teszi a bevonatos és a referenciafelület azonos kísérleti körülmények között történő párhuzamos ellipszometriai vizsgálatát, melynek köszönhetően a mért eredmények összehasonlítása megbízhatóbbá válik. Üvegből készült félhenger alkalmazásával tettem lehetővé több beesési szög alkalmazását és az időosztásos többcsatornás mérést. A rendszer kis mintaigényét és a minta gyors keveredését a kis cellatérfogattal (kb. 10 µL) biztosítottam. A hordozó felületén található arany vékonyréteg plazmonikus hatása következtében a mérés érzékenysége nőtt, a kimutatási határ – a hagyományos cellával végzett ellipszometriai mérések 80 pg/mm^2-es értékéhez képest – 40 pg/mm^2-re csökkent [T2].

4.a   A 3. tézispontban bemutatott ellipszometriai elrendezést nátrium-poli(sztirol-szulfonát) és poli(allilamin-hidroklorid) polielektrolit rétegek építésének monitorozására is alkalmaztam. Igazoltam, hogy a kétféle felületen egyidejűleg épülő rétegek közül 8-as pH-n a TNP rétegen az optikai mérésből származtatott effektív vastagság nagyobbnak adódott (10 rétegpár esetén kb. 35%-kal). Azonos TNP felületen, 4-es és 8-as pH-n épített rétegek teljes vastagságát összehasonlítva pedig megmutattam, hogy 8-as pH-n kb. 9,7-szer vastagabb rétegek épültek, mint 4-es pH-n [T2].

4.b   Az új ellipszometriai elrendezést elsőként alkalmaztam borjú szérumból származó fibrinogén fehérje adszorpciójának vizsgálatára TNP bevonaton, illetve arany kontrollfelületen egy folyamatban történő leválasztás során. A mérésekkel megmutattam, hogy a fehérjék kitapadását elősegítette a nanoszemcsés bevonat, a mérésekből származtatott effektív felületi tömegsűrűség kb. 30%-kal nagyobb volt a TNP-vel borított felületen.

Elsőként alkalmaztam a kétcsatornás *in situ* Kretschmann elrendezésű spektroszkópiai ellipszometriát élő sejtek vizsgálatára. A mérésekkel megmutattam, hogy a különböző kísérleti szakaszok jól elkülöníthetők az időben ábrázolt mérési adatok alapján, és igazoltam, hogy a két különböző felszínen mért adatok jelentősen eltérnek egymástól. A kísérlet után a sejtekről készített fáziskontraszt mikroszkópos képekkel demonstráltam, hogy a mérés utolsó, mosási szakasza után jól láthatóan több sejt maradt a titán-dioxid nanoszemcsékkel borított felületen, mint az arany kontrollfelületen [T2].

8. List of publications

8.1. Publications related to the Ph.D. thesis

[T1] J. Nador, N. Orgovan, M. Fried, P. Petrik, A. Sulyok, J. J. Ramsden, L. Korosi, R. Horvath, "Enhanced protein adsorption and cellular adhesion using transparent titanate nanotube thin films made by a simple and inexpensive room temperature process: Application to optical biochips", Colloids and Surfaces B Biointerfaces **122**, 491–497, Elsevier B.V. (2014) [doi:10.1016/j.colsurfb.2014.07.015]. Impact factor: 4.152

[T2] J. Nador, B. Kalas, A. Saftics, E. Agocs, P. Kozma, L. Korosi, I. Szekacs, M. Fried, R. Horvath, and P. Petrik, "Plasmon-enhanced two-channel in situ Kretschmann ellipsometry of protein adsorption, cellular adhesion and polyelectrolyte deposition on titania nanostructures," Opt. Express **24**(5), 4812–4823 (2016) [doi:10.1364/OE.24.004812]. Impact factor: 3.488

[T3] B. Peter, J. Nador, K. Juhasz, A. Dobos, L. Korosi, I. Szekacs, D. Patko, R. Horvath: "Incubator proof miniaturized Holomonitor to *in situ* monitor cancer cells exposed to green tea polyphenol and preosteoblast cells adhering on nanostructured titanate surfaces: validity of the measured parameters and their corrections", J. Biomed. Opt. **20**(6), 067002 (2015) [doi:10.1117/1.JBO.20.6.067002]. Impact factor: 2.859

8.2. Oral and poster presentations related to the Ph.D. thesis

[T4] J. Nador, D. Patko, N. Orgovan, B. Peter, L. Korosi, M. Fried, P. Petrik, R. Horvath: "Nanostructured Biosensor Coatings Using Titanate Nanotubes", 3rd International Conference on Bio-Sensing Technology, Sitges, Spain, 12-15 May 2013, poster presentation.

[T5] J. Nador, D. Patko, N. Orgovan, B. Peter, L. Korosi, M. Fried, P. Petrik, R. Horvath: "Nanostructured Biosensor Coatings Using Titanate Nanotubes", A Magyar Biofizikai Társaság XXIV. Kongresszusa, Veszprém, 27-30 August 2013,

poster presentation.

[T6] E. Agocs, P. Kozma, J. Nador, B. Kalas, A. Hamori, M. Janosov, S. Kurunczi, B. Fodor, M. Fried, P. Petrik, R. Horvath: "Grating Coupled Optical Waveguide Interferometry Combined with In-situ Spectroscopic Ellipsometry to Monitor Surface Processes in Aqueous Solutions", 13th European Vacuum Conference, Aveiro, Portugal, 8-12 September 2014, poster presentation.

[T7] Nádor J, Petrik P, Horváth R: "Fehérjeadszorpció és sejtadhézió erősítése titanát-nanocsövekből készített nanostrukturált bevonatok segítségével", MTA Természettudományi Kutatóközpont Doktori Konferencia, Budapest, 10-12 December 2014, oral presentation.

[T8] E. Agocs, P. Kozma, J. Nador, B. Kalas, A. Hamori, M. Janosov, S. Kurunczi, B. Fodor, M. Fried, R. Horvath, P. Petrik: "In-situ simultaneous monitoring of layer adsorption in aqueous solutions using grating coupled optical waveguide interferometry combined with spectroscopic ellipsometry", 9th Workshop Ellipsometry, Enschede, Hollandia, 23-25 February 2015, poster presentation.

[T9] J. Nador, B. Kalas, E. Agocs, P. Kozma, L. Korosi, I. Szekacs, M. Fried, R. Horvath, P. Petrik: "High-sensitivity in situ Kretschmann ellipsometry of protein adsorption and cellular adhesion on titania nanostructures", 4th International Conference on Bio-Sensing Technology, Lisbon, Portugal, 10-13 May 2015, poster presentation.

[T10] P. Petrik, E. Agocs, B. Fodor, B. Kalas, J. Nador, T. Lohner, P. Kozma, G. Juhasz, C. Major, M. Fried: Methods for optical modeling and cross-checking. 7th International Workshop "Advanced optical and X-ray characterization techniques of multifunctional materials for information and communication technologies, sensing and renewable energy applications", Bucharest, Romania, 16-18 September 2015, invited.

[T11] Nádor J, Kalas B, Saftics A, Agócs E, Kozma P, Kőrösi L, Székács I, Fried M, Horváth R, Petrik P: Biológiai objektumok és nanorétegek TiO_2 nanorészecskés bevonaton történő kitapadásának vizsgálata nagyérzékenységű *in situ* Kretschmann-ellipszometria alkalmazásával. A Magyar Biofizikai Társaság XXV.

Kongresszusa, Budapest, Semmelweis Egyetem, 25-28 August 2015, oral presentation.

[T12] P. Petrik, E. Agocs, B. Kalas, P. Kozma, B. Fodor, <u>J. Nador</u>, C. Major, M. Fried: Multiple angle of incidence, spectroscopic, plasmon-enhanced, internal reflection ellipsometry for the characterization of solid-liquid interface processes. SPIE Conference on Optical Methods for Inspection, Characterization, and Imaging of Biomaterials II. Munich, Germany, 22-24 June 2015, oral presentation.

[T13] P. Petrik, B. Fodor, E. Agocs, P. Kozma, <u>J. Nador</u>, N. Kumar, J. Endres, G. Juhasz, C. Major, S. F. Pereira, T. Lohner, H. P. Urbach, B. Bodermann, M. Fried: Methods for optical modeling and cross-checking in ellipsometry and scatterometry. SPIE Conference on Modeling Aspects in Optical Metrology V, 9526, Munich, Germany, 21-25 June 2015, invited.

8.3. *Other publications*

[T14] P. Petrik, E. Agocs, B. Kalas, P. Kozma, B. Fodor, <u>J. Nador</u>, C. Major, M. Fried: Multiple angle of incidence, spectroscopic, plasmon-enhanced, internal reflection ellipsometry for the characterization of solid-liquid interface processes. Proc. SPIE 9529, Optical Methods for Inspection, Characterization, and Imaging of Biomaterials II, 95290W (2015)

[T15] P. Petrik, B. Fodor, E. Agocs, P. Kozma, <u>J. Nador,</u> N. Kumar, J. Endres, G. Juhasz, C. Major, S. F. Pereira, T. Lohner, H. P. Urbach, B. Bodermann, M. Fried: Methods for optical modeling and cross-checking in ellipsometry and scatterometry. Proc. SPIE 9526, Modeling Aspects in Optical Metrology V, 95260S (2015)

9. Acknowledgements

10. References

[1]   K. Riehemann, S. W. Schneider, T. A. Luger, B. Godin, M. Ferrari, and H. Fuchs, "Nanomedicine--challenge and perspectives.," *Angew. Chem. Int. Ed. Engl.*, vol. 48, no. 5, pp. 872–97, 2009.

[2]   M. Davoren, "Nanotechnology...Small particles, big risks?" [Online]. Available: https://www.pacific-environment.com/news/nanotechnology-small-particles-big-risks/.

[3]   O. Thomas, A. Ponchet, and S. Forest, *Mechanics of Nano-objects*. Presses des MINES, 2011.

[4]   J. N. Tiwari, R. N. Tiwari, and K. S. Kim, "Zero-dimensional, one-dimensional, two-dimensional and three-dimensional nanostructured materials for advanced electrochemical energy devices," *Prog. Mater. Sci.*, vol. 57, no. 4, pp. 724–803, 2012.

[5]   B. O. Dabbousi, J. Rodriguez, F. V Mikulec, J. R. Heine, H. Mattoussi, R. Ober, K. F. Jensen, and M. G. Bawendi, "(CdSe)ZnS Core - Shell Quantum Dots : Synthesis and Characterization of a Size Series of Highly Luminescent Nanocrystallites," *J. Phys. Chem. B*, vol. 101, no. 97, pp. 9463–9475, 1997.

[6]   D. A. Schwartz, N. S. Norberg, Q. P. Nguyen, J. M. Parker, and D. R. Gamelin, "Magnetic quantum dots: synthesis, spectroscopy, and magnetism of Co^{2+} - and Ni^{2+}-doped ZnO nanocrystals.," *J. Am. Chem. Soc.*, vol. 125, no. 43, pp. 13205–13218, 2003.

[7]   D. Gerion, F. Pinaud, S. C. Williams, W. J. PArak, D. Zanchet, S. Weiss, and P. A. Alivisatos, "Synthesis and properties of biocompartible water-soluble silica-coated CdSe/ZnS semiconductor quantum dots," *J. Phys. Chem. B*, vol. 105, pp. 8861–8871, 2001.

[8]   J. Yu and X. Yu, "Hydrothermal synthesis and photocatalytic activity of zinc oxide hollow spheres.," *Environ. Sci. Technol.*, vol. 42, no. 13, pp. 4902–4907, 2008.

[9]   O. E. Semonin, J. M. Luther, S. Choi, H.-Y. Chen, J. Gao, A. J. Nozik, and M. C. Beard, "Peak External Photocurrent Quantum Efficiency Exceeding 100% via MEG in a Quantum Dot Solar Cell," *Science (80-.).*, vol. 334, no. 6062, pp. 1530–1533, 2011.

[10]   D. L. Huffaker, G. Park, Z. Zou, O. B. Shchekin, and D. G. Deppe, "1.3 micrometer room-temperature GaAs-based quantum-dot laser," *Appl. Phys. Lett.*, vol. 73, no. 18, pp. 2564–2566, 1998.

[11]   P. O. Anikeeva, J. E. Halpert, M. G. Bawendi, and V. Bulović, "Quantum dot light-emitting devices with electroluminescence tunable over the entire visible spectrum," *Nano Lett.*, vol. 9, no. 7, pp. 2532–2536, 2009.

[12]   V. G. Mokerov, Y. V Fedorov, L. E. Velikovski, and M. Y. Scherbakova, "New quantum dot transistor," *Nanotechnology*, vol. 12, no. 4, pp. 552–555, 2001.

[13]   X. Michalet, F. F. Pinaud, L. A. Bentolila, J. M. Tsay, S. Doose, J. J. Li, G. Sundaresan, A. M. Wu, S. S. Gambhir, S. Weiss, and A. Manuscript, "Quantum dots for live cells, in vivo imaging, and diagnostics.," *Science*, vol. 307, no. 5709, pp. 538–44, 2005.

[14]   C. J. Murphy, "Optical Sensing with Quantum Dots," *Anal. Chem.*, vol. 74, no. 19, p. 520 A–526 A, 2002.

[15]   C. C. Berry and A. S. G. Curtis, "Functionalisation of magnetic nanoparticles for applications in biomedicine," *J. Phys. D. Appl. Phys.*, vol. 36, no. 13, pp. R198–

R206, 2003.

[16] Z. Ren, Z. Huang, J. Xu, J. Wang, P. Bush, M. Siegal, and P. Provencio, "Synthesis of large arrays of well-aligned carbon nanotubes on glass," *Science*, vol. 282, no. 5391, pp. 1105–7, 1998.

[17] K. Hata, D. Futaba, K. Mizuno, T. Namai, M. Yumura, and S. Iijima, "Water-assisted highly efficient synthesis of impurity-free single-walled carbon nanotubes.," *Science*, vol. 306, no. 5700, pp. 1362–1364, 2004.

[18] M. S. Gudiksen, L. J. Lauhon, J. Wang, D. C. Smith, and C. M. Lieber, "Growth of nanowire superlattice structures for nanoscale photonics and electronics.," *Nature*, vol. 415, no. 6872, pp. 617–620, 2002.

[19] S. E. Lohse and C. J. Murphy, "The quest for shape control: A history of gold nanorod synthesis," *Chem. Mater.*, vol. 25, no. 8, pp. 1250–1261, 2013.

[20] Z. W. Pan, Z. R. Dai, and Z. L. Wang, "Nanobelts of semiconducting oxides," *Science (80-.).*, vol. 291, no. 5510, pp. 1947–1949, 2001.

[21] J. Wang, "Nanomaterial-based electrochemical biosensors," pp. 421–426, 2005.

[22] A. R. Harutyunyan, B. K. Pradhan, G. U. Sumanasekera, and A. A. Kuznetsov, "Carbon Nanotubes for Medical Applications," *Eur. Cells Mater.*, vol. 3, pp. 84–87, 2002.

[23] S. Chen and D. L. Carroll, "Synthesis and Characterization of Truncated Triangular Silver Nanoplates," *Nano Lett.*, vol. 2, no. 9, pp. 1003–1007, 2002.

[24] S. Stankovich, D. A. Dikin, R. D. Piner, K. A. Kohlhaas, A. Kleinhammes, Y. Jia, Y. Wu, S. T. Nguyen, and R. S. Ruoff, "Synthesis of graphene-based nanosheets via chemical reduction of exfoliated graphite oxide," *Carbon N. Y.*, vol. 45, no. 7, pp. 1558–1565, 2007.

[25] D. Aherne, D. M. Ledwith, M. Gara, and J. M. Kelly, "Optical properties and growth aspects of silver nanoprisms produced by a highly reproducible and rapid synthesis at room temperature," *Adv. Funct. Mater.*, vol. 18, no. 14, pp. 2005–2016, 2008.

[26] T. Yu, Y. Zhu, X. Xu, Z. Shen, P. Chen, C. T. Lim, J. T. L. Thong, and C. H. Sow, "Controlled growth and field-emission properties of cobalt oxide nanowalls," *Adv. Mater.*, vol. 17, no. 13, pp. 1595–1599, 2005.

[27] M. Maillard, P. Huang, and L. Brus, "Silver Nanodisk Growth by Surface Plasmon Enhanced Photoreduction of Adsorbed [Ag +]," *Nano Lett.*, vol. 3, no. 11, pp. 1611–1615, 2003.

[28] K. J. Koski and Y. Cui, "The new skinny in two-dimensional nanomaterials," *ACS Nano*, vol. 7, no. 5, pp. 3739–3743, 2013.

[29] S. Balendhran, S. Walia, H. Nili, S. Sriram, and M. Bhaskaran, "Elemental analogues of graphene: Silicene, germanene, stanene, and phosphorene," *Small*, vol. 11, no. 6, pp. 640–652, 2015.

[30] A. K. Geim and K. S. Novoselov, "The rise of graphene.," *Nat. Mater.*, pp. 183–191, 2007.

[31] Z. Ni, Q. Liu, K. Tang, J. Zheng, J. Zhou, R. Qin, Z. Gao, D. Yu, and J. Lu, "Tunable bandgap in silicene and germanene," *Nano Lett.*, vol. 12, no. 1, pp. 113–118, 2012.

[32] N. Yang, J. Zhai, D. Wang, Y. Chen, and L. Jiang, "Two-dimensional graphene bridges enchanced photoinduced charge transport in dye-sensitized solar cells," *ACS Nano*, vol. 4, no. 2, p. 887, 2010.

[33] X. Sun, Z. Liu, K. Welsher, J. T. Robinson, A. Goodwin, S. Zaric, and H. Dai, "Nano-Graphene Oxide for Cellular Imaging and Drug Delivery," *Nano Res*, vol. 1, no. 3, pp. 203–212, 2008.

[34] S. Goenka, V. Sant, and S. Sant, "Graphene-based nanomaterials for drug delivery and tissue engineering," *J. Control. Release*, vol. 173, no. 1, pp. 75–88, 2014.

[35] Y. Yang, A. M. Asiri, Z. Tang, D. Du, and Y. Lin, "Graphene based materials for biomedical applications," *Mater. Today*, vol. 16, no. 10, pp. 365–373, 2013.

[36] A. Carlmark, C. Hawker, A. Hult, and M. Malkoch, "New methodologies in the construction of dendritic materials," *Chem. Soc. Rev.*, vol. 38, no. 2, pp. 352–362, 2009.

[37] S. N. Naess, A. Elgsaeter, G. Helgesen, and K. D. Knudsen, "Carbon nanocones: wall structure and morphology," *Sci. Technol. Adv. Mater.*, vol. 10, no. 6, p. 065002, 2009.

[38] L. Pan, M. Zhang, and Y. Nakayama, "Growth mechanism of carbon nanocoils," *J. Appl. Phys.*, vol. 91, no. 12, pp. 10058–10061, 2002.

[39] S. Zeng, K. Tang, T. Li, Z. Liang, D. Wang, Y. Wang, Y. Qi, and W. Zhou, "Facile route for the fabrication of porous hematite nanoflowers: Its synthesis, growth mechanism, application in the lithium ion battery, and magnetic and photocatalytic properties," *J. Phys. Chem. C*, vol. 112, no. 13, pp. 4836–4843, 2008.

[40] H. Heli, I. Eskandari, N. Sattarahmady, and A. A. Moosavi-Movahedi, "Cobalt nanoflowers: Synthesis, characterization and derivatization to cobalt hexacyanoferrate - Electrocatalytic oxidation and determination of sulfite and nitrite," *Electrochim. Acta*, vol. 77, pp. 294–301, 2012.

[41] Z. Fan, H. Razavi, J. Do, A. Moriwaki, O. Ergen, J. L. Chueh, P. W. Leu, J. C. Ho, T. Takahashi, L. A. Reichertz, S. Neale, K. Yu, M. Wu, J. W. Ager, and A. Javey, "Three-dimensional nanopillar-array photovoltaics on low-cost and flexible substrates," *Nat. Mater.*, vol. 8, no. 8, pp. 648–653, 2009.

[42] J.-H. Ahn, H.-S. Kim, K. J. Lee, S. Jeon, S. J. Kang, Y. Sun, R. G. Nuzzo, and J. A. Rogers, "Heterogeneous Three-Dimensional Electronics by Use of Printed Semiconductor Nanomaterials," *Science (80-.).*, vol. 314, no. 5806, pp. 1754–1757, Dec. 2006.

[43] M. Cao, X. He, J. Chen, and C. Hu, "Self-assembled nickel hydroxide three-dimensional nanostructures: A nanomaterial for alkaline rechargeable batteries," *Cryst. Growth Des.*, vol. 7, no. 1, pp. 170–174, 2007.

[44] S.-W. Kim, D.-H. Seo, H. Gwon, J. Kim, and K. Kang, "Fabrication of FeF3 Nanoflowers on CNT branches and their application to high power lithium rechargeable batteries.," *Adv. Mater.*, vol. 22, no. 46, pp. 5260–5264, 2010.

[45] T. Dvir, B. P. Timko, M. D. Brigham, S. R. Naik, S. S. Karajanagi, O. Levy, H. Jin, K. K. Parker, R. Langer, and D. S. Kohane, "Nanowired three-dimensional cardiac patches.," *Nat. Nanotechnol.*, vol. 6, no. 11, pp. 720–5, 2011.

[46] E. R. Gillies and J. M. J. Frechet, "Dendrimers and dendritic polymers in drug delivery," *Drug Discov. Today*, vol. 10, no. 1, pp. 35–43, 2005.

[47] C. Dufès, I. F. Uchegbu, and A. G. Schätzlein, "Dendrimers in gene delivery," *Adv. Drug Deliv. Rev.*, vol. 57, no. 15, pp. 2177–2202, 2005.

[48] J. Xie, Q. Zhang, J. Y. Lee, and D. I. C. Wang, "The Synthesis of SERS-Active Gold Nanoflower Tags for In Vivo Applications," vol. 2, no. 12, pp. 2473–2480, 2008.

[49] E. Martinez, E. Engel, J. A. Planell, and J. Samitier, "Effects of artificial micro- and nano-structured surfaces on cell behaviour," *Ann. Anat.*, vol. 191, no. 1, pp. 126–135, 2009.

[50] J. Y. Lim and H. J. Donahue, "Cell sensing and response to micro- and

nanostructured surfaces produced by chemical and topographic patterning.," *Tissue Eng.*, vol. 13, no. 8, pp. 1879–91, 2007.

[51] E. Palin, H. Liu, and T. J. Webster, "Mimicking the nanofeatures of bone increases bone-forming cell adhesion and proliferation," *Nanotechnology*, vol. 16, no. 9, p. 1828, 2005.

[52] S. Bonde, N. Buch-Manson, K. R. Rostgaard, T. K. Andersen, T. Berthing, and K. L. Martinez, "Exploring arrays of vertical one-dimensional nanostructures for cellular investigations," *Nanotechnology*, vol. 25, no. 36, p. 362001, 2014.

[53] K. M. Kim, S. Han, and C. S. Hwang, "Electronic bipolar resistance switching in an anti-serially connected Pt/TiO2/Pt structure for improved reliability.," *Nanotechnology*, vol. 23, no. 3, p. 035201, 2012.

[54] F. Mumm, K. M. Beckwith, S. Bonde, K. L. Martinez, and P. Sikorski, "A transparent nanowire-based cell impalement device suitable for detailed cell-nanowire interaction studies," *Small*, vol. 9, no. 2, pp. 263–272, 2013.

[55] J. J. Vandersarl, A. M. Xu, and N. A. Melosh, "Nanostraws for direct fluidic intracellular access," *Nano Lett.*, vol. 12, no. 8, pp. 3881–3886, 2012.

[56] A. K. Shalek, J. T. Gaublomme, L. Wang, N. Yosef, N. Chevrier, M. S. Andersen, J. T. Robinson, N. Pochet, D. Neuberg, R. S. Gertner, I. Amit, J. R. Brown, N. Hacohen, A. Regev, C. J. Wu, and H. Park, "Nanowire-mediated delivery enables functional interrogation of primary immune cells: Application to the analysis of chronic lymphocytic leukemia," *Nano Lett.*, vol. 12, no. 12, pp. 6498–6504, 2012.

[57] L. Hanson, Z. C. Lin, C. Xie, Y. Cui, and B. Cui, "Characterization of the cell-nanopillar interface by transmission electron microscopy," *Nano Lett.*, vol. 12, no. 11, pp. 5815–5820, 2012.

[58] C. Xie, L. Hanson, W. Xie, Z. Lin, B. Cui, and Y. Cui, "Noninvasive neuron pinning with nanopillar arrays," *Nano Lett.*, vol. 10, no. 10, pp. 4020–4024, 2010.

[59] S. T. Kim, D. J. Kim, T. J. Kim, D. W. Seo, T. H. Kim, S. Y. Lee, K. Kim, K. M. Lee, and S. K. Lee, "Novel streptavidin-functionalized silicon nanowire arrays for CD4 + T lymphocyte separation," *Nano Lett.*, vol. 10, no. 8, pp. 2877–2883, 2010.

[60] G. Piret, M. T. Perez, and C. N. Prinz, "Neurite outgrowth and synaptophysin expression of postnatal CNS neurons on GaP nanowire arrays in long-term retinal cell culture," *Biomaterials*, vol. 34, no. 4, pp. 875–887, 2013.

[61] S. Kar and P. K. Tewari, *Nanotechnology in Eco-Efficient Construction*. 2013.

[62] P. M. Martin, Ed., "Deposition Technologies: An Overview," in *Handbook of Deposition Technologies for Films and Coatings*, 3rd ed., Boston: William Andrew Publishing, 2010, pp. 1–31.

[63] X. Wang, M. Sieger, and B. Mizaikoff, "Toward on-chip mid-infrared chem/bio sensors using quantum cascade lasers and substrate-integrated semiconductor waveguides," *Proc. SPIE*, vol. 8631, no. February, p. 86312M–86312M–11, 2013.

[64] J. Vörös, J. J. Ramsden, G. Csucs, I. Szendrő, S. M. De Paul, M. Textor, and N. D. Spencer, "Optical grating coupler biosensors," *Biomaterials*, vol. 23, pp. 3699–3710, 2002.

[65] J. J. Ramsden, "Experimental methods for investigating protein adsorption kinetics at surfaces," *Q. Rev. Biophys.*, vol. 27, no. 01, pp. 41–105, 1994.

[66] B. Cunningham, P. Li, B. Lin, and J. Pepper, "Colorimetric resonant reflection as a direct biochemical assay technique," *Sensors Actuators, B Chem.*, vol. 81, no.

2–3, pp. 316–328, 2002.

[67] N. Orgovan, D. Patko, C. Hos, S. Kurunczi, B. Szabó, J. J. Ramsden, and R. Horvath, "Sample handling in surface sensitive chemical and biological sensing: A practical review of basic fluidics and analyte transport," *Adv. Colloid Interface Sci.*, vol. 211, pp. 1–16, Sep. 2014.

[68] "OW 2400 - Optical Waveguide Grating Coupler Sensor Chip." [Online]. Available: http://www.owls-sensors.com/sensorchip_ow2400.

[69] F. Höök, J. Vörös, M. Rodahl, R. Kurrat, P. Böni, J. J. Ramsden, M. Textor, N. D. Spencer, P. Tengvall, J. Gold, and B. Kasemo, "A comparative study of protein adsorption on titanium oxide surfaces using in situ ellipsometry, optical waveguide lightmode spectroscopy, and quartz crystal microbalance/dissipation," *Colloids Surfaces B Biointerfaces*, vol. 24, no. 2, pp. 155–170, 2002.

[70] T. S. Hug, J. E. Prenosil, P. Maier, and M. Morbidelli, "Optical waveguide lightmode spectroscopy (OWLS) to monitor cell proliferation quantitatively.," *Biotechnol. Bioeng.*, vol. 80, no. 2, pp. 213–21, Oct. 2002.

[71] N. Orgovan, R. Salánki, N. Sándor, Z. Bajtay, A. Erdei, B. Szabó, and R. Horvath, "In-situ and label-free optical monitoring of the adhesion and spreading of primary monocytes isolated from human blood: Dependence on serum concentration levels.," *Biosens. Bioelectron.*, vol. 54, pp. 339–44, Apr. 2014.

[72] I. R. Cooper, S. T. Meikle, G. Standen, G. W. Hanlon, and M. Santin, "The rapid and specific real-time detection of Legionella pneumophila in water samples using Optical Waveguide Lightmode Spectroscopy," *J. Microbiol. Methods*, vol. 78, no. 1, pp. 40–44, 2009.

[73] K. Majer-Baranyi, A. Székács, I. Szendro, A. Kiss, and N. Adányi, "Optical waveguide lightmode spectroscopy technique-based immunosensor development for deoxynivalenol determination in wheat samples," *Eur. Food Res. Technol.*, vol. 233, no. 6, pp. 1041–1047, 2011.

[74] N. Orgovan, B. Peter, S. Bősze, J. J. Ramsden, B. Szabó, and R. Horvath, "Dependence of cancer cell adhesion kinetics on integrin ligand surface density measured by a high-throughput label-free resonant waveguide grating biosensor.," *Sci. Rep.*, vol. 4, p. 4034, Jan. 2014.

[75] N. Orgovan, R. Ungai-Salánki, S. Lukácsi, N. Sándor, Z. Bajtay, A. Erdei, B. Szabó, and R. Horvath, "Adhesion kinetics of human primary monocytes, dendritic cells, and macrophages: Dynamic cell adhesion measurements with a label-free optical biosensor and their comparison with end-point assays," *Biointerphases*, vol. 11, no. 3, p. 031001, 2016.

[76] Y. Fang, A. M. Ferrie, N. H. Fontaine, J. Mauro, and J. Balakrishnan, "Resonant Waveguide Grating Biosensor for Living Cell Sensing," *Biophys. J.*, vol. 91, no. 5, pp. 1925–1940, 2006.

[77] R. Slavik and J. Homola, "Ultrahigh resolution long range surface plasmon-based sensor," *Sensors Actuators, B Chem.*, vol. 123, no. 1, pp. 10–12, 2007.

[78] M. Mrksich, G. B. Sigal, and G. M. WHITESIDES, "Surface-Plasmon Resonance Permits in-Situ Measurement of Protein Adsorption on Self-Assembled Monolayers of Alkanethiolates on Gold," *Langmuir*, vol. 11, no. 11, pp. 4383–4385, 1995.

[79] J. Homola, S. S. Yee, and G. Gauglitz, "Surface plasmon resonance sensors: review," *Sensors Actuators B Chem.*, vol. 54, no. 1–2, pp. 3–15, 1999.

[80] S. A. Meyer, E. C. Le Ru, and P. G. Etchegoin, "Combining Surface Plasmon Resonance (SPR) Spectroscopy with Surface-Enhanced Raman Scattering (SERS)," pp. 2337–2344, 2011.

[81] T. M. Chinowsky, S. B. Saban, and S. S. Yee, "Experimental data from a trace metal sensor combining surface plasmon resonance with anodic stripping voltammetry," *Sensors Actuators B Chem.*, vol. 35, no. 1–3, pp. 37–43, 1996.

[82] P. Westphal and A. Bornmann, "Biomolecular detection by surface plasmon enhanced ellipsometry," *Sensors Actuators, B Chem.*, vol. 84, no. 2–3, pp. 278–282, 2002.

[83] M. A. Cooper, "Optical biosensors in drug discovery.," *Nat. Rev. Drug Discov.*, vol. 1, no. 7, pp. 515–528, 2002.

[84] P. Kozma, A. Hamori, K. Cottier, S. Kurunczi, and R. Horvath, "Grating coupled interferometry for optical sensing," *Appl. Phys. B Lasers Opt.*, vol. 97, no. 1, pp. 5–8, 2009.

[85] D. Patko, K. Cottier, A. Hamori, and R. Horvath, "Single beam grating coupled interferometry: high resolution miniaturized label-free sensor for plate based parallel screening," *Opt. Express*, vol. 20, no. 21, p. 23162, 2012.

[86] S. Simhony, E. M. Kosower, and A. Katzir, "Novel attenuated total internal reflectance spectroscopic cell using infrared fibers for aqueous solutions," *Appl. Phys. Lett.*, vol. 49, no. 5, pp. 253–254, 1986.

[87] A. Messica, A. Greenstein, and A. Katzir, "Theory of fiber-optic, evanescent-wave spectroscopy and sensors.," *Appl. Opt.*, vol. 35, no. 13, pp. 2274–2284, 1996.

[88] H. Tai, H. Tanaka, and T. Yoshino, "Fiber-optic evanescent-wave methane-gas sensor using optical absorption for the 3.392-microm line of a He-Ne laser.," *Opt. Lett.*, vol. 12, no. 6, pp. 437–439, 1987.

[89] F. Villuendas and J. Pelayo, "Optical Fibre Device for Chemical Sensing Based on Surface Plasmon Excitation," vol. 423, pp. 1142–1145, 1990.

[90] A. K. Sharma, R. Jha, and B. D. Gupta, "Fiber-optic sensors based on surface plasmon resonance: A comprehensive review," *IEEE Sens. J.*, vol. 7, no. 8, pp. 1118–1129, 2007.

[91] D. Monzón-Hernández and J. Villatoro, "High-resolution refractive index sensing by means of a multiple-peak surface plasmon resonance optical fiber sensor," *Sensors Actuators, B Chem.*, vol. 115, no. 1, pp. 227–231, 2006.

[92] S. Shukla, N. K. Sharma, and V. Sajal, "Sensitivity enhancement of a surface plasmon resonance based fiber optic sensor using ZnO thin film: A theoretical study," *Sensors Actuators, B Chem.*, vol. 206, pp. 463–470, 2015.

[93] N. Zhong, M. Zhao, L. Zhong, Q. Liao, X. Zhu, B. Luo, and Y. Li, "A high-sensitivity fiber-optic evanescent wave sensor with a three-layer structure composed of Canada balsam doped with GeO2," *Biosens. Bioelectron.*, vol. 85, pp. 876–882, 2016.

[94] X. Liu and W. Tan, "A fiber-optic evanescent wave DNA biosensor based on novel molecular beacons.," *Anal. Chem.*, vol. 71, no. 22, pp. 5054–5059, 1999.

[95] A. P. Abel, M. G. Weller, G. L. Duveneck, M. Ehrat, and H. M. Widmer, "Fiber-optic evanescent wave biosensor for the detection of oligonucleotides," *Anal. Chem.*, vol. 68, no. 17, pp. 2905–2912, 1996.

[96] H. Fujiwara, *Spectroscopic Ellipsometry: Principles and Applications*. Chichester, UK: John Wiley & Sons, Ltd, 2007.

[97] M. Fried, T. Lohner, and P. Petrik, "Handbook of Surfaces and Interfaces of Materials," in *Handbook of Surfaces and Interfaces of Materials*, Elsevier, 2001, pp. 335–367.

[98] M. Dressel, B. Gompf, D. Faltermeier, A. K. Tripathi, J. Pflaum, and M. Schubert, "Kramers-Kronig-consistent optical functions of anisotropic crystals:

generalized spectroscopic ellipsometry on pentacene.," *Opt. Express*, vol. 16, no. 24, pp. 19770–19778, 2008.

[99] P. Petrik, E. Agocs, J. Volk, I. Lukacs, B. Fodor, P. Kozma, T. Lohner, S. Oh, Y. Wakayama, T. Nagata, and M. Fried, "Resolving lateral and vertical structures by ellipsometry using wavelength range scan," *Thin Solid Films*, vol. 571, no. P3, pp. 579–583, 2014.

[100] P. Petrik, "Parameterization of the dielectric function of semiconductor nanocrystals," *Phys. B Condens. Matter*, vol. 453, pp. 2–7, 2014.

[101] P. Kozma, D. Kozma, A. Nemeth, H. Jankovics, S. Kurunczi, R. Horvath, F. Vonderviszt, M. Fried, and P. Petrik, "In-depth characterization and computational 3D reconstruction of flagellar filament protein layer structure based on in situ spectroscopic ellipsometry measurements," *Appl. Surf. Sci.*, vol. 257, no. 16, pp. 7160–7166, Jun. 2011.

[102] J. N. Hilfiker, R. A. Synowicki, and H. G. Tompkins, "Spectroscopic Ellipsometry Methods for Thin Absorbing Coatings," *Soc. Vac. Coaters*, no. 1, pp. 511–516, 2008.

[103] A. Rothen, "The ellipsometer, an apparatus to measure thicknesses of thin surface films," *Rev. Sci. Instrum.*, vol. 16, no. 2, pp. 26–30, 1945.

[104] B. Y. Alexandre, "Immunological antigen reactions and antibody," *October*, pp. 75–97, 1946.

[105] A. Rothen, "Long Range Enzymatic Action on Films of Antigen," *J. Am. Chem. Soc.*, vol. 70, no. 8, pp. 2732–2740, 1948.

[106] A. A. Fisk, "The Thicknesses of Hemoglobin and Bovine Serum Albumin Molecules as Unimolecular Layers Adsorbed onto Films of Barium Stearate," *Proc. Natl. Acad. Sci. U. S. A.*, pp. 518–523, 1950.

[107] H. J. Trurnit, "Symposium on Monomolecular Layers," *American Association for the Advancement of Science*. Philadelphia, 1951.

[108] H. J. Trurnit, "Studies of enzyme systems at a solid-liquid interface. I. The system chymotrypsin-serum albumin," *Arch. Biochem. Biophys.*, vol. 47, no. 2, pp. 251–271, 1953.

[109] H. J. Trurnit, "Studies on enzyme systems at a solid-liquid interface. II. The kinetics of adsorption and reaction.," *Arch. Biochem. Biophys.*, vol. 51, no. 1, pp. 176–99, 1954.

[110] L. VROMAN and A. LUKOSEVICIUS, "Ellipsometer Recordings of Changes in Optical Thickness of Adsorbed Films associated with Surface Activation of Blood Clotting," *Nature*, vol. 204, no. 4959, pp. 701–703, Nov. 1964.

[111] D. E. Aspnes and A. A. Studna, "High precision scanning ellipsometer.," *Appl. Opt.*, vol. 14, no. 1, pp. 220–228, 1975.

[112] P. A. Cuypers, W. T. Hermens, and H. C. Hemker, "Ellipsometry as a Tool to Study Protein Interfaces Films at," *Anal. Biochem.*, vol. 67, pp. 56–67, 1978.

[113] P. T. PUGLIESE and A. J. MILLIGAN, "Ellipsometric measurement of skin refractive index in vivo," in *Bioengineering and the Skin*, vol. 13, no. 4, R. Marks and P. A. Payne, Eds. Dordrecht: Springer Netherlands, 1981, pp. 291–302.

[114] H. Arwin, "Optical Properties of Thin Layers of Bovine Serum Albumin, γ-Globulin, and Hemoglobin," *Appl. Spectrosc.*, vol. 40, no. 3, pp. 313–318, 1986.

[115] U. Jönsson, M. Malmqvist, and I. Ronnberg, "Adsorption of immunoglobulin G, protein A, and fibronectin in the submonolayer region evaluated by a combined study of ellipsometry and radiotracer techniques," *J. Colloid Interface Sci.*, vol. 103, no. 2, pp. 360–372, 1985.

[116] J. Måtensson, H. Arwin, I. Lundström, and T. Ericson, "Adsorption of

Lactoperoxidase on Hydrophilic and Hydrophobic Silicon Dioxide Surfaces: An Ellipsometric Study," *Journal of Colloid and Interface Science*, vol. 155, no. 1. pp. 30–36, 1993.

[117] D. R. Miller and N. A. Peppas, "The use of ellipsometry to study adsorption on hydrogels," *Biomaterials*, vol. 6, no. 1, pp. 33–40, 1985.

[118] G. Jin, R. Jansson, and H. Arwin, "Imaging ellipsometry revisited: Developments for visualization of thin transparent layers on silicon substrates," *Rev. Sci. Instrum.*, vol. 67, no. 8, pp. 2930–2936, 1996.

[119] E. G. Bortchagovsky, "Possibilities of Ellipsometry with the Surface Plasmon Excitation in the Investigation of Thin Films in Comparism with Separated Ellipsometry and Surface plasmon spectroscopy," in *SPIE*, 1997, vol. 3094, pp. 239–249.

[120] H. Arwin, M. Poksinski, and K. Johansen, "Total internal reflection ellipsometry: principles and applications.," *Appl. Opt.*, vol. 43, no. 15, pp. 3028–3036, 2004.

[121] T. W. H. Oates, H. Wormeester, and H. Arwin, "Characterization of plasmonic effects in thin films and metamaterials using spectroscopic ellipsometry," *Prog. Surf. Sci.*, vol. 86, no. 11–12, pp. 328–376, 2011.

[122] M. Poksinski and H. Arwin, "Protein monolayers monitored by internal reflection ellipsometry," *Thin Solid Films*, vol. 455–456, pp. 716–721, 2004.

[123] H. Arwin, M. Poksinski, and K. Johansen, "Enhancement in ellipsometric thin film sensitivity near surface plasmon resonance conditions," *Phys. Status Solidi Appl. Mater. Sci.*, vol. 205, no. 4, pp. 817–820, 2008.

[124] Z. Balevicius, A. Ramanaviciene, I. Baleviciute, A. Makaraviciute, L. Mikoliunaite, and A. Ramanavicius, "Evaluation of intact- and fragmented-antibody based immunosensors by total internal reflection ellipsometry," *Sensors Actuators, B Chem.*, vol. 160, no. 1, pp. 555–562, 2011.

[125] A. Nooke, U. Beck, A. Hertwig, A. Krause, H. Kröger, V. Lohse, D. Negendank, and J. Steinbach, "On the application of gold based SPR sensors for the detection of hazardous gases," *Sensors Actuators, B Chem.*, vol. 149, no. 1, pp. 194–198, 2010.

[126] A. Nooke, U. Beck, A. Hertwig, A. Krause, H. Kröger, V. Lohse, D. Negendank, and J. Steinbach, "Ellipsometric detection of gases with the surface plasmon resonance effect on gold top-coated with sensitive layers," *Thin Solid Films*, vol. 519, no. 9, pp. 2659–2663, 2011.

[127] A. V. Nabok, A. Tsargorodskaya, A. K. Hassan, and N. F. Starodub, "Total internal reflection ellipsometry and SPR detection of low molecular weight environmental toxins," *Appl. Surf. Sci.*, vol. 246, no. 4, pp. 381–386, 2005.

[128] L. Liu, A. Viallat, and G. Jin, "Vesicle adhesion visualized with total internal reflection imaging ellipsometry biosensor," *Sensors Actuators, B Chem.*, vol. 190, pp. 221–226, 2014.

[129] M. D. Rosenberg, "Microexudates from Cells Grown in Tissue Culture," *Biophys. J.*, vol. 1, no. 2, pp. 137–159, 1960.

[130] G. Poste, L. W. Greenham, L. Mallucci, P. Reeve, and D. J. Alexander, "The study of cellular 'microexudates' by ellipsometry and their relationship to the cell coat," *Exp. Cell Res.*, vol. 78, no. 2, pp. 303–313, Apr. 1973.

[131] S.-H. Kim, W. Chegal, J. Doh, H. M. Cho, and D. W. Moon, "Study of cell-matrix adhesion dynamics using surface plasmon resonance imaging ellipsometry.," *Biophys. J.*, vol. 100, no. 7, pp. 1819–28, Apr. 2011.

[132] S. M. Yang, S. J. Choi, H. S. Kim, and S. Y. Kim, "In vitro characterization of optical property of mouse myoblast cells by spectroscopic ellipsometry," *Thin*

Solid Films, vol. 571, pp. 468–472, 2014.

[133] M. Minunni, M. Mascini, G. G. Guilbault, and B. Hock, "The Quartz Crystal Microbalance as Biosensor. A Status Report on Its Future," *Anal. Lett.*, vol. 28, no. 5, pp. 749–764, 1995.

[134] K. A. Marx, T. Zhou, A. Montrone, H. Schulze, and S. J. Braunhut, "A quartz crystal microbalance cell biosensor: Detection of microtubule alterations in living cells at nM nocodazole concentrations," *Biosens. Bioelectron.*, vol. 16, no. 9–12, pp. 773–782, 2001.

[135] T. Hianik, V. Ostatná, Z. Zajacová, E. Stoikova, and G. Evtugyn, "Detection of aptamer-protein interactions using QCM and electrochemical indicator methods," *Bioorganic Med. Chem. Lett.*, vol. 15, no. 2, pp. 291–295, 2005.

[136] R. Z. Hao, H. Bin Song, G. M. Zuo, R. F. Yang, H. P. Wei, D. B. Wang, Z. Q. Cui, Z. Zhang, Z. X. Cheng, and X. E. Zhang, "DNA probe functionalized QCM biosensor based on gold nanoparticle amplification for Bacillus anthracis detection," *Biosens. Bioelectron.*, vol. 26, no. 8, pp. 3398–3404, 2011.

[137] C. Yao, T. Zhu, J. Tang, R. Wu, Q. Chen, M. Chen, B. Zhang, J. Huang, and W. Fu, "Hybridization assay of hepatitis B virus by QCM peptide nucleic acid biosensor," *Biosens. Bioelectron.*, vol. 23, no. 6, pp. 879–885, 2008.

[138] P. Sedlak, J. Majzner, J. Šikula, and K. Hajek, "Noise Measurement Setup for Quartz Crystal Microbalance," *Radioengineering*, vol. 21, no. 1, pp. 207–212, 2012.

[139] J. Rishpon, A. Redondo, C. Derouin, and S. Gotttesfeld, "Simultaneous ellipsometric and microgravimetric measurements during the electrochemical growth of polyaniline," *J. Electroanal. Chem.*, vol. 294, no. 1–2, pp. 73–85, 1990.

[140] J. J. Iturri Ramos, S. Stahl, R. P. Richter, and S. E. Moya, "Water content and buildup of poly(diallyldimethylammonium chloride)/poly(sodium 4-styrenesulfonate) and poly(allylamine hydrochloride)/poly(sodium 4-styrenesulfonate) polyelectrolyte multilayers studied by an in situ combination of a quartz crystal microb," *Macromolecules*, vol. 43, no. 21, pp. 9063–9070, 2010.

[141] N. Kananizadeh, C. Rice, J. Lee, K. B. Rodenhausen, D. Sekora, M. Schubert, E. Schubert, S. Bartelt-Hunt, and Y. Li, "Combined quartz crystal microbalance with dissipation (QCM-D) and generalized ellipsometry (GE) to characterize the deposition of titanium dioxide nanoparticles on model rough surfaces," *J. Hazard. Mater.*, 2015.

[142] E. Agocs, P. Kozma, J. Nador, A. Hamori, M. Janosov, B. Kalas, S. Kurunczi, B. Fodor, E. Ehrentreich-Förster, M. Fried, R. Horvath, and P. Petrik, "Grating coupled optical waveguide interferometry combined with in situ spectroscopic ellipsometry to monitor surface processes in aqueous solutions," *Appl. Surf. Sci. (in press)*, 2016.

[143] F. Rosei, "Nanostructured surfaces: challenges and frontiers in nanotechnology," *J. Phys. Condens. Matter*, vol. 16, no. 17, pp. S1373–S1436, 2004.

[144] T. H. Maiman, "Stimulated Optical Radiation in Ruby," *Nature*, vol. 187, no. 4736, pp. 493–494, 1960.

[145] M. Birnbaum, "Semiconductor surface damage produced by Ruby lasers," *J. Appl. Phys.*, vol. 36, no. 11, pp. 3688–3689, 1965.

[146] V. R. Manfrinato, L. Zhang, D. Su, H. Duan, R. G. Hobbs, E. A. Stach, and K. K. Berggren, "Resolution limits of electron-beam lithography toward the atomic scale," *Nano Lett.*, vol. 13, no. 4, pp. 1555–1558, 2013.

[147] Q. Xia, K. J. Morton, R. H. Austin, and S. Y. Chou, "Sub-10 nm self-enclosed

self-limited nanofluidic channel arrays," *Nano Lett.*, vol. 8, no. 11, pp. 3830–3833, 2008.

[148] R. Spohr, *International School-Seminar on Heavy Ion Physics*. Alushta: Press Office of Joint Institute for Nuclear Research, 1983.

[149] E. W. Becker, W. Ehrfeld, P. Hagmann, A. Maner, and D. Munchmeyer, "Fabrication of microstructures with high aspect ratios and great structural heights by synchrotron radiation lithography, galvanoforming, and plastic moulding (LIGA process)," *Microelectron. Eng.*, vol. 4, no. 1, pp. 35–56, 1986.

[150] R. Chen, M. C. Lu, V. Srinivasan, Z. Wang, H. H. Cho, and A. Majumdar, "Nanowires for enhanced boiling heat transfer," *Nano Lett.*, vol. 9, no. 2, pp. 548–553, 2009.

[151] B. Bhushan and Y. C. Jung, "Wetting, adhesion and friction of superhydrophobic and hydrophilic leaves and fabricated micro/nanopatterned surfaces," *J. Phys. Condens. Matter*, vol. 20, no. 22, p. 225010, 2008.

[152] P. Roach, D. Farrar, and C. C. Perry, "Interpretation of protein adsorption: Surface-induced conformational changes," *J. Am. Chem. Soc.*, vol. 127, no. 22, pp. 8168–8173, 2005.

[153] H. Chen, W. Song, F. Zhou, Z. Wu, H. Huang, J. Zhang, Q. Lin, and B. Yang, "The effect of surface microtopography of poly(dimethylsiloxane) on protein adsorption, platelet and cell adhesion," *Colloids Surfaces B Biointerfaces*, vol. 71, no. 2, pp. 275–281, 2009.

[154] P. E. Scopelliti, A. Borgonovo, M. Indrieri, L. Giorgetti, G. Bongiorno, R. Carbone, A. Podestà, and P. Milani, "The effect of surface nanometre-scale morphology on protein adsorption," *PLoS One*, vol. 5, no. 7, pp. 1–9, 2010.

[155] K. Rechendorff, M. B. Hovgaard, M. Foss, V. P. Zhdanov, and F. Besenbacher, "Enhancement of protein adsorption induced by surface roughness," *Langmuir*, vol. 22, no. 26, pp. 10885–10888, 2006.

[156] M. N. Sela, L. Badihi, G. Rosen, D. Steinberg, and D. Kohavi, "Adsorption of human plasma proteins to modified titanium surfaces," *Clin. Oral Implants Res.*, vol. 18, no. 5, pp. 630–638, 2007.

[157] P. Elter, R. Lange, and U. Beck, "Atomic force microscopy studies of the influence of convex and concave nanostructures on the adsorption of fibronectin," *Colloids Surfaces B Biointerfaces*, vol. 89, no. 1, pp. 139–146, 2012.

[158] Y. Koc, a J. de Mello, G. McHale, M. I. Newton, P. Roach, and N. J. Shirtcliffe, "Nano-scale superhydrophobicity: suppression of protein adsorption and promotion of flow-induced detachment.," *Lab Chip*, vol. 8, no. 4, pp. 582–586, 2008.

[159] J. Zheng, W. Song, H. Huang, and H. Chen, "Protein adsorption and cell adhesion on polyurethane/Pluronic surface with lotus leaf-like topography," *Colloids Surfaces B Biointerfaces*, vol. 77, no. 2, pp. 234–239, 2010.

[160] L. Rizzello, B. Sorce, S. Sabella, G. Vecchio, A. Galeone, V. Brunetti, R. Cingolani, and P. P. Pompa, "Impact of nanoscale topography on genomics and proteomics of adherent bacteria," *ACS Nano*, vol. 5, no. 3, pp. 1865–1876, 2011.

[161] A. Z. Komaromy, S. Li, H. Zhang, D. V. Nicolau, R. I. Boysen, and M. T. W. Hearn, "Arrays of nano-structured surfaces to probe the adhesion and viability of bacteria," *Microelectron. Eng.*, vol. 91, pp. 39–43, 2012.

[162] A. V. Singh, V. Vyas, R. Patil, V. Sharma, P. E. Scopelliti, G. Bongiorno, A. Podestà, C. Lenardi, W. N. Gade, and P. Milani, "Quantitative characterization of the influence of the nanoscale morphology of nanostructured surfaces on

bacterial adhesion and biofilm formation," *PLoS One*, vol. 6, no. 9, 2011.

[163] V. A. Schulte, M. Diez, M. Müller, and M. C. Lensen, "Topography-induced cell adhesion to acr-sP(EO-stat-PO) hydrogels: The role of protein adsorption," *Macromol. Biosci.*, vol. 11, no. 10, pp. 1378–1386, 2011.

[164] P. Premnath, A. Tavangar, B. Tan, and K. Venkatakrishnan, "Tuning cell adhesion by direct nanostructuring silicon into cell repulsive/adhesive patterns," *Exp. Cell Res.*, vol. 337, no. 1, pp. 44–52, 2015.

[165] M. J. Dalby, S. J. Yarwood, M. O. Riehle, H. J. H. Johnstone, S. Affrossman, and A. S. G. Curtis, "Increasing fibroblast response to materials using nanotopography: morphological and genetic measurements of cell response to 13-nm-high polymer demixed islands.," *Exp. Cell Res.*, vol. 276, no. 1, pp. 1–9, 2002.

[166] G. S. Leventhal, "Titanium, a metal for surgery," *J. Bone Jt. Surg.*, vol. 33 A, no. 2, pp. 473–74, 1951.

[167] O. E. Beder and G. Eade, "An investigation of tissue tolerance to titanium metal implants in dogs," *Surgery*, vol. 39, pp. 470–473, 1956.

[168] O. E. Beder and W. J. Ploger, "Intraoral titanium implants," *Oral Surgery, Oral Med. Oral Pathol.*, vol. 12, no. 7, pp. 787–799, Jul. 1959.

[169] P. I. Brånemark, R. Adell, U. Breine, B. O. Hansson, J. Lindström, and a Ohlsson, "Intra-osseous anchorage of dental prostheses. I. Experimental studies.," *Scand. J. Plast. Reconstr. Surg.*, vol. 3, no. 2, pp. 81–100, 1969.

[170] M. A. Meenaghan, J. R. Natiella, J. E. Armitage, and R. H. Wood, "Evaluation of the crypt surface adjacent to metal endosseous implants: An electron microscopic study in clinically successful implants," *J. Prosthet. Dent.*, vol. 31, no. 5, pp. 574–581, May 1974.

[171] A. B. Ferguson, Y. Akahoshi, P. G. Laing, and E. S. Hodge, "Trace Metal Ion Concentration in the Liver, Kidney, Spleen, and Lung of Normal Rabbits," *J. Bone Jt. Surg.*, vol. 44, no. 2, pp. 317–322, Mar. 1962.

[172] A. Schroeder, E. Vanderzypen, H. Stich, and F. Sutter, "the Reactions of Bone, Connective-Tissue, and Epithelium To Endosteal Implants With Titanium-Sprayed Surfaces," *J. Maxillofac. Surg.*, vol. 9, no. 1, pp. 15–25, 1981.

[173] F. A. Young, "Porous titanium dental implants," *J. Biomed. Mater. Res.*, vol. 8, no. 4, pp. 401–407, 1974.

[174] K. Suzuki, K. Aoki, and K. Ohya, "Effects of surface roughness of titanium implants on bone remodeling activity of femur in rabbits," *Bone*, vol. 21, no. 6, pp. 507–514, 1997.

[175] D. Buser, R. K. Schenk, S. Steinemann, J. P. Fiorellini, C. H. Fox, and H. Stich, "Influence of surface characteristics on bone integration of titanium implants. A histomorphometric study in miniature pigs.," *J. Biomed. Mater. Res.*, vol. 25, no. 7, pp. 889–902, 1991.

[176] T. Masuda, P. K. Yliheikkilä, D. A. Felton, and M. S. L. F. Cooper, "Generalizations Regarding the Process and Phenomenon of Osseointegration. Part I. In Vivo Studies," *Int. J. Oral Maxillofac. Implant.*, vol. 13, no. 1, pp. 17–29, 1998.

[177] L. F. Cooper, T. Masuda, P. K. Yliheikkilä, and D. a Felton, "Generalizations regarding the process and phenomenon of osseointegration. Part II. In vitro studies.," *Int. J. Oral Maxillofac. Implants*, vol. 13, no. 2, pp. 163–174, 1998.

[178] E. Luong-Van, I. Rodriguez, H. Y. Low, N. Elmouelhi, B. Lowenhaupt, S. Natarajan, C. T. Lim, R. Prajapati, M. Vyakarnam, and K. Cooper, "Review: Micro- and nanostructured surface engineering for biomedical applications," *J.*

Mater. Res., vol. 28, no. 2, pp. 165–174, 2013.

[179] U. Meyer, A. Büchter, H. P. Wiesmann, U. Joos, and D. B. Jones, "Basic reactions of osteoblasts on structured material surfaces.," *Eur. Cell. Mater.*, vol. 9, no. August, pp. 39–49, 2005.

[180] L. F. Cooper, "A role for surface topography in creating and maintaining bone at titanium endosseous implants," *J. Prosthet. Dent.*, vol. 84, no. 5, pp. 522–534, 2000.

[181] D. Khang, J. Lu, C. Yao, K. M. Haberstroh, and T. J. Webster, "The role of nanometer and sub-micron surface features on vascular and bone cell adhesion on titanium," *Biomaterials*, vol. 29, no. 8, pp. 970–983, 2008.

[182] X. Zhu, J. Chen, L. Scheideler, T. Altebaeumer, J. Geis-Gerstorfer, and D. Kern, "Cellular reactions of osteoblasts to micron- and submicron-scale porous structures of titanium surfaces," *Cells Tissues Organs*, vol. 178, no. 1, pp. 13–22, 2004.

[183] R. C.-C. Wang, M.-C. Hsieh, and T.-M. Lee, "Effects of nanometric roughness on surface properties and fibroblast's initial cytocompatibilities of Ti6Al4V.," *Biointerphases*, vol. 6, no. 3, p. 87, 2011.

[184] M. Jayaraman, U. Meyer, M. Bühner, U. Joos, and H. P. Wiesmann, "Influence of titanium surfaces on attachment of osteoblast-like cells in vitro," *Biomaterials*, vol. 25, no. 4, pp. 625–631, 2004.

[185] K. C. Popat, L. Leoni, C. A. Grimes, and T. A. Desai, "Influence of engineered titania nanotubular surfaces on bone cells," *Biomaterials*, vol. 28, no. 21, pp. 3188–3197, 2007.

[186] H. Kim, J. Seo, T. Kim, and B. Lee, "Nanometrology and its perspectives in environmental research," *Environ. Health Toxicol.*, vol. 29, pp. 1–9, 2014.

[187] "Refractometers – Measuring Principle." [Online]. Available: http://www.gpsil.com/our-products/refractometers/measuring-pri/.

[188] L. Korosi, S. Papp, V. Hornok, A. Oszko, P. Petrik, D. Patko, R. Horvath, and I. Dekany, "Titanate nanotube thin films with enhanced thermal stability and high-transparency prepared from additive-free sols," *J. Solid State Chem.*, vol. 192, pp. 342–350, 2012.

[189] D. P. Birnie III, "Spin Coating Technique," *Sol-Gel Technol. Glas. Prod. Users*, pp. 49–55, 2004.

[190] L. E. Scriven, "Physics and Applications of Dip Coating and Spin Coating," *Better Ceram. Through Chem. III*, vol. 121, pp. 717–729, 1988.

[191] L. Korosi, M. Prato, A. Scarpellini, A. Riedinger, J. Kovács, M. Kus, V. Meynen, and S. Papp, "Hydrothermal synthesis, structure and photocatalytic activity of PF-co-doped TiO2," *Mater. Sci. Semicond. Process.*, vol. 30, pp. 442–450, 2015.

[192] L. Kőrösi, A. Scarpellini, P. Petrik, S. Papp, and I. Dékány, "Sol–gel synthesis of nanostructured indium tin oxide with controlled morphology and porosity," *Appl. Surf. Sci.*, vol. 320, pp. 725–731, Nov. 2014.

[193] D. Nečas and P. Klapetek, "Gwyddion: an open-source software for SPM data analysis," *Open Phys.*, vol. 10, no. 1, pp. 181–188, 2012.

[194] G. Binnig and C. F. Quate, "Atomic Force Microscope," *Phys. Rev. Lett.*, vol. 56, no. 9, pp. 930–933, 1986.

[195] D. Fotiadis, "Atomic force microscopy for the study of membrane proteins," *Curr. Opin. Biotechnol.*, vol. 23, no. 4, pp. 510–515, 2012.

[196] F. J. Giessibl, "AFM's path to atomic resolution," *Mater. Today*, vol. 8, no. 5, pp. 32–41, 2005.

[197] L. Ressier and V. Le Nader, "Electrostatic nanopatterning of PMMA by AFM

charge writing for directed nano-assembly.," *Nanotechnology*, vol. 19, no. 13, p. 135301, 2008.

[198] W. H. Roos and G. J. L. Wuite, "Nanoindentation studies reveal material properties of viruses," *Adv. Mater.*, vol. 21, no. 10–11, pp. 1187–1192, 2009.

[199] W.-C. Mo, Z.-J. Zhang, D.-L. Wang, Y. Liu, P. F. Bartlett, and R.-Q. He, "Shielding of the Geomagnetic Field Alters Actin Assembly and Inhibits Cell Motility in Human Neuroblastoma Cells," *Sci. Rep.*, vol. 6, no. April 2015, p. 22624, 2016.

[200] A. Holm, K.-E. Magnusson, and E. Vikström, "Pseudomonas aeruginosa N-3-oxo-dodecanoyl-homoserine Lactone Elicits Changes in Cell Volume, Morphology, and AQP9 Characteristics in Macrophages," *Front. Cell. Infect. Microbiol.*, vol. 6, no. March, pp. 1–15, 2016.

[201] H. Persson, Z. Li, J. O. Tegenfeldt, S. Oredsson, and C. N. Prinz, "From immobilized cells to motile cells on a bed-of-nails: effects of vertical nanowire array density on cell behaviour.," *Sci. Rep.*, vol. 5, no. November, p. 18535, 2015.

[202] M. Sebesta, P. J. Egelberg, A. Langberg, J.-H. Lindskov, K. Alm, and B. Janicke, "HoloMonitor M4: holographic imaging cytometer for real-time kinetic label-free live-cell analysis of adherent cells," vol. 9718, p. 971813, 2016.

[203] "Holographic Microscopy." [Online]. Available: http://www.phiab.se/technology/holographic-microscopy.

[204] F. Zernike, "Phase contrast, a new method for the microscopic observation of transparent objects," *Physica*, vol. 9, no. 7, pp. 686–698, Jul. 1942.

[205] F. Zernike, "Phase contrast, a new method for the microscopic observation of transparent objects part II," *Physica*, vol. 9, no. 10, pp. 974–986, Dec. 1942.

[206] "Introduction to Phase Contrast Microscopy," 2010. [Online]. Available: http://www.bwoptics.com/newsend2.asp?id=3.

[207] R. Horvath, H. C. Pedersen, N. Skivesen, D. Selmeczi, and N. B. Larsen, "Optical waveguide sensor for on-line monitoring of bacteria," *Opt. Lett.*, vol. 28, no. 14, pp. 1233–1235, 2003.

[208] L. Marcotte and M. Tabrizian, "Sensing surfaces: Challenges in studying the cell adhesion process and the cell adhesion forces on biomaterials," *Irbm*, vol. 29, no. 2–3, pp. 77–88, Apr. 2008.

[209] T. S. Hug, J. E. Prenosil, and M. Morbidelli, "Optical waveguide lightmode spectroscopy as a new method to study adhesion of anchorage-dependent cells as an indicator of metabolic state.," *Biosens. Bioelectron.*, vol. 16, no. 9–12, pp. 865–74, Dec. 2001.

[210] R. Horváth, G. Fricsovszky, and E. Papp, "Application of the optical waveguide lightmode spectroscopy to monitor lipid bilayer phase transition.," *Biosens. Bioelectron.*, vol. 18, no. 4, pp. 415–28, Apr. 2003.

[211] J. De Feijter, J. Benjamins, and F. Veer, "Ellipsometry as a tool to study the adsorption behavior of syntetic and biopolyers at the air water interface," *Biopolymers*, vol. 17, no. 7, pp. 1759–1772, 1978.

[212] V. Ball and J. J. Ramsden, "Buffer dependence of refractive index increments of protein solutions," *Biopolymers*, vol. 46, no. 7, pp. 489–492, 1998.

[213] R. Kurrat, M. Textor, and J. Ramsden, "Instrumental improvements in optical waveguide light mode spectroscopy for the study of biomolecule adsorption," *Rev. Sci. ...*, vol. 68, no. 5, pp. 2172–2176, 1997.

[214] R. W. Carpick and M. Salmeron, "Scratching the surface: fundamental investigations of tribology with atomic force microscopy.," *Chem. Rev.*, vol. 97, no. 4, pp. 1163–1194, Jun. 1997.

[215] F. Giessibl, "Advances in atomic force microscopy," *Rev. Mod. Phys.*, vol. 75, no. July, pp. 949–983, 2003.

[216] J. J. Ramsden, *Biomedical surfaces*. Norwood: ARTECH HOUSE, 2008.

[217] E. S. Gadelmawla, M. M. Koura, T. M. A. Maksoud, I. M. Elewa, and H. H. Soliman, "Roughness parameters," *J. Mater. Process. Technol.*, vol. 123, no. 1, pp. 133–145, Apr. 2002.

[218] J. Woollam, P. Snyder, and M. Rost, "Variable angle spectroscopic ellipsometry: a non-destructive characterization technique for ultrathin and multilayer materials," *Thin Solid Films*, vol. 166, pp. 317–323, 1988.

[219] G. J. Jellison, "Data analysis for spectroscopic ellipsometry," *Thin Solid Films*, vol. 234, pp. 416–422, 1993.

[220] G. J. Jellison, "Spectroscopic ellipsometry data analysis: measured versus calculated quantities," *Thin Solid Films*, vol. 313–314, pp. 33–39, 1998.

[221] P. Langhoff and M. Karplus, "Pade summation of the cauchy dispersion equation," *J. Opt. Soc. Am.*, vol. 59, no. 7, pp. 863–871, 1969.

[222] F. Jenkins and H. White, *Fundamentals of optics*, 3rd ed. New York: McGraw-Hill, 1957.

[223] K. Tiefenthaler and W. Lukosz, "Sensitivity of grating couplers as integrated-optical chemical sensors," *J. Opt. Soc. Am. B*, vol. 6, no. 2, p. 209, Feb. 1989.

[224] R. Kurrat, J. Prenosil, and J. J. Ramsden, "Kinetics of human and bovine serum albumin adsorption at silica-titania surfaces," *J. Colloid Interface Sci.*, vol. 185, no. 1, pp. 1–8, Jan. 1997.

[225] J. J. Ramsden and R. Horvath, "Optical biosensors for cell adhesion.," *J. Recept. Signal Transduct. Res.*, vol. 29, no. 3–4, pp. 211–223, Jan. 2009.

[226] S. Kurunczi, A. Németh, T. Hülber, P. Kozma, P. Petrik, H. Jankovics, A. Sebestyén, F. Vonderviszt, M. Fried, and I. Bársony, "In situ ellipsometric study of surface immobilization of flagellar filaments," *Appl. Surf. Sci.*, vol. 257, no. 1, pp. 319–324, 2010.

[227] A. Nemeth, P. Kozma, T. Hülber, S. Kurunczi, R. Horvath, P. Petrik, A. Muskotál, F. Vonderviszt, C. Hős, M. Fried, J. Gyulai, and I. Bársony, "In Situ Spectroscopic Ellipsometry Study of Protein Immobilization on Different Substrates Using Liquid Cells," *Sens. Lett.*, vol. 8, no. 5, pp. 730–735, 2010.

[228] B. Johs and J. S. Hale, "Dielectric function representation by B-splines," *Phys. Status Solidi Appl. Mater. Sci.*, vol. 205, no. 4, pp. 715–719, 2008.

[229] E. D. Palik, *Handbook of Optical Constants of Solids*. Elsevier, 1997.

[230] H. G. Tompkins and E. A. Irene, Eds., *Handbook of Ellipsometry*. Norwich, NY: William Andrew Publishing, 2005.

[231] J. J. Ramsden, Y. M. Lvov, and G. Decher, "Determination of optical constants of molecular films assembled via alternate polyion adsorption," *Thin Solid Films*, vol. 254, no. 1–2, pp. 246–251, 1995.

[232] M. Alba, P. Formentín, J. Ferré-Borrull, J. Pallarès, and L. F. Marsal, "pH-responsive drug delivery system based on hollow silicon dioxide micropillars coated with polyelectrolyte multilayers.," *Nanoscale Res. Lett.*, vol. 9, no. 1, p. 411, 2014.